THE PRESSURE LEACHING OF PYRITE AND WOLFRAMITE IN SODIUM HYDROXIDE SOLUTIONS

A thesis

presented for the degree of

Doctor of Philosophy

in the

University of London

by

Aidan Miller Edwards; B.Sc.,Eng.(Met.) Rand.

April, 1963.

ABSTRACT.

A study has been made of the behaviour of pyrite and wolframite when leached in sodium hydroxide solutions.

Oxygen was essential to both systems but the mechanisms of behaviour during leaching was different; with pyrite the reaction rate was controlled by the interaction of oxygen atoms at the mineral surface, and with wolframite, a small quantity of oxygen resulted in extensive mineral dissolution, the oxygen not being consumed by reaction between mineral and reactant ions.

In the leaching of pyrite, determinations were made of the energy of activation and order of reaction with respect to reactant ions.

The important aspect of both systems was the "in situ" deposition of the insoluble products of dissolution on the parent mineral. The nature and porosity of the product was critically affected by the leaching environment and their density and porosity controlled the rate of diffusion of reactants through the product and, therefore, the rate of mineral dissolution.

Microscopic and X-ray studies have been made of the partially leached residues from which useful evidence regarding the reaction mechanisms and nature of the insoluble product has been obtained. Of particular importance is the structural relationship between pyrite and iron oxides of the cubic system and the apparent topotactic transformation from pyrite, through wustite and magnetite configuration to maghemite.

CONTENTS.

ABSTRACT. Page

SECTION 1

HYDROMETALLURGICAL PROCESSES

1.1. Introduction 1

1.2. General Considerations on Hydrometallurgical Processes 3

1.3. Review of Leach Reaction Variables 7

1.3.1. Oxygen Consumption 7
1.3.2. Oxidising Agents 10
1.3.3. Leach Solution Concentration 13
1.3.4. Effect of Temperature Change 15
1.3.5. Nature of Particle Surface 16

1.4. Insoluble Products of Reaction 18

1.4.1. Iron oxides or hydroxides 18
1.4.2. Elemental Sulphur on Sulphides 21
1.4.3. Precipitation from solution 22

1.5. Mechanisms of Reaction 23

1.5.1. Pyrite in Sulphuric Acid Solution 24
1.5.2. Pentlandite in Ammonia Solution 26
1.5.3. Galena in Sodium Hydroxide Solution 27
1.5.4. Molybdenite in Potassium Hydroxide Solution 27
1.5.5. Pyrolusite using Pyrite as Reagent 29
1.5.6. Uraninite using Pyrite as Solution 30
1.5.7. Uraninite in Sodium Carbonate Solution ... 30
1.5.8. Copper in Ammonia Solution 32

Page

1.6. Review of Topotactic Transformations. 33

1.6.1. Iron Oxides and Hydroxides 35
1.6.2. Aluminium Oxides and Hyroxides 42
1.6.3. Manganese Oxides and Hydroxides 44
1.6.4. Removal of Atoms from Crystalline Lattice... 45

1.7. Topotactic Transformation in Hydrometallurgy.. 46

SECTION 2.

GEOLOGY OF PYRITE AND WOLFRAMITE 48

2.1. Pyrite 48

2.1.1. General 48
2.1.2. Minerals Used 52

2.2. Wolframite 54

2.2.1. General 54
2.2.2. Minerals Used 56

SECTION 3.

RESULTS AND DISCUSSION: LEACHING OF PYRITE 57

3.1. Leach Reaction Variables 62

3.1.1. Dependence of Reaction on Oxygen and Sodium Hydroxide Concentration 62
3.1.2. Effect of Reaction Time 68
3.1.3. Effect of Air Pressure 78
3.1.4. Effect of Sodium Hydroxide Variation 1.. ... 90
3.1.5. Effect of Particle Size 92

Page

3.2. Reagent Consumption 96

3.3. Relation Between Particle Surface Area and Extent of Mineral Dissolution 99

3.3.1. Actual Reaction Rates per Unit Surface Area... 105

3.4. Study of Leach Residues 112

3.4.1. Microscopic Examination 112
3.4.2. Examination Using Microscan Analyser 120
3.4.3. X-ray powder photographs... 131

SECTION 3 - continued

RESULTS AND DISCUSSION: LEACHING OF WOLFRAMITE 134

3.5. Leach Reaction Variables 136

3.5.1. Effect of Particle Surface Area 136
3.5.2. Effect of Sodium Hydroxide Concentration . .. 137
3.5.3. Effect of Air Pressure 139
3.5.4. Effect of Reaction Time 147
3.5.5. Effect of Agitation Rate 149

3.6. Reagent Consumption ... .150

3.7. Promotion of Reaction Using Chelating Agent ...151

3.8. Relation Between Particle Size and Reduction in Surface Area. 153

3.9. Study of Leach Residues 155

3.9.1. Microscopic Examination 155
3.9.2. Examination Using Microscan Analyser 159
3.9.3. X-ray Powder Diffraction Studies 163

Page

SECTION 4.

MECHANISMS OF REACTION

4.1. Pyrite Section 164

4.1.1. Reaction at Mineral-Solution Interface ... 164
4.1.2. Behaviour of the Insoluble Iron Oxide Products 168

4.2. Wolframite Section 172

4.2.1. Reaction at Mineral-Solution Interface ... 172
4.2.2. Behaviour of the Insoluble Oxide Products.. 175

SECTION 5.

EXPERIMENTAL WORK.

5.1. Apparatus 177

5.2. Operation of the Autoclave.. 181

5.2.1. Pyrite 181
5.2.2. Wolframite 182

5.3. Analytical 183

5.3.1. Pyrite 183
5.3.2. Wolframite.. 184

5.4. Preparation of Polished Specimens 187

SECTION 6

SUMMARY

6.1. Pyrite 189

6.2. Wolframite 192

ACKNOWLEDGEMENTS 195

LIST OF REFERENCES 196

SECTION 1.

HYDROMETALLURGICAL PROCESSES.

1.1. Introduction.

The leaching of minerals in either alkaline or acidic solutions under conditions of elevated temperatures and pressures is a comparatively new approach in the field of hydrometallurgy, most of the research having been carried out in the last ten years.

By decomposing ores under these conditions it has been possible to promote reactions which may, in many cases, be very sluggish under normal atmospheric conditions with the restriction in temperature at the normal boiling point of the leach solutions. The use of sealed reaction vessels enables high temperatures and gas pressures to be employed. This favourably displaces the thermodynamic equilibrium of the dissolution process, and, especially where oxygen is essential to the reaction, the rate of dissolution into the liquid phase.

In this work, particular attention has been given to the insoluble products of decomposition of iron bearing minerals which are invariably deposited on to the unleached mineral in alkaline or weakly acidic solutions. The products usually cause the rate of reaction to be considerably reduced, and leads, in some cases, to the effective cessation of the reaction.

Except in very strong alkaline or acid solutions, the insoluble products are deposited as a pseudomorphic coating, in which the oxidation state may vary through its thickness depending on the leaching conditions. Similarly, the structure and porosity of the coating depends on these conditions and controls the rate of diffusion of solutes to the mineral surface and soluble products of reaction to the liquid phase. Thus, the rate of mineral decomposition depends on the concentrations of the reactants for two separate reasons; firstly, the direct relation between reaction rate and reagent activity and secondly, their control of the nature of the insoluble product.

The two examples of iron bearing minerals studied in this work are pyrite and wolframite which have been leached in 0.50 N sodium hydroxide solutions at temperatures up to 150°C and air pressures up to 600 p.s.i. In both cases pseudomorphic products were deposited on to the unleached mineral during the dissolution process, though the mechanisms of reaction and oxide formation were essentially different.

Examination of the partially leached residues microscopically has provided valuable information in elucidating the conditions under which a strongly adherent coating is most likely to be deposited. X-ray analysis has enabled the concentration of the constituent elements in the oxidation product to be determined.

The observations made have led to theories on both the mechanisms of mineral dissolution, and the structural changes,

which take place during reaction, of the insoluble product.

The effect of each reaction variable has been discussed with the experimental results in section 3, and a summary of the conclusions arrived at has been tabulated in section 4, in which the proposed mechanisms of reaction and oxide formation are discussed. A summary of the thesis is given in section 6.

1.2. General Considerations on Hydrometallurgical Processes.

The leaching rate of minerals may be dependent on any one or more of the following variables which determine the rate of reaction between mineral and reactants in the leach liquor :-

a) The rate of dissolution of gaseous molecules into the liquid phase.

b) The rate of diffusion of dissolved gases and reactant ions in solution to the mineral surface.

c) Adsorption of reactants on to the mineral surface.

d) Reaction at the surface.

e) Desorption of soluble products from the surface and the deposition of insoluble products either on or away from the surface.

f) Transference of soluble products into the bulk of the solution.

g) Reaction between soluble products and reactant ions.

h) Reaction between insoluble products and reactants and/or rate of structural change of the insoluble product.

i) Diffusion of reactants through an insoluble product to the free surface and outward diffusion of products or liberated mineral ions to react with reactants in the solution.

j) Reduction of reactant ion concentration by reaction with the mineral.

k) Interference of soluble products by increase in their concentration with progress of reaction.

Provided that the rate of mineral dissolution is not too rapid, efficient agitation of the leach solution and sufficiently high gas pressure should enable the above rate controlling factors, (a), (b) and (f) to be reduced to a minimum. Cases (j) and (k) can be eliminated by employing a sufficiently low solids to liquid ratio.

When an insoluble reaction product is deposited on the unleached mineral, the rate of diffusion of reactants through it becomes progressively more important. A sufficiently large thickness of coating is eventually produced which causes diffusion to become rate controlling. The coating itself may alter in porosity either by chemical reaction or by structural change thereby causing a further change of rate at a given temperature.

With change of temperature, the rate of reaction at the surface, i.e. a heterogeneous reaction, may be superceded by homogeneous reaction between soluble products and reactant ions, e.g. in the sodium hydroxide leaching of chromium oxide (13) (24). At temperatures up to 230°C, the reaction is heterogeneous with liberation of chromite ions being a slow process :

$$Cr_2O_3 = CrO_2' \quad \ldots\ldots\ldots \quad (1)$$

However, at 250°, the oxidation of chromite ions tends to become rate controlling;

$$CrO_2' = CrO_4'' \quad \ldots\ldots\ldots \quad (2)$$

This is the only example mentioned of such behaviour in the pressure leaching of minerals. In all other cases the reaction is heterogeneous and is directly related to the effective area of the mineral used.

Further reaction rate controlling factors are provided by the physical nature of the mineral. Minerals occurring in nature are seldom, if ever, structurally perfect and, therefore, accurate correlation of reaction rates between similar minerals from different geological sources cannot be expected. In the leaching of pyrite in sulphuric acid solutions, Warren (74)

studied the behaviour of pyrite from three sources in Australia and found a difference in the rate of oxidation of up to 10%. These were in comparatively good agreement. However, a comparison of activation energies obtained by three different workers showed a variation from 13 to 20 kcal per mole (16), (50) (74).

It was observed in this work that high purity pyrite is a good deal less reactive than the less pure Rio Tinto ore which was used.

a) More reactive sites are provided at defects in the crystal lattice which may be due to :-

   i. Lattice vacancies.
   ii. Interstitial foreign elements.
   iii. Replacement by foreign elements.

b) During the dissolution process, the actual reaction rate is frequently seen to increase substantially, or remain constant, despite the expected diminution of reaction rate with decrease in particle surface area. This may be due to a number of factors:-

   i. Non-uniform reaction by preferential decomposition at more reactive sites with resultant increase in surface area by pitting etc.
   ii. Penetration along mineral cleavage planes with increase in surface area.
   iii. Penetration along grain boundaries when the mineral is found in a finely disseminated state.

It is thus evident that, in a hydrometallurgical leaching process, a large number of reaction rate affecting factors must be considered. In particular, allowance should be made, when possible, for the inherent physical characteristics of the mineral in question. This is a factor which has frequently been overlooked in the past due to a lack of the necessary equipment for such a study to be made. Furthermore, it has been shown that extraneous rate controlling factors can have a considerable retarding effect on the dissolution rate and experimental conditions should, therefore, be controlled to reduce these effects to a minimum.

1.3. Review of Leach Reaction Variables.

1.3.1. Oxygen Consumption.

Oxygen or an oxidising agent is usually essential to the reaction and plays an important role in controlling the rate of dissolution of the mineral. When the mineral is decomposed rapidly, the experimental agitation rate may be too slow so that it may be impossible to provide a constant supply of oxygen molecules to the particle surface.

In the leaching of copper in ammonium hydroxide (38) Halpern found that at low oxygen partial pressures the rate was proportional to the pressure and the initial rate of reaction was limited by transport of dissolved oxygen to the copper surface. However, at high oxygen pressures, the chemical reaction at the surface became rate controlling. Similarly, in the leaching of

pentlandite in ammonium hydroxide solution, Forward and Mackiw, (31) found that in the initial stages, the concentration of oxygen in solution became depleted and the leaching rate was determined by the dissolution of oxygen from the gas phase. In the early stages, fresh reaction sites were abundant so that there was a high oxygen requirement for sulphide oxidation and for the oxidation of intermediate sulphide products to sulphate and sulphamate. In the later stages, the oxygen demand was less and the oxygen pressure was superceded as the rate controlling factor with the build up of an insoluble iron oxide coating and the diffusion control of reactants through it.

In the sodium hydroxide leaching of arsenopyrite, Plaskin and Masurova, (60) found that increments of oxygen pressures up to 10 atm. promoted reaction but had little effect at higher concentrations. This was also attributed to the physical transport of oxygen molecules to the mineral surface owing to the high rate of reaction. (The reaction was virtually complete in 1 hr at 150°C.)

The rate controlling step has been reported as various functions of the oxygen partial pressure but there is lack of correlation in some cases; e.g. Warren (74) found that the reaction rate was proportional to the square root of the oxygen partial pressure in the sulphuric acid leaching of pyrite whereas Mackay and Halpern (50) found the rate to be directly proportional to the oxygen pressure. In the sulphuric acid leaching of

chalcopyrite, covellite, and chalcocite, Warren (73) found the rate to be dependent on oxygen partial pressure in moderate acidity, (4g H_2SO_4/l) and proportional to the square root of the oxygen pressure with higher oxygen pressures from 150 to 200 p.s.i. at high acidity (20g H_2SO_4/l) for chalcopyrite. In the sodium hydroxide leaching of pyrite, (Stenhouse and Armstrong) (69) and of galena, (Anderson et al) (1), the rate was proportional to the square root of the oxygen partial pressure and to a more complex power in the potassium hydroxide leaching of molybdenite, (Dresher et al) (22).

In the sodium (30) (51) and ammonium carbonate (44) leaching of Uraninite, the rate is determined by the chemical oxidation of the uranium in the mineral to Carnotite;

$$U_3O_8 + \tfrac{1}{2}O_2 = 3UO_3 \quad \ldots.(3)$$

this being the only hexavalent form of uranium soluble in carbonate solutions.

It is a well known fact that oxygen is essential in controlling the rate of reaction during the cyanidation of gold (76) (42) and silver ores (19). Tronev and Bondin (72) found that the rate of dissolution of gold increased directly with the oxygen partial pressure. Deitz and Halpern (19), in their study of the cyanide leaching of gold and silver,found that the rate of dissolution was controlled by the transport of the reactants to the metal surface.

With the minerals wolframite, (this work) and columbite (14) in alkaline solution, the presence of oxygen is essential in initiating

and maintaining reaction. Further increments above an initial low pressure do not promote reaction and, in fact may considerably suppress the reaction by oxidation of the insoluble oxide product to a form less pervious to reactant ions. This is attributed to the presence of a thin layer of ferric ions at the mineral-oxide interface which is necessary for the initiation and maintenance of the reaction by oxidation of the mineral. Oxygen, however, was not required in the overall reaction.

Oxygen was found to have a deleterious effect in the leaching of pyrolusite in ferric sulphate and sulphuric acid solutions (16), in which there was a reduction in reaction rate in the presence of oxygen. This was attributed to the competitive adsorption between various ions at active sites on the MnO_2 surface.

1.3.2. Oxidising agents.

Oxygen has been found to be a relatively weak oxidising agent compared with chloride, ferric ions, or manganese dioxide, (16) (71) and (24). Ferric ions as the chloride or sulphate, have been used by Gray (35) and Sullivan (70) to oxidise the copper sulphides, chalcocite, bornite, and covellite. They were found to have little effect on chalcopyrite and pyrite.

Manganese Dioxide is used extensively in the sulphuric acid leaching of uraninite (45). This produces a very high Fe^{+++} to Fe^{++} ratio and ensures good extractions in industrial practice :

$$2H_2SO_4 + 2FeSO_4 + MnO_2 = Fe_2(SO_4)_3 + MnSO_4 + 2H_2O \quad ..(4)$$

It was observed, in the leaching of sphalerite by Nelen and Sobol (56), that the rate increased with increase in copper ion concentration, the cupric ions providing a considerable catalytic effect. In the ammonia leaching of pentlandite (31), cupric salts in solution acted as oxidising catalysts in the conversion of the thiosulphate, to thionate ion. In the sodium hydroxide leaching of chromite (24) the reaction promoting influence of manganese dioxide was used to enhance the rate of mineral dissolution.

Chlorine has been used by Sherman and Strickland for studies of the mechanics of dissolution of pyrite (64) and galena (65). In the leaching of galena, the rate of reaction of chlorine in aqueous solutions was of first order and both sulphate and elemental sulphur were produced simultaneously, the overall reactions being :-

$$PbS + Cl_2 = Pb^{\bullet\bullet} + 2Cl' + S^{\circ} \quad \cdots(5)$$

$$\text{and } PbS + 4Cl_2 + 4H_2O = Pb^{\bullet\bullet} + 8Cl' + 8H^{\bullet} + SO_4'' \quad \cdots(6)$$

The reaction was transport controlled at temperatures above $45^{\circ}C$, and a feature of the production of sulphur was that, under certain conditions, its formation was of zero order with respect to chlorine concentration.

In the leaching of pyrite, only sulphate was produced by the action of aqueous chlorine solutions :-

$$2FeS_2 + 15Cl_2 + 16H_2O = 2Fe^{\bullet\bullet\bullet} + 30Cl' + 32H^{\bullet} + 4SO_4'' \quad \cdots(7)$$

Bryner and Anderson (12) and (2) have shown the interesting example of bacteria being used to oxidise ferrous to ferric ions. Molybdenite was oxidised by a sulphide oxidising autotrophic bacteria. Innoculation of this bacteria into the solution produced a seven fold increase in the rate of solution, but in the presence of pyrite, the molybdenite was oxidised 29 times more rapidly than the MoS_2 in the sterile control. This is a very slow process, 36% of the molybdenum having been dissolved from the ore in nine months compared with 55% in the presence of pyrite;

$$2FeSO_4 + H_2SO_4 + \tfrac{1}{2}O_2 \xrightarrow{\text{Bacteria}} Fe_2(SO_4)_3 + H_2O \quad ...(8)$$

In the leaching of pyrolusite (MnO_2) (71) pyrite was used to produce ferrous sulphate which was oxidised by reaction with the mineral and then reduced by further pyrite. In this continuous cycle, the iron was therefore alternately oxidised and reduced by pyrite and the reaction so maintained until all the pyrolusite had been digested. (i.e. 90% in 4 hours at 90°C.)

$$Fe^{\bullet\bullet} \underset{FeS_2}{\overset{MnO_2}{\rightleftharpoons}} Fe^{\bullet\bullet\bullet} \quad ....(9)$$

1.3.3. Leach solution concentration.

Many sulphides have been observed to go into solution in water alone although some minerals need moderate acidity or alkali concentration.

The alkali concentration usually plays a secondary role to the oxygen dissolved in the solution from the gaseous phase which is normally the rate controlling reactant. In the potassium hydroxide leaching of molybdenite (22), it was found that the rate increased with concentrations up to 1 N at temperatures from 112-156°. However, beyond this concentration up to 6 M, potassium hydroxide, there was a progressive decrease in rate, attributed to a combination of; reduced solubility of oxygen, change in activity coefficient of KOH,*, and a lowering of diffusion rate of oxygen in solution with increase in viscosity of the solution. In the sodium hydroxide leaching of galena (1) it was found that high stirring velocities and related oxygen supply from the gas phase became increasingly important with increase in alkali concentration, but, at low concentrations of sodium hydroxide, (0.5 M) it was found that changes in velocity of the stirrer had no effect.

---

* This is an incorrect assumption, since the activity coefficient has been found to increase substantially with increase of potassium hydroxide concentration.

In the ammonia leaching of sphalerite (56) it was found that the reaction rate increased with increase in ammonium hydroxide concentration and this was attributed to the fact that oxygen solubility increases with increase of NH_4OH concentration. Similarly in the leaching of copper (38) the rate becomes independent of the oxygen partial pressure and levels off at a value which depends on the concentration of ammonia.

In the sodium hydroxide leaching of arsenopyrite (60), it was found that increments in sodium hydroxide concentration up to 15% w/v improved the transfer of arsenic into solution at temperatures below 150°.

Stenhouse and Armstrong (69) observed that increases in sodium hydroxide concentration from 1 N to 2 N resulted in an increase in the rate of oxidation. This was not found to be the case in this work. (See fig. 2.). They attributed this increased rate of oxidation to reactions between the sodium hydroxide and silica in the ore.

When pyrite was leached in dilute sulphuric acid solution (50), it was found that increase of initial acid concentration from 0.0 to 0.15M had little effect on the rate of oxidation. Warren (74) similarly found little difference between values of pH from 3 to 1, the natural pH of the solution.

1.3.4. Effect of Temperature Change.

Poor correlation has been reached in the determination of activation energy, as shown in the values obtained for the leaching of pyrite in sulphuric acid solutions in the presence of oxygen. McKay and Halpern (50) obtained the value of 13.2 ± 2 kcal/mole at 100 - 130°, Cornelius and Woodcock (16) the value 18.5 in the temperature range of 130-165° and Warren (74) the value 20.0 in the range of 130-210°C.

Anderson et al (1) obtained the value of 6.3 kcal/mole for the leaching of galena in 0.5 N sodium hydroxide at 93-175° and Warren (73) found a number of values for experiments conducted in sulphuric acid medium, of various copper-bearing sulphide minerals; viz; 23.0 kcal/mole for chalcopyrite at 120-180°, 11.7 for covellite at 120-180° and the values 6.6 and 1.8 kcal/mole for the two stages of reaction of chalcocite at 100-200°. This indicated that in the first stage, the process of chalcocite dissolution, was heterogeneous at the surface of the mineral and it was suggested that diffusion of copper ions within the mineral lattice was rate controlling. The low temperature coefficient in the second stage was attributed to the stifling of reaction with molten elemental sulphur. (See also page 46)

In the leaching of galena in ammonium acetate solution, Seraphim and Samis (63), calculated the activation energy at

15.5 kcal/mole in the temperature range of 91-159°. In the leaching of uranium ores in carbonate solutions the value of 9.7 kcal/mole was obtained (30) in the range of 60-115°C, which was calculated as being a 50% increase in the rate of reaction per 10°C rise in temperature.

In the ammonia leaching of copper (38) the values obtained were 5.54 kcal/mole at high oxygen pressures and 1.33 at low oxygen pressures. The higher value was more consistent with a rate process controlled by a chemical reaction and the lower value indicated a diffusion or transport controlled rate.

In the acid chlorine leaching of galena, (65) the energy of activation was found to be 21 kcal/mole in the temperature range of 10-40°C and for pyrite (64), a value was found which indicated a diffusion controlled reaction, viz; 4.90 kcal/mole between 10° and 40°C (33).

1.3.5. Nature of the particle surface.

The apparent increase in particle surface area during leaching plays an important part in the rate of mineral dissolution. McKay and Halpern (50) found in the sulphuric acid leaching of pyrite, (which was allowed to decompose to the extent of 25-50%) a uniform rate of reaction per initial surface area. It might be

expected that the resulting reduction in size would be accompanied by a decrease in surface area which would lead to a progressive reduction in rate. The explanation given was that there was an accompanying increase in surface roughness which compensated for the reduction in macroscopic surface area, the effective area therefore remaining constant. Microscopic examination of some large pyrite crystals revealed a considerable degree of surface etching which provided support for the assumption that the surface area had remained constant within the range. The reaction rate was directly proportional to the surface area when no insoluble reaction products were formed on the surface of the mineral.

Cornelius and Woodcock (16) found that the observed rate of reaction for the oxidation of pyrite in acid solution remained constant until about 90% of the particles had been dissolved provided that a correction was made for the reduction in surface area by calculation from particle size measurements.

In the leaching of galena (1), large crystals of the mineral were polished so that accurate measurements could be made of the surface area. Calculations of the ~~specific~~ absolute reaction rate were therefore possible.

The penetration of reactants at relatively few active sites on pyrite, with resultant pit formation, was mentioned by Warren (74) and Cornelius (16). It was suggested that these

sites were possible where dislocations existed, the heterogeneous process occurring at a limited number of sites on the pyrite surface. On this basis they have suggested an electrochemical behaviour in reaction. However, judging from the surface appearance of the leached and unleached particles, it would appear that the pyrite existed initially in a finely crystalline state, in which case penetration at more reactive sites at the grain boundaries would have been expected to have taken place and would explain the irregular reaction at the exposed surface.

In the sodium hydroxide leaching of molybdenite, (22) it was suggested that reaction was concentrated at the edges of platelets in the mineral structure, the faces of these platelets being relatively stable. They assumed adsorption of oxygen and removal of MoS_2 in a series of steps. However, no visual examinations were made, this present work being the first in which polished sections of minerals after leaching have been examined.

1.4. Insoluble products of reactions.

1.4.1. Iron oxides or hydroxides.

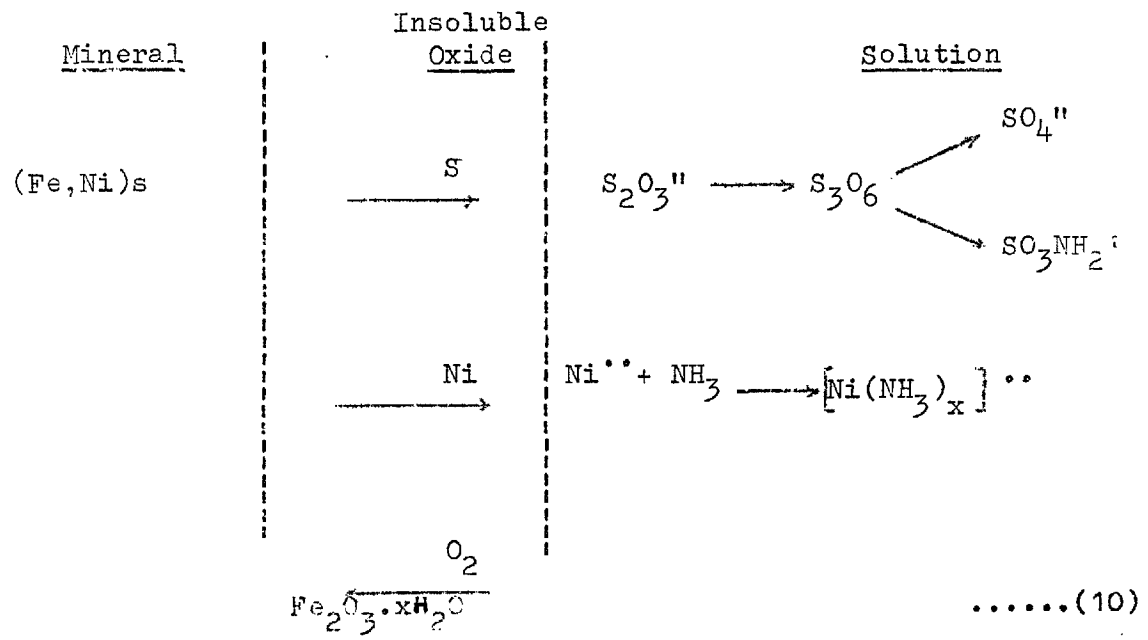
When iron bearing minerals are leached in alkaline solutions

insoluble iron oxides are formed as coatings pseudomorphic with the parent mineral. When this coating has attained sufficient thickness, the rate of diffusion of reactants through it becomes rate controlling and there is a parabolic decrease in the rate of mineral decomposition. In some cases, the product may become sufficiently impervious to stifle completely further dissolution of the mineral as was found with wolframite (this work) and by Burkin (14) in the potassium hydroxide leaching of columbite. Even with potassium hydroxide solution up to 10 N, the oxide was deposited pseudomorphically despite the tendency for increased solubility of iron oxides with ferroate formation (14).

Stenhouse and Armstrong (69), in the sodium hydroxide leaching of pyrite, suggested that iron was first formed in the ferrous state which was then oxidised and deposited in situ, with sulphur diffusing out as the positive ion and oxygen inwards to the mineral surface. They were unable to detect, by X-ray powder analysis the expected oxides Fe_2O_3 and Fe_3O_4. Warren (74) used this assumption to explain the behaviour of pyrite in acid solutions: Under conditions of high acidity (20g H_2SO_4/l) the iron appeared to leave the pyrite surface in the ferrous state, becoming oxidised in solution, and forming a precipitate by hydrolysis of the hydrated ferric oxide. However, when leached under conditions of low acidity (4 g H_2SO_4/l), the iron was thought

to oxidise at the pyrite surface, forming a film of oxide on the pyrite. The rate of oxidation of sulphur in the pyrite was then controlled by diffusion of sulphur through the oxide film.

Forward and Mackiw (31) suggested a similar behaviour in the ammonia leaching of pentlandite (chalcopyrite and pyrrhotite) in which nickel and sulphur ions diffused out and reacted with oxygen at the liquid-solid interface and oxygen diffused through the oxide to the mineral surface. Sulphur was not converted in a single step to sulphate ions but followed a series of reactions in which the first product was thiosulphate. This was further oxidised to thionate which, in turn was oxidised to sulphate and sulphamate;



.....(10)

These experiments were carried out at 40-100°C. Higher temperatures limited reaction with the increase of ammonia vapour

pressure and the promotion of hydrolysis. At the experimental temperature it was noted that pyrite did not react measurably and remained unaltered in the leach residue.

Warren (74) found that additions of calcium carbonate, used to raise the pH during leaching of pyrite, drastically curtailed the dissolution rate with the formation of an iron oxide film on the surface.

1.4.2. Elemental sulphur on sulphides.

The formation of a film of sulphur during leaching has been frequently suggested. In the leaching of galena with ammonium acetate solution (63) elemental sulphur formed as a coating and the diffusion controlling barrier resulted in the reaction being independent of both oxygen pressure and ammonium acetate concentration;

$$PbS + \tfrac{1}{2}O_2 + 2NH_4Ac = PbAc_2 + S^\circ + 2\,NH_3 + H_2O \quad \ldots(11)$$

Downes and Bruce (21) obtained elemental sulphur from pyrrhotite by treating aqueous suspensions of the mineral, having pH less than 1.5, with compressed air :

$$4FeS + 3O_2 = 2Fe_2O_3 + 4S^\circ \quad \ldots(12)$$

When carried out at temperatures above the melting point of sulphur (120°), the sulphur agglomerated into nodules which could be separated from the finely divided iron oxide by screening. This method was suggested as suitable for the industrial production of sulphur.

Warren (73) suggested that, in the leaching of chalcopyrite, covellite and chalcocite, a similar sulphur coating of the minerals occurred during leaching (100-200°). Trace quantities of sulphur were found after leaching in high acidity. Cementing of unreacted mineral particles with sulphur was common with chalcocite.

Warren further suggested (74) that sulphur was oxidised to the elemental form but was never of sufficient magnitude to account for the low predicted concentration in the presence of oxygen with pyrite leaching.

Sherman and Strickland (65) found that sulphur was produced on galena in acid chlorine solutions. From their observations, they concluded that, although all the galena surface could react with chlorine, only a comparatively small fraction, or a certain number of reactive sites, could give rise to sulphur formation. The sulphur thus produced inhibited the subsequent reaction at these sites, since the rate of sulphur production ceased at an early stage, although the rate of sulphate produced, was maintained.

1.4.3. Precipitation of insoluble products from solution.

The precipitation of products from the solution may stifle the

reaction, a notable example being given by the insoluble niobate, $NaNbO_3$ deposited on columbite in sodium hydroxide solutions (14) which completely stops reaction in the very early stages of dissolution. In potassium hydroxide solutions the niobate produced is much more soluble but was presumed to cause rate retarding effects at high temperatures (280°).

In the ammonia leaching of pentlandite (31), the presence of calcium was deleterious due to the tendency for deposition of insoluble calcium sulphate on the particle surfaces thereby obstructing access of oxygen. However when carbon dioxide was introduced into the leach solution calcium carbonate was precipitated which prevented this occurrence.

At temperatures greater than 150°, Plaskin and Masurova (60) in the sodium hydroxide leaching of arsenopyrite, found that arsenic and sulphur were precipitated. The pH influenced the equilibrium by the precipitation of iron arsenates at pHs less than 8.

1.5. Mechanisms of Reaction.

Reaction mechanisms will only be discussed briefly, most of the interpretation being provided by chemical equations.

1.5.1. Leaching of pyrite in sulphuric acid solution.

McKay and Halpern (50)

Two main reactions are :

$$2FeS_2 + 2O_2 = FeSO_4 + S \quad \ldots.(13)$$

$$\text{and } 2FeS_2 + 7O_2 + 2H_2O = 2\,FeSO_4 + H_2SO_4 \quad \ldots.(14)$$

The rate controlling step involves, at the surface, only an oxygen molecule. This is supported by the observation that the rate is of first order in oxygen and independent of solution composition.

Therefore reactions are represented by ;

$$FeS_2 + H_2SO_4 = FeSO_4 + H_2S + S \quad \ldots(15)$$

$$2H_2S + O_2 = 2H_2O + 2\,S \quad \ldots(16)$$

$$\text{and } H_2S + 2O_2 = H_2SO_4 \quad \ldots(17)$$

Ferric sulphate contributes to the oxidation of pyrite and

hydrogen sulphide by ;

$$FeS_2 + 8Fe(SO_4)_{1.5} + 4H_2O = 9FeSO_4 + 4H_2SO_4 + S \quad .. (18)$$

$$FeS_2 + 14Fe(SO_4)_{1.5} + 8H_2O = 15FeSO_4 + 8H_2SO_4 \quad .. (19)$$

$$H_2S + 2Fe(SO_4)_{1.5} = 2FeSO_4 + H_2SO_4 + S \quad .. (20)$$

$$H_2S + 8Fe(SO_4)_{1.5} + 4H_2O = 8FeSO_4 + 5H_2SO_4 \quad .. (21)$$

The formation of sulphur is favoured by high acidity and low temperatures and conversely, low acidity and high temperatures favoured formation of sulphuric acid.

Therefore the reaction of pyrite occurs predominantly by equation (13) leading to $FeSO_4$ and S°

Thus;

a) oxygen is chemisorbed on pyrite producing a monolayer comprising one oxygen molecule at each FeS_2 site;

$$FeS_2 + O_{2aq} \xrightarrow{\text{fast}} FeS_2 \cdot O_2 \quad .. (22)$$

b) the slow step in the reaction is the attachment of a seconnd oxygen molecule on an oxygen covered site;

$$FeS_2 \cdot O_2 + O_{2(aq)} \overset{\text{slow}}{=} [FeS_2 \cdot 2O_2] = FeSO_4 + S^\circ \quad \cdot (23)$$

activated complex

Elemental sulphur, once formed, is oxidised by oxygen or ferric ions;

$$2S^{o} + 3O_2 + 2H_2O = 2H_2SO_4 \quad ...(24)$$

and $$S^{o} + 6Fe(SO_4)_{1.5} + 4H_2O = 6FeSO_4 + 4H_2SO_4 \quad .(25)$$

1.5.2. Leaching of pentlandite in ammonia solutions.

Forward and Mackiw (31)

The mechanism of diffusion through the insoluble coating has been explained. (Page 20)

The following reactions take place in sequence, although, at any given time all are in progress simultaneously.

i) Heterogeneous:

$$NiS:FeS + 3FeS + 7O_2 + 10NH_3 + 4H_2O = Ni(NH_3)_6SO_4 + 2Fe_2O_3 \cdot H_2O + 2(NH_4)_2S_2O_3. \quad .(26)$$

ii) Homogeneous :

$$2(NH_4)_2S_2O_3 + 2O_2 = (NH_4)_2S_3O_6 + (NH_4)_2SO_4. \quad ...(27)$$

$$(NH_4)_2S_3O_6 + 2O_2 + 4NH_3 + H_2O = NH_4SO_3.NH_2 + 2(NH_4)_2SO_4. \quad ...(28)$$

1.5.3. Leaching of Galena in sodium hydroxide solution.

Anderson, Halpern and Samis (1)

The overall reaction is;

$$PbS + 2O_2 + 3OH^- = SO_4^{--} + HPbO_2^- + H_2O \quad ..(29)$$

Proposed stages involving adsorption and dissociation are :

$$PbS + \tfrac{1}{2}O_{2aq} \underset{\leftarrow}{\overset{\text{fast}}{\rightleftharpoons}} Pb\begin{smallmatrix}O\\ \diagdown\ \diagup\\ -\ S\end{smallmatrix} \quad ...(30)$$

$$Pb\begin{smallmatrix}O\\ \diagdown\ \diagup\\ -\ S\end{smallmatrix} + H_2O \xrightarrow{\text{slow}} \text{activated complex} \longrightarrow Pb\begin{smallmatrix}OH\ OH\\ |\ \ |\\ -S\end{smallmatrix} \quad ..(31)$$

$$Pb\begin{smallmatrix}OH\ OH\\ |\ \ |\\ -S\end{smallmatrix} + 1\tfrac{1}{2}O_{2aq} + 3OH^- \xrightarrow{\text{fast}} SO_4^{--} + HPbO_2^- + 2H_2O \quad ..(32)$$

1.5.4. Leaching of molybdenite in potassium hydroxide solution.

Dresher, Wadsworth and Fassell (22)

The overall reaction is ;

$$MoS_2 + 4\tfrac{1}{2}O_2 + 6OH^- \longrightarrow MoO_4^{--} + 2SO_4^{--} + 3H_2O \quad ...(33)$$

Proposed stages involving adsorption and dissociation are :-

$$MoS_2 + O_2 \xrightarrow{\text{fast}} MoS_2...O \qquad ...(34)$$

$$MoS_2...O_2 + O_2 \underset{\leftarrow}{\overset{\text{slow}}{\rightarrow}} MoS_2...2O_2 \qquad ...(35)$$

$$MoS_2...2O_2 \xrightarrow{\text{slow}} [MoS_2...2O_2] \qquad ...(36)$$

activated complex

$$[MoS_2...2O_2] + OH' \xrightarrow{\text{fast}} MoO_2(OH)^{\bullet} + S_2O_2'' \qquad ...(37)$$

activated complex

$$MoO_2(OH)^{\bullet} + OH' \xrightarrow{\text{fast}} MoO_4'' + 2H^{\bullet} \qquad ...(38)$$

$$H^{\bullet} + OH' \xrightarrow{\text{fast}} H_2O \qquad ...(39)$$

$$S_2O_2'' + \tfrac{1}{2}O_2 \xrightarrow{\text{fast}} S_2O_3'' \qquad ...(40)$$

The thionates cannot exist for any appreciable time in alkaline solutions in the absence of ammonia ions due to their decomposition by hydroxyl ion to thiosulphate.

1.5.5. Leaching of pyrolusite using pyrite as reagent.

Cornelius and Woodcock (16).

The pyrite reacts with oxygen to give ferrous sulphate which decomposes the manganese dioxide. The overall reaction is :

$$4MnO_2 + 4FeS_2 + 13O_2 + 4H_2O = 4MnSO_4 + 4H_2SO_4 + 2Fe_2O_3 \quad ..(41)$$

The oxidation of pyrite has been dealt with (Page 24)

MnO_2 is decomposed according to the reactions ;

$$4Fe^{\bullet\bullet} + O_2 + 4H^{\bullet} = 4Fe^{\bullet\bullet\bullet} + 2H_2O \quad ...(42)$$

The ferric ion hydrolyses;

$$2Fe^{\bullet\bullet\bullet} + 3H_2O = Fe_2O_3 + 6H^{\bullet} \quad ..(43)$$

The authors have proposed an electrochemical explanation for the dissolution of pyrolusite by ferrous ions, in which ferrous ions diffuse to the mineral surface, are adsorbed, and diffuse across the surface to an active site where they give up electrons to form

ferric ions which desorb and diffuse into the bulk solution phase. At the same time electrons are transferred through the semiconducting MnO_2 lattice and liberate manganous ions from the lattice.

1.5.6. Leaching of uraninite using pyrite as reagent.

Forward and Halpern (29).

Pyrite was used to generate sulphuric acid in the presence of oxygen.

The oxidation of pyrite has been dealt with above. (Page 24) The ferric salts are hydrolysed because of the high temperature and low acidity and the minerals are attacked and dissolved by the sulphuric acid solution ;

$$U_3O_8 + \tfrac{1}{2}O_2 + 3H_2SO_4 = 3UO_2SO_4 + 3H_2O \quad ..(44)$$

1.5.7. Leaching of uraninite in sodium carbonate solution.

Forward, Halpern and Peters (30)

As mentioned earlier, (page 9) uranium will not react in carbonate solution until the uraninite has been oxidised to the mineral carnotite ;

$$U_3O_8 + \tfrac{1}{2}O_2 = 3UO_3 \quad ..(45)$$

the overall reaction is ;

$$U_3O_8 + \tfrac{1}{2}O_2 + 9CO_3'' + 3H_2O = 3UO_2(CO_3)_3'''' + 6OH' \quad ..(46)$$

The OH' ion may result in reprecipitation of uranium as sodium uranate ;

$$UO_2(CO_3)_3'''' + 4OH' + 2Na^{\bullet} = Na_2UO_4 + 3CO_3'' + 2H_2O \quad ..(47)$$

which lowers efficiency. Therefore bicarbonate ions are introduced which react with the hydroxyl ions ;

$$U_3O_8 + \tfrac{1}{2}O_2 + 3CO_3'' + 6HCO_3' = 3UO_2(CO_3)_3'''' + 3H_2O \quad ..(48)$$

The sodium carbonate leach process, in practise, does not yield as high an extraction of uranium as the acid leach and is not attractive for economic reasons when treating ores that are high in sulphates or sulphides.

1.5.8. Leaching of copper in ammonium hydroxide solution.

Halpern (38).

Two reactions take place simultaneously. Both are first order with respect to concentrations of NH_3 and NH_4^+ resp., and independent of oxygen concentration when present in excess.

Step i) Adsorption of dissolved oxygen on copper

$$Cu + \tfrac{1}{2}O_2 \xrightarrow{\text{fast}} Cu...O \qquad \ldots (49)$$

ii) Reaction of NH_3 molecule or NH_4^+ ion with the Cu...O complex ;

$$Cu...O + NH_3 \xrightarrow{\text{slow}} \left[{}^{++}Cu \begin{matrix} NH_3 \\ O'' \end{matrix} \right] + HOH \xrightarrow{\text{fast}} Cu(NH_3)^{++} + 2OH^- \qquad (50)$$

activated complex

or ;

$$Cu...O + NH_4^+ \xrightarrow{\text{slow}} \left[{}^{++}Cu \begin{matrix} NH_3 \\ H \\ O' \end{matrix} \right] + OH^- \xrightarrow{\text{fast}} Cu(NH_3)^{++} + 2OH^- \qquad (51)$$

It was considered likely that, in the presence of excess oxygen at the surface, such as was maintained in the system, oxidation to the cupric state would occur at the surface and the copper would dissolve in the first instance as the cupric ion.

Comprehensive Reviews of hydrometallurgical processes have been given by Halpern and Forward (39) and Woodcock (78).

1.6. Review of Topotactic Transformations.

An insoluble product of reaction may be formed by the decomposition of a solid by; a) " do novo " recrystallisation independent of the initial solid or b) topotactically. This latter kind of solid state transformation takes place during reaction when the crystal structure of the reaction product conforms with that of the original crystalline solid. The structure and crystalline orientation of the original solid controls the orientation and even the nature of the products. These reactions frequently give rise to compounds which cannot be obtained at all by other methods such as analogous reactions in the gas phase or in solution.

A topotactic product is therefore distinct from a pseudomorphic

one in which a crystal may become converted into another solid substance without change in its external form. The crystal structure of this product however, may be quite independent of the structure of the parent mineral. Thus a pseudomorphic casting need only be topotactic in a restricted number of cases. An epitaxial transformation is one in which the products grow on the surface of the host mineral in certain definite orientations although the host need not be a reactant or chemically related to the overgrowth.

The term "topotaxy" has only recently been used, (61), (48). Lotgering defined the term as "all chemical solid state reactions that lead to a material with crystalline orientations which are correlated with crystal orientations of the initial material." Bernal et al (9) have since defined topotaxy more narrowly to cover transformations in which the majority of the atomic positions in the original and in the transformed material are substantially the same and there is accord in three dimensions between the initial and the final lattices. This name is due to Dr. E.W. Gorter (9) and is derived from the Greek, "topos" - place and "taxis" - arrangement, and has only been generally used in the last four years though transformations of this nature have been suggested by various workers in the last forty years.

Factors which may influence the degree of orientation in any particular reaction include; temperature, pressure, physical state, specific experimental conditions such as the time and rate

of heating and the sizes and electronegativities of the cations which frequently decide which ions move in the lattice. With small cations such as $Mg^{\bullet\bullet}$, $Al^{\bullet\bullet\bullet}$, $Fe^{\bullet\bullet\bullet}$, $Si^{\bullet\bullet\bullet\bullet}$, the oxygen framework may be maintained, change taking place by regrouping of cations in the lattice so that the number of oxygen atoms per unit volume will not be appreciably changed. However the oxygen packing may change, as has been found with $Mg^{\bullet\bullet}$, and less readily with $Al^{\bullet\bullet\bullet}$ and $Fe^{\bullet\bullet\bullet}$, in transformations from a cubic close packed lattice to a hexagonal close packed lattice.

1.6.1. Iron oxides and Hydroxides.

In early works, Gruner (37) and Greig et al (36) studied the transformations in magnetite under oxidising conditions. Haematite was formed as needles conforming with the octahedral planes of the magnetite, giving rise to intersecting lamellae of hematite in the magnetite. Gruner (37) found that the lines of hematite became progressively thicker and would have covered the whole surface if left at high temperature (ca 1000°C.) for a sufficiently long time. There was no hematite formation at any areas around the magnetite unless the contact was an octahedral plane, when a fine line of hematite at the contact was produced. Thus the hematite forms as exsolution lamellae, orientated so as to allow the best possible fit between the close packed oxygen planes of the magnetite and the

Table I.

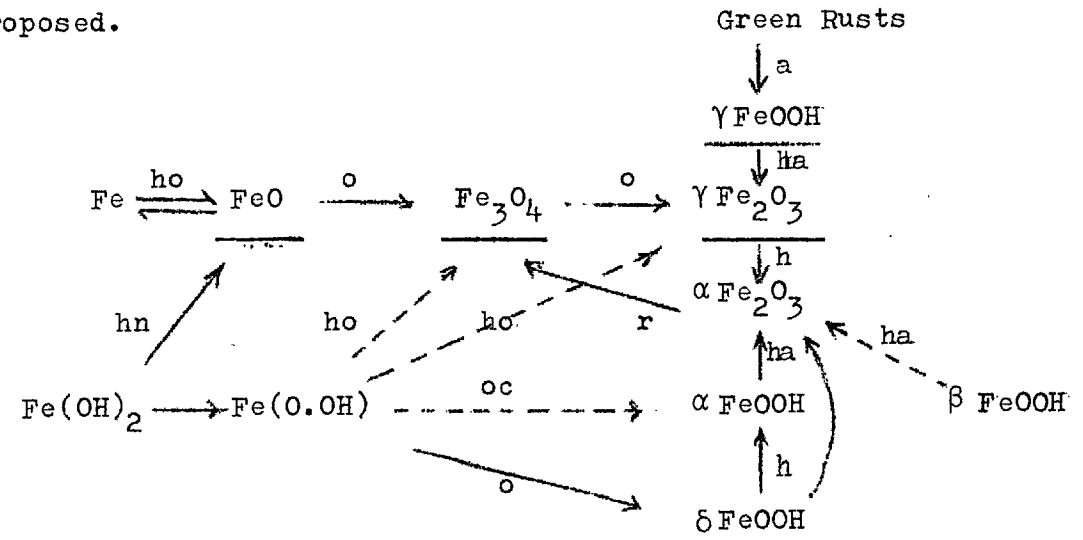
Crystal Structures of oxides and hydroxides of iron (9)

Composition	Mineral Name.	Unit Cell Dimensions A.	Z	Notes.
α -Fe_2O_3	Hematite	a= 5.0345 c= 13.749	6 (hex)	H.C.P. Oxygen with Fe^{***} in oct.positions.
Fe_3O_4	Magnetite	a= 8.3963	8	Inverse Spinel Fe^{***}-tet.Fe^{***}+Fe^{**}- oct. O_4
γ-Fe_2O_3	Maghemite	a= 8.338	$10\frac{2}{3}$	Spinel-various degrees of ordering
FeO	Wustite	a= 4.302 -high Fe a= 4.275 -low Fe	4	NaCl Type.
	or	a= 6.04 c= 8.54	16	Tet. Martensite transformation
α -FeOOH	Goethite	a= 4.587 b= 9.937 c= 3.015	4	H.C.P. oxygen
β -FeOOH	-	a=10.48 c= 3.06	8	-MnO_2 structure ?
γ -FeOOH	Lepidocrocite	a= 3.87 b=12.51 c= 3.06	4	C.C.P. oxygen
δ -FeOOH	-	a= 2.941 c= 4.58	1	M.C.P. Oxygen-disordered CdI_2 struct.
$Fe(OH)_2$	-	a= 3.262 c= 4.596	1	CdI_2 structure.
$FeCO_3$	Chalybite	a= 4.711 c=15.436	2 6 (hex)	Calcite structure.

sharing of atoms common to both solids.

Bernal et al. (8) studied in detail the orientated transformations in iron oxides and hydroxides. They have shown that transformations from tetragonal lepidocrocite, γFeOOH through maghemite, γFe_2O_3 to hematite, αFe_2O_3, take place, the transformation from maghemite suggesting that this does not include any loss of material but only a restacking of the hexagonally close packed atoms on the 111 faces of the maghemite. A similar relation to the above structural change was observed by X-rays for the magnetite, (Fe_3O_4)-ilmenite, ($FeTiO_3$) transformation, the ilmenite being isostructural with hematite. This occurs in natural titaniferous magnetite systems with ilmenite crystals orientated in relation to magnetite with the 0001 ilmenite axis parallel to the 111 axis of the magnetite.

More recent studies by Bernal et al. (9) (17) (49) show an examination particularly of the oxyhydroxides βFeOOH and δFeOOH The topotactic transformations FeCO to FeO and $Fe(OH)_2$ to FeO are reported (9). The following sequence of topotactic transformations was proposed.

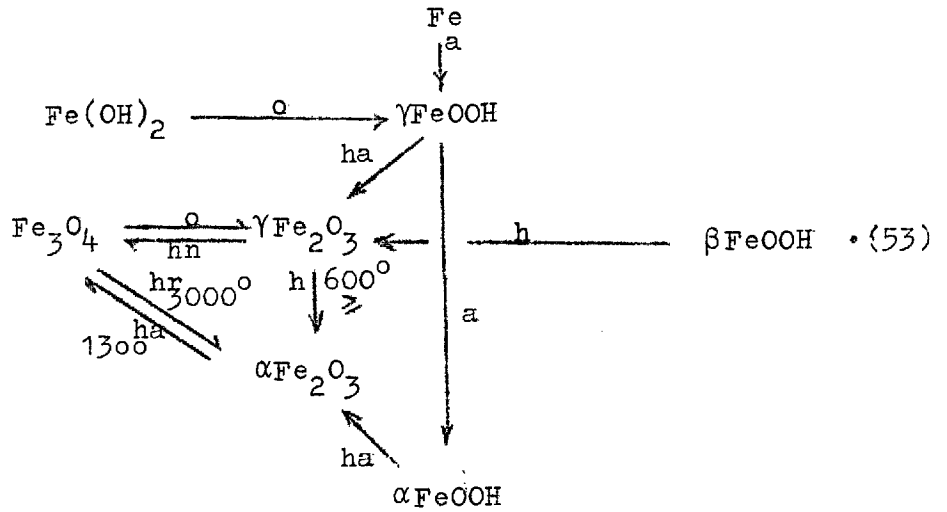


....(52)

The underlined compounds have oxygen atoms in a cubic close packed and the rest in a hexagonal close packed configuration except for β FeOOH, which is of a more complex nature. The broken lines indicate non-topotactic transformations.

This is somewhat different from the sequence mentioned by Wells (75).

No distinction was made between recrystallised and topotactically deposited compounds :



KEY:

h = heating
a = atmospheric oxidation
c = in alkali
n = in nitrogen or in vaccuo
o = on oxidation
r = on reduction

Bernal et al found that $Fe(OH)_2$ is surprisingly stable though extremely sensitive to water and the structure could be maintained

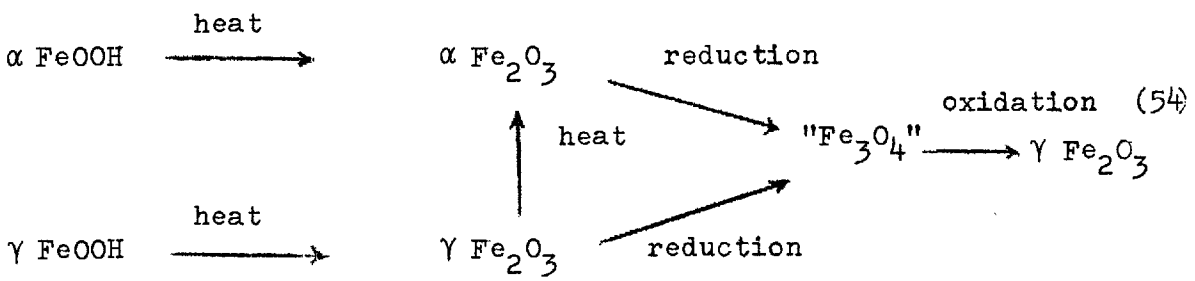
until ca20% of ferric ions was present in the lattice. It could then transform with dehydration to either Fe_3O_4 or topotactically by disproportion to FeO. $Fe(OH)_2$ was oxidised in strong alkali to give αFeOOH but was never found to form γFeOOH. δ FeOOH was produced from $Fe(OH)_2$ by very rapid oxidation with excess hydrogen peroxide or ammonium persulphate. It was brown and strongly magnetic and began to transform to αFe_2O_3 at temperatures greater than 130°, the reaction being complete at 200°. αFe_2O_3 could then be reduced at 200° to give magnetite, and ferrite, α Fe. Cubic maghemite could be produced by the oxidation of $Fe(OH)_2$ with dilute peroxide or ammonium persulphate and could also be made by dehydrating lepidocrocite. In an earlier study of the oxidation of ferrous hydroxide, Mayne (52) found that oxidation of $Fe(OH)_2$ in weak acid solutions (pH 4-5) gave γ FeOOH irrespective of the rate of oxidation, and in alkaline solutions, αFeOOH with rapid oxidation and a compound of composition intermediate between Fe_3O_4 and γFe_2O_3 when the rate of oxidation was slow. He suggested that, when oxidation was slow, the FeOOH first formed, interacted with the remaining $Fe(OH)_2$ to form magnetite.

FeO could be produced from the $FeCO_3$ lattice by expulsion of carbon dioxide and change of the angles between the sheets of ions from 72° to 90°, i.e. a change from the rhombohedral to cubic structure. (9). It was remarkable that, despite the loss of more than half the oxygen atoms, the orientation of the lattice was still preserved and

and it was assumed that the thermal vibrations at this temperature were not sufficiently large to cause complete disorganisation of the lattice. The only reactions which were not topotactic were the changes from β FeOOH to αFe_2O_3, $Fe(OH)_2$ to α FeOOH, and $Fe(OH)_2$ to Fe_3O_4 and γFe_2O_3 which are all dissimilar in structure renucleation being necessary for the transformation process.

Feitknecht (26) has shown that δ FeOOH transforms topotactically to αFeOOH in 10 N sodium hydroxide at 70° but through solution to α-FeOOH in IN sodium hydroxide.

van Oosterhout. (57) found that the α FeOOH and γFeOOH Compounds could be transformed into γFe_2O_3 by the following processes :



(54)

in which the "Fe_3O_4" symbolises a ferrous ferric oxide having a spinel lattice but not exactly the composition of Fe_3O_4 being more a disordered maghemite than magnetite.

Mackay (49) has reported that the tetragonal β FeOOH can transform when heated in the beam of the electron microscope to the spinel

structure, presumably γFe_2O_3, by the migration of iron atoms to tetrahedral sites. There was an accompanied expansion of the O-O distance from 3.49 to 4.77 A in one direction and a contraction from 3.49 to 2.95 A in a perpendicular direction.

The systems have been represented in the following equations, which include the relation between the oxygen atoms in the crystal lattice of the host mineral and the product ;

$$\alpha \text{ FeOOH } (0001)\ (10\bar{1}0) \longrightarrow Fe_3O_4\ (111)\ (1\bar{1}0). \qquad (55)$$

and

$$\gamma \text{ FeOOH } (100)\ (001) \longrightarrow \gamma Fe_2O_3\ (001)\ (110) \qquad (56)$$

in which case the FeO_2 chain direction becomes the 110 direction of the spinel structure. Electron diffraction patterns of maghemite prepared from lepidocrocite by reduction and oxidation are shown (57) in which very weak spots were found which indicated an a:c ratio of 3 in the tetragonal superstructure.

Normally, wüstite, FeO has a number of $Fe^{\bullet\bullet}$ sites vacant so that the stoichiometric composition of FeO is never obtained, (75), (79) Wyckoff has shown that when FeO is heated in excess iron and quenched from a series of temperatures, the lattice parameter is greater the higher the quenching temperature, i.e. at elevated temperatures iron dissolves in and swells the FeO structure so that it represents an attempt to complete the lattice by approaching the 1:1 composition ratio .

Bernal et al. (8) have mentioned that the iron oxides and hydroxides, all have oxygen atoms in cubic close packed or hexagonal

close packed configuration except for β FeOOH. They predicted that whenever powder photographs indicate two series of transformations of the same chemical compound leading to different end products, that topotactic or epitaxial types of transformation were involved.

Until recently it was reported that transformations from maghemite to hematite were irreversible (54). However, Finch and Sinha (27) in electron diffraction studies, contended that the α to γ transformation was a necessary step preceding the solid state spinelisation reaction involving the formation of ferrospinel and, at 900°, the surface crystallites of maghemite were observed. They suggested that the basal plane of the hexagonal close packed lattice was equivalent in packing to the 111 plane of the cubic close packed lattice, with epitaxial growth of maghemite in two degree 111 orientation on the cubic close packed lattice on the hematite basal plane. They mentioned the existence of a βFe_2O_3 phase intermediate between maghemite and hematite, being a defect α phase and possibly the cause of an unusual magnetic behaviour of the hematite.

1.6.2. Aluminium oxides and hydroxides.

Aluminium behaves in a somewhat similar manner to iron, by forming a related series of oxides and oxyhydroxides. Francombe

and Rooksby (32) and Rooksby and Rooymans (32) (62) showed that the decomposition of bayerite, $Al(OH)_3$ and boehmite AlOOH, lead to metastable aluminas before transformation to corundum, $\alpha\ Al_2O_3$, finally occurs.

Brindley and Choe (11) gave the following series of reactions depending on experimental conditions;

$$\begin{array}{l} Al(OH)_3 \text{ gibbsite} \longrightarrow \chi\, Al_2O_3 \longrightarrow \kappa\, Al_2O_3 \longrightarrow \alpha\ Al_2O_3 \qquad (57) \\ \qquad\searrow \\ \quad AlOOH \text{ boehmite} \longrightarrow \gamma\ Al_2O_3 \longrightarrow \theta\, Al_2O_3 \rightarrow \alpha\, Al_2O_3. \\ \qquad\qquad\qquad\qquad\qquad\qquad\qquad\qquad\qquad\qquad\qquad\qquad \text{corundum} \end{array}$$

in which boehmite and gamma alumina have oxygen atoms in cubic close packed configuration, and in corundum, hexagonal close packed configuration. There was a progressive reduction in unit cell size from 2.88 for gibbsite to 2.81 for $\theta\, Al_2O_3$

Ervin (23) suggested the concept of structural continuity in relation to the numerous intermediate products formed when gibbsite and other aluminas are converted to the final stable alpha alumina, corundum.

1.6.3. Manganese oxides and hydroxides.

Faulring et al (25) showed the relative orientations of manganese oxides parallel to the 001 axis of cryptomelane ;

$$KMn_8O_{16} \longrightarrow \begin{matrix}(110)\\(100)\\Mn_2O_3\end{matrix} \longrightarrow \begin{matrix}(100)\\Mn_3O_4\end{matrix} \longrightarrow \begin{matrix}(1\bar{1}0)\\Mn_3O_4\end{matrix} \quad \ldots(58)$$

Cryptomelane Hausmannite, Spinel

Thermogravimetric examination indicated that the Mn_3O_4 phase forms from the Mn_2O_3 phase, the critical temperature for formation of Mn_2O_3 from cryptomelane needles being ca600°, for Mn_3O_4 ca825°, and, for spinel, 1050°. The naturally occurring cryptomelane always contains potassium, but manganese oxides having X-ray diffraction patterns like those of cryptomelane can be produced in the absence of potassium.

Topotactic transformations appear to have taken place in the series of transformations (7)

$$Mn(OH)_2 \longrightarrow MnOOH \longrightarrow MnO_2 \quad \ldots\ldots(59)$$

1.6.4. Removal of atoms from crystal lattice.

A few examples of the topotactic reduction of oxides to metals are mentioned. Goswami and Trehan (34) showed that cuprite, (Cu_2O) could be reduced to copper. In the cubic Cu_2O lattice copper ions are at face centred positions and the oxygen ions at the body centred positions, each oxygen atom being surrounded tetragonally by copper ions. In copper, cubic system, the atoms also occupy face-centre positions. By removal of oxygen, the compound transformed to copper, with a progressive reduction in cell size from 4.252A to 3.608 A respectively. In monoclinic tenorite (CuO) each oxygen atom is surrounded by a distorted tetrahedron of copper ions and each copper, by a square of oxygen ions. In this case, the copper atoms were assumed to rearrange to the cubic face centred lattice from the distorted tetrahedral positions.

Piggot (59) obtained smooth surface crystals of copper with similar orientation to the original Cu_2O structure by reduction with atomic hydrogen produced from dry hydrogen.

Ball and Taylor (6), in the dehydration of brucite, $(Mg,Fe)(OH)_2$, assumed cation migration and the occurrence of the spinel-like phase, periclase MgO. They postulated that the crystal developed donor and acceptor regions, the acceptor regions being converted to periclase, by gain of cations and the loss of protons, and the donor regions, which were completely destroyed, became the pores that were shown to

exist in the pseudomorph. This transformation indicated a change in oxygen atom configuration from the hexagonal close packed configuration to the cubic close packed configuration. It was further postulated that a spinel-like intermediate hypothetical stage was needed having the formula, $Mg_3O_4H_2$, through which the donor regions pass and that this was where the spinel-like structure began to appear.

Liebau et al (47) found that elemental silver was produced topotactically from the silicate, $Ag_2Si_2O_5$ by reduction in the presence of sodium silicate and silver nitrate at 280°.

Numerous other examples are cited, particularly transformations of naturally occurring silicates, in a concise review by Dent-Glasser, et al (20).

1.7. Topotactic Transformations in Hydrometallurgy.

This form of transformation has not previously been reported in hydrometallurgical systems though it is possible that the process mentioned below took place in such a manner.

In the acid leaching of chalcocite using ferric sulphate, Sullivan (70), in 1933, found that the reaction proceeded in two stages: He observed that the particles retained the original

outline of the unleached mineral throughout the process with production of the intermediate product, CuS, and the ultimate complete removal of the copper atoms and the retention of elemental sulphur. (Experiments were carried out at 35°C.) Reactions were :

$$Cu_2S + Fe_2(SO_4)_3 = CuS + CuSO_4 + 2FeSO_4 \quad ...(60)$$

and

$$CuS + Fe_2(SO_4)_3 = CuSO_4 + 2FeSO_4 + S^o \quad ...(61)$$

The intermediate CuS did not resemble the common form of the naturally occurring mineral, covellite, (CuS) and it is suggested that the mineral had undergone a series of topotactic transformations from Cu_2S to CuS to S. Warren (73) has shown two distinct rate processes during the sulphuric acid leaching of chalcocite indicative of the two successive stages in the reaction.

Burkin has recently suggested (13) that, in the leaching of columbite and chromite, in potassium and sodium hydroxide solutions respectively, the oxidation product goes through a series of topotactic transformations the inverse spinel structure of the chromite altering to the similar structure of magnetite.

SECTION 2.

GEOLOGY OF WOLFRAMITE AND PYRITE.

2.1. Pyrite.

2.1.1. General.

Pyrite belongs to the cubic system of minerals having the sodium chloride structure with cell edge a = 5.42A, and four formula units per unit cell, (18) (79). The iron atoms are at the corners and face centres of the cube and the S_2 atoms in homopolar bonding centred at the midpoints of the cube edges and the cube's body centre. The four S-S bonds are respectively parallel to four non-intersecting body diagonal directions.

Each iron atom is surrounded by six sulphur atoms at the corners of an octahedron and each sulphur atom is equidistant from three iron atoms forming a triangular planar group to one side of it, i.e. each S-S pair may be considered to be in close packed cubic arrangement with an iron atom in each of the octahedral holes.

The interatomic distances are given as, S-S = 2.14 A and S-Fe = 2.26 A (58) and, assuming ideal chemical composition, the density

has been determined as 5.012 g/cc.

Small variations in the cell edge may be due to either diminution in specimens with low sulphur, or to the presence of atoms other than iron and sulphur, such as substitution by nickel atoms for iron, which shows an increase in cell size. There is invariably a departure from the ideal formula, FeS_2 which usually seems to be in the direction towards a deficiency in sulphur, the value varying from $FeS_{2.01}$ to $FeS_{1.93}$. Iron has been assumed to take the place of some sulphur in such crystals so affecting the lattice dimensions and probably also its symmetry (67). Smith showed that variables in composition seemed to affect the conductivity of pyrite so that, the lower the sulphur of the pyrite, the lower was the resistance. This was attributed to iron replacement of some sulphur deficient areas so that, when this occurred the mineral was much more "metallic" in character than the iron-sulphur linkage. The other alternative is that the structure has sulphur sites vacant.

Kullerud and Yoder (43) believed on the basis of present analyses and cell measurements, that pyrite has a metal to sulphur ratio of 1:2.00, within the limits of experimental error.

The presence of minor elements other than sulphur and iron has frequently been reported (28), but these minerals are more frequently present as impurities such as copper in chalcopyrite, lead in galena, arsenic in arsenopyrite and zinc in sphalerite. In this work, an X-ray Microscan analysis of the Rio Tinto pyrite, (which indicated appreciable proportions, (ca8%) of the elements Cu,Pb,As, and Zn,)

showed these elements to be absent in the pyrite mineral. These impurities were present as the corresponding sulphide minerals mentioned above, occurring as very small grains associated with the pyrite. Similarly, a considerable variation in sulphur across an apparently uniform particle of pyrite showed that a sulphur deficiency is not uniformly prevalent throughout a crystal but shows a definite gradation across its surface. However, little change in iron variation was found to compensate completely for the sulphur deficiency despite the fact that all other elements (heavier than aluminium) were absent. It is suggested therefore, that, with the possible retention of the iron atomic lattice despite sulphur deficiency, the iron X-ray emission from the surface had not increased substantially.

The Rio Tinto ore body is known to contain appreciable amounts of arsenic. In considering the solubility of arsenic in pyrite, Fleischer mentioned that pyrite had been observed to contain up to 5% arsenic, the mineral then having a unit cell structure with $a = 5.44$ A.

It is possible that very small amounts of the above mentioned elements may be present in solid solution. On the other hand, when elements have related properties and atomic structures, their corresponding sulphide, MS_2, may be isostructural with pyrite and could replace iron from the lattice, e.g. nickel, cobalt, and manganese to a very limited extent. The mineral, bravoite is a

derivative of pyrite containing large amounts of nickel and cobalt.

The stability relations of pyrite in the iron-sulphur system have been studied, (43) and (3). In the phase diagram, pyrrhotite in equilibrium shows an increasing iron deficiency with increase in temperature, while the pyrite remains constant, being stable up to 743°C.

Pyrite is by far the most widespread and commonly occurring of the sulphide minerals (10) and may be found in almost every type of geological environment e.g. as a primary crystallisation from both acidic and basic magmas, as a magmatic segregation from igneous rocks, in contact metamorphic deposits (Premier), in hydrothermal sulphide veins (Cassandra) and (Rio Tinto), as a sublimation deposit, and in sedimentary rocks, principally argillaceous and carbonaceous. Pyrite is rarely of economic importance but is used, to a large extent, in the production of sulphuric acid either by roasting to liberate sulphur dioxide, or in the decomposition to pyrrhotite and liberation of elemental sulphur. (21)

2.1.2. Minerals Used.

In this work, pyrite from three geological sources has been studied :

a) Rio Tinto (Spain)

The sulphide deposits in the Rio Tinto ore body are most probably of hydrothermal origin though there are many conflicting views held as to the mode of formation. Pyrite is the most important sulphide. Arsenic is always present as an impurity and the minerals, galena, arsenopyrite, sphalerite and chalcopyrite are intimately associated with the mineral in a finely disseminated state.

b) Cassandra (Greece)

This deposit is also of hydrothermal origin (55), being derived from an intrusive acid granite, and was probably emplaced under mesothermal temperature conditions (175-300°) associated with marble. The chief minerals are pyrite, sphalerite and galena, which occur in lenticular veins and wall rock disseminations and are accompanied by minor quantities of marcasite, FeS_2 , Stibnite , Sb_2S_3 , Chalcopyrite, $CuFeS_2$,

arsenopyrite, FeAsS, tetrahedrite, Cu_3SbS_2, and boulangerite, $Pb_5Sb_4S_{11}$. Also reported are traces of the elements, Ag, Bi, Mo, Se, Ga, and Ge. In this work, large well-formed crystals (1 cm) of very high purity were used, containing only trace quantities of the elements, zinc and lead.

c) Premier (South Africa)

In this deposit (55), the pyrite is normally associated with basic intrusive dolerite which is replaced in a diamondiferous kimberlite pipe. The dolerite has caused extensive carbonatisation of the kimberlite and subsequent movement has caused the formation of numerous shears and joints which contain asbestos, pyrite, calcite and prehnite. The genetic aspects of the pyrite occurrence suggest that the pyrite has been formed from aqueous volatile phases associated with the dolerites as volcano-hydrothermal emanations. The mineral, either during, or after formation was subjected to high stress conditions so that a platy appearance has been imparted to the outer surface. In this work, the crystals used were also large and well-formed (1 cm)

and of very high pyrity with only a trace of nickel (observed by X-ray fluorescence examination), which is probably present as an substitional lattice replacement.

The geology demonstrates that the Cassandra pyrite owes its origin to acid intrusives and the Premier occurrence to the activity of basic intrusives.

2.2. Wolframite.

2.2.1. General.

Tungsten minerals can broadly be divided into two groups, viz; the wolframite group and the scheelite group (10) and (46).

The minerals of the wolframite group of economic importance are the tungstates of iron and manganese, and are graded according to the proportion of the one relative to the other. Wolframite is the most important mineral and is of intermediate composition ranging from 20 to 80 atomic percent of either metal. Ferberite, on the other hand, consists predominantly of iron tungstate, $FeWO_4$,

while Hübnerite is mainly the manganese tungstate, $MnWO_4$.

All these minerals belong to the monoclinic system, the WO_4" anionic group forming a distorted tetrahedron. The cell dimensions are a = 4.81, b = 5.73, c = 4.97 $\beta = 90^{\circ}49'$ with two formula units per unit cell. The dimensions are slightly larger for $MnWO_4$ and slightly smaller with $\beta = 90^{\circ}$ for $FeWO_4$. They exhibit a perfect cleavage in one direction, have specific gravities ranging from 7.1. to 7.5, a colour variation from dark grey to black, and have feebly magnetic properties.

The tungsten content of pure wolframite is 60.6%. The mineral generally occurs as irregular masses or radiating groups of bladed crystals and are found largely in greissen, quartz-rich veins, in pegmatites in close association with granitic intrusive rocks or in high temperature hydrothermal veins with sulphides such as pyrrhotite, pyrite, chalcopyrite, or bismuthinite. The major economical sources of wolframite are in the Nanling range in Souther China and also in Colorado, Portugal, Cornwall, Bolivia and Malaya.

Of the second group of minerals, the only important one is scheelit $CaWO_4$ which belongs to the tetragonal system.

A partial or complete series exists between some molybdates and tungstates, both series of minerals having the general formula, $A_m(XO_4)_n$, X being either Mo or W.

2.2.2. Minerals Used.

In this work wolframite from two sources has been used, both of which showed identical X-ray powder diffraction pictures. The main body of the work was carried out on a wolframite ore of unknown origin. X-ray analysis of the metal constituents on a particle using the Cambridge Microscan X-ray analyser gave 55.5% W, 11.5% Mn, 13.0% Fe, therefore giving oxygen, by difference, as 20.0%. The idealised formula $(Fe,Mn)WO_4$ requires 61% W, 18% (Fe + Mn) and 21% oxygen. The other sample of ore consisted of a hand specimen of wolframite from South Crofty, Cornwall, but owing to the small quantity available only a restricted number of experimental runs could be made. However a correlation im the behaviour of the two minerals was reached.

SECTION 3.

RESULTS AND DISCUSSION.

LEACHING OF PYRITE.

This section comprises a study of the behaviour of pyrite and its insoluble oxide products when leached in sodium hydroxide solutions with concentrations up to 4.00N and at temperatures up to 150°C. An atmosphere of compressed air was introduced into the reaction vessel and the effect of the oxygen partial pressure studied, for air pressures varying from zero to 600 p.s.i. and its relationship to the above variables of temperature, and NaOH concentration for increments of time up to 120 min.

The only work dealing with the caustic leaching of pyrite was carried out by Stenhouse and Armstrong in 1952 (69), from which notable observations made were :

i) The reaction was heterogeneous at the pyrite particle surface.

ii) A pseudomorphic iron oxide coating was formed about unleached pyrite during leaching.

iii) The rate of reaction was directly proportional to the square root of the oxygen pressure. This indicated dissociation of oxygen molecules to atoms at the particle surface followed by transference of sulphur atoms as positive ions through the oxide coating to oxygen at the surface where combination to form the sulphate, SO_4" took place. It was further postulated that lattice defects were created at the pyrite oxide interface by sulphur removed to the surface of the particle. Diffusion of oxygen atoms into the oxide layer took place so that the oxidation of iron was assumed to occur by this substitutional diffusion into the oxide layer.

In the light of observations obtained from this work, some agreement is obtained with the deductions of this early paper, the reaction mechanism and nature of oxidation product produced being further elucidated by examination of the partially leached residues. The oxide product was found to exist as a pseudomorphic coating only when the mineral had a deficiency of sulphur atoms in its lattice, or in places where the oxide could be physically held in contact with pyrite by its penetration along defects or along the grain boundaries of a particle consisting of a matrix of finely crystalline

material. The rate of reaction has been found to be proportional to the square root of the oxygen partial pressure implying an order of reaction of 0.5 with respect to oxygen and explained by the dissociation of oxygen molecules at the particle surface. It has been possible to determine the effective proportion of free pyrite surface available for reaction under varying conditions of time and temperature when the product formed tends to be non-adherent. From these values, calculations of the actual reaction rate per unit exposed pyrite surface area have been made.

Pyrite used, consisted of :

i) A finely crystalline material from Rio Tinto, Spain of comparatively low purity;

ii) Large crystals of very high purity from Cassandra, Greece, and

iii) Large high purity crystals from the Kimberlite diamond pipes of the Premier diamond mine in South Africa.

An X-ray fluorescence analysis of the above minerals, showed that the impurities in the Rio Tinto ore consisted of Copper, Zinc,

lead and arsenic in appreciable proportions. Trace quantities of the elements arsenic and lead were found in the Cassandra crystals and of nickel in the Premier pyrite. A study of individual grains of Rio Tinto pyrite was made using the Cambridge Microscan X-ray Analyser. Observations confirmed that the impurities were not present in the pyrite lattice but rather on a macro scale as the minerals chalcopyrite, sphalerite, galena and arsenopyrite. When the relation between alkali consumption and pyrite decomposed was studied, the amount of sulphur consumed per mole of hydroxide was greater than the stoichiometric requirement for pyrite as FeS_2, the difference therefore was due to sulphur liberated when the impurities were decomposed. The arsenic and lead impurities in the Cassandra ore were in extremely low proportion and were expected to play a negligible part in the reaction, as was the nickel in the Premier pyrite, where it was probably present as a substitional replacement in the pyrite lattice.

In order to study the mechanism of reaction for the expected heterogeneous behaviour of a solid-liquid reaction, the pyrite was ground and dry-screened to particle sizes of 48-100 mesh Tyler and 100-200 mesh Tyler. Throughout the series of experiments, the solution in the pressure vessel was agitated at a high rate. It was a disadvantage that the impeller was driven by compressed air motor since absolute agitation rates and their relationship with the reaction

could not be obtained, due to the appreciable changes in the agitation rate with variation of compressed air pressure. However, the high rates employed, enabled a maximum amount of air at operating pressure to be dissolved in the solution throughout the duration of the experiments. The rate of diffusion from liquid-gaseous phase to the liquid-solid phase thus had negligible effect as a rate controlling factor.

Sulphur liberated from pyrite during leaching as sulphate was determined by its precipitation as barium sulphate, and provided the criterion for the determination of the extent of pyrite dissolution after leaching under the prescribed experimental conditions. The sulphate ion was thermodynamically the only stable product under the experimental conditions.

Experimental results are discussed below :-

3.1. Leach Reaction Variables.

3.1.1. Dependence of reaction on Oxygen and Sodium hydroxide concentration.

In the determination of the effect of changes of oxygen partial pressure and alkali concentration, the Rio Tinto pyrite of particle size 100 - 200 mesh, was heated with 750 cc 0.5N sodium hydroxide solution to temperatures of 100, 120, 150 and 200°C. All oxygen was eliminated before heating and, when a steady temperature had been reached, air was introduced to pressures up to 250 p.s.i., maintained at temperature for the required reaction time of 120 min, and then eliminated and replaced by an atmosphere of nitrogen. The extent of reaction at 150°C was directly proportional to the amount of oxygen present and was negligible in its absence at 0.74% pyrite dissolution at 100°, see fig 1. A similar low value was obtained when the sodium hydroxide concentration was increased to 2.50N.

Results for 10.000 gm pyrite were :

Table II.

Run	Temperature °C	Air pressure p.s.i.	NaOH Conc. (N)	SO_4"(g) produced
73	150	250	0.50	10.06
74	120	250	0.50	8.71
75	100	250	0.50	8.38
79	200	50	0.50	2.05
78	150	50	0.50	2.01
77	120	50	0.50	2.01
76	100	50	0.50	2.18
82	75	50	0.50	1.79
80	150	0	0.50	0.31
81	150	0	2.50	0.42

When the air pressure was maintained at 200 p.s.i. progressive increases of sodium hydroxide concentration from 0.25 to 2.00 N at 100° for 60 min using Cassandra pyrite and 0.50 to 4.00 N at 90° for 30 min using Rio Tinto pyrite were studied. In Fig. 2, it is shown that below 0.50 N sodium hydroxide concentration, the extent of reaction dropped rapidly, but above 0.50 N, the extent of mineral decomposition remained practically constant. This shows a zero order of reaction with respect to alkali concentration, above 0.5 N sodium hydroxide.

Table III

Run	Leach time min	Temp. °C	Air press. p.s.i.	NaOH N	SO_4"(g) produced.
Cassandra					
161	60	100	200	0.25	1.54
152	60	100	200	0.50	2.23
160	60	100	200	1.00	2.25
165	60	100	200	2.00	2.16
Rio Tinto					
184	30	90	200	0.50	0.52
202	30	90	200	2.00	0.57
207	30	90	200	4.00	0.55

Thus, at concentrations above 0.50 N, sodium hydroxide is essential in maintaining reaction as long as oxygen is present in the system but the proportion of oxygen determines the extent to which the mineral will be dissolved even when the sodium hydroxide concentration is as high as 4.00 N, (16% w/v).

These observations show that pyrite is particularly suited for study under the above experimental conditions since accurate control of reaction time can be obtained with the respective introduction and elimination of air before and after the required experimental time. This prevents reaction during heating and cooling and the initial fluctuations of temperature before stable conditions have been reached. These ideal conditions have enabled many of the useful observations mentioned below, to be made, especially when very short reaction times were required.

Fig 1. RELATION BETWEEN INITIAL OXYGEN PARTIAL PRESSURE AND SULPHATE PRODUCED

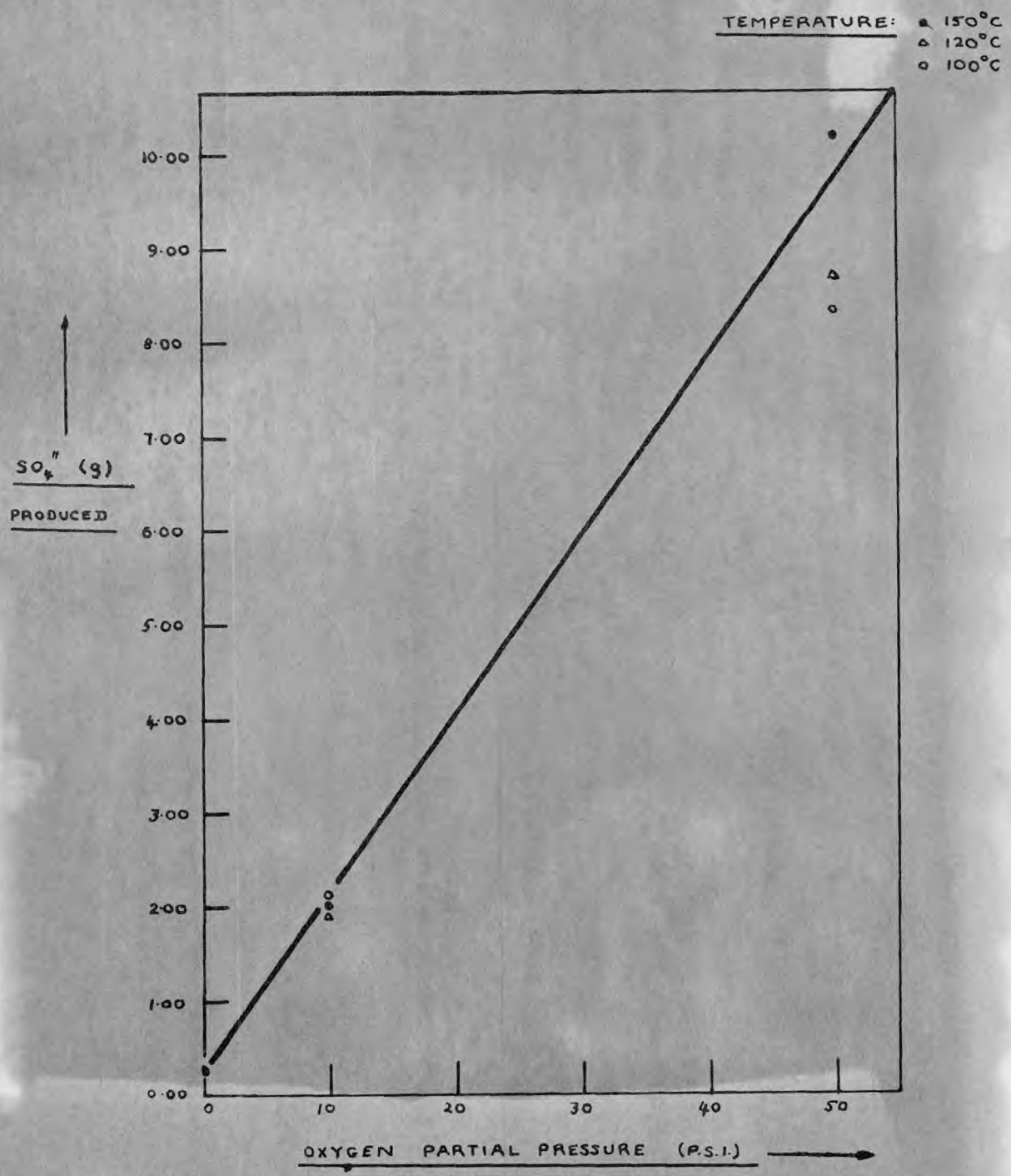
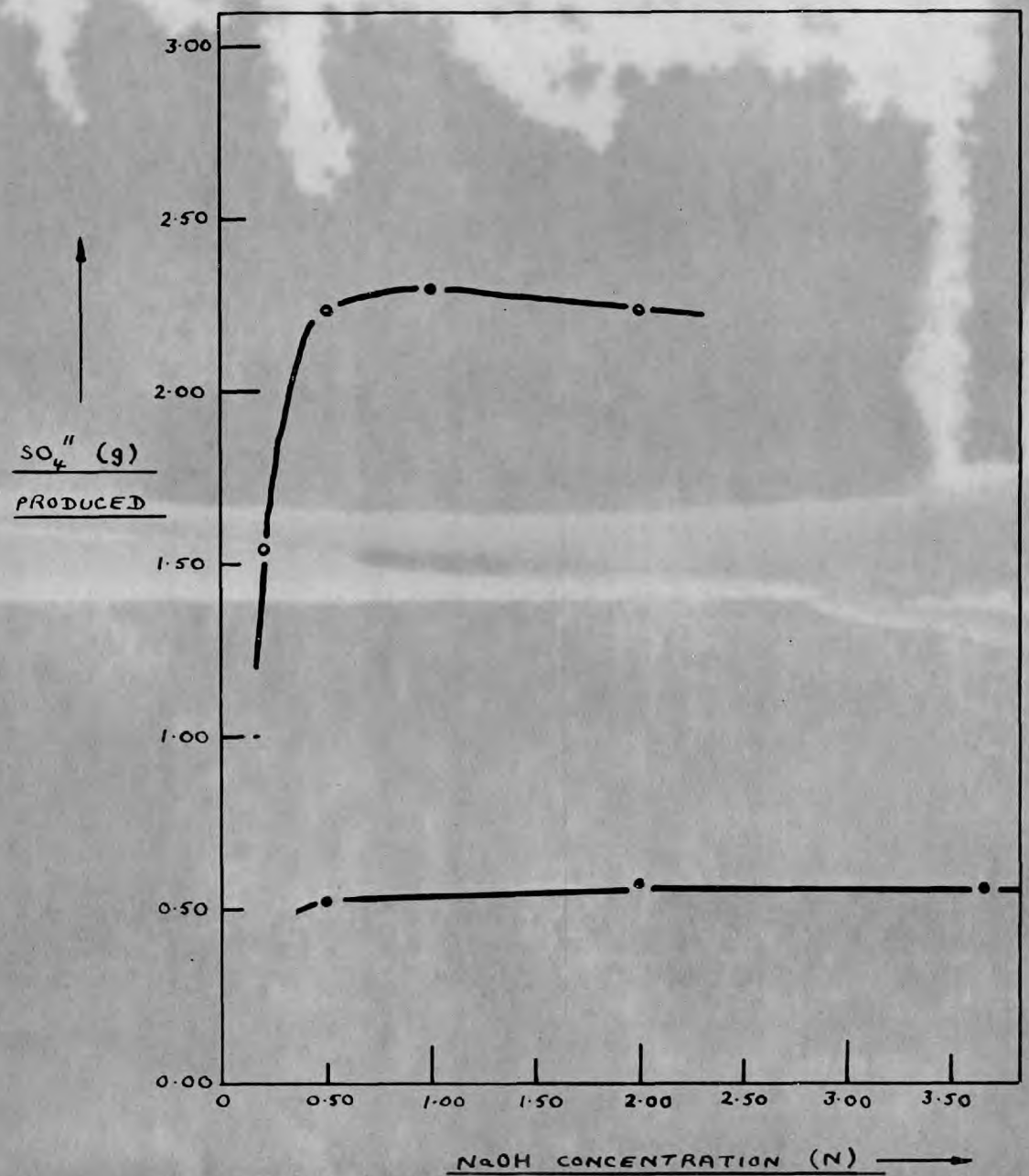


Fig 2.

RELATION BETWEEN SODIUM HYDROXIDE CONCENTRATION AND SULPHATE PRODUCED

PYRITE : ○ : CASSANDRA .
● : RIO TINTO



3.1.2. Effect of reaction time with temperature variation.

With the high purity Cassandra (and Premier) pyrite, there was a steady change of reaction rate with increase of time from 15 to 120 min. as shown in fig (3) * An effectively adherent reaction inhibiting coating was not formed and much of the residue of unleached pyrite exhibited the same high degree of lustre and colour of the unleached pyrite. Only on a small fraction of the particles was an adherent oxide coating noticed, the greater bulk of the oxide product having been deposited as the typically amorphous hydrated iron oxide, away from the mineral surface.

The Rio Tinto pyrite, exhibited a different form of behaviour, as shown in fig 4. being initially more reactive than the Cassandra pyrite. The dissolution rate actually increased below 100° but slowed down abruptly after a time, decreasing linearly with increase in temperature. However, after a short time the reaction rate once again began to increase repidly. The residue exhibited the colour of the iron oxide product, and, since there was no change in particle size or shape, it was apparent that the oxide product had been deposited in situ about the unleached pyrite as a pseudomorphic

---

* The interpolated values were obtained from figs. (20) and (21).

coating. The initial increase in reaction rate before the abrupt retardation was due to an increase in effective pyrite surface area caused by the extensive reactant ion penetration along the pyrite grain boundaries of the finely granular material. The induction period can be attributed to a slowing down of the diffusion rate of reactant ions through the oxide coating with an alteration in the nature of the insoluble product, and the subsequent increase after this period by either the expansion or contraction of the altered product. At temperatures above 90°C these changes of reaction rate became less evident as the induction period became progressively shorter and the reaction rate considerably greater.

It is shown, therefore, that an effectively adherent oxide coating is found when the pyrite consists of a matrix of small grains or is relatively impure (Rio Tinto) and its reaction inhibiting effect becomes less effective when the pyrite particles are larger and of higher purity as with the Cassandra ore. Furthermore the coating, when formed, undergoes a change, either physical or chemical during the course of pyrite dissolution.

It had been suggested that the slowing down of reaction rate and its subsequent increase,was due to the presence of two forms of pyrite of different geological history, one being more reactive, e.g. due to impurities in the lattice or to sulphur vacancies. However, if this were the case, there would not be the linear variation shown by the broken line in fig 4, for the beginning of the induction period, and the line would rather have tended to be parallel with the

abcissa for changes in temperature. The effect, therefore, appears, more likely, to be due to changes in porosity of the oxide.

Experimental results for 5.000 g of pyrite of 100-200 mesh size at 200 p.s.i. air pressure and 0.50 N sodium hydroxide concentration were :

Table IV.

Cassandra pyrite

Run	Time min.	Temperature °C	SO_4"(g) produced.
158	15	150	1.85
145	30	150	2.68
146	60	150	4.95
159	30	120	1.87
155	60	120	3.65
156	15	100	0.71
157	30	100	1.30
152	60	100	2.23
154	120	100	3.22
153	30	90	0.91
149	60	90	1.66
151	120	90	2.45
150	30	80	0.52
147	60	80	1.19
148	120	80	1.83

Table V.

Rio Tinto Pyrite.

Run	Time min	Temperature °C	SO_4" g produced.
132	15	150	3.16
142	60	150	4.95
133	15	120	1.92
126	30	120	3.53
119	60	120	4.46
127	30	100	2.28
134	45	100	3.20
120	60	100	3.55
114	120	100	5.04
228	15	90	0.80
128	30	90	1.60
135	45	90	2.52
121	60	90	2.65
140	90	90	3.44
227	90	90	3.35
115	120	90	4.64
143	30	80	1.08
136	45	80	1.70
139	45	80	1.86
122	60	80	2.47
138	90	80	2.88
116	120	80	3.32
130	30	70	0.71
123	60	70	2.03
137	90	70	2.22
117	120	70	2.58
131	30	60	0.34
124	60	60	0.79
141	90	60	1.37
118	120	60	1.50

Kinetic Measurements: The rate curves shown in figs, (3) and (4) have been used for the determination of the activation energies for the initial stages of the reaction. It was not possible to establish Arrhenius plots for rates after prolonged times of reaction as the reaction inhibiting coating particularly in the case of the Rio Tinto pyrite, caused the diffusion of reactants through it to become rate controlling at an early stage. Furthermore it was difficult to account accurately for changes in particle surface area after the longer times. For the Cassandra and Premier pyrite, although corrections have been made for the effective reduction in surface area, a proportion of the pyrite surface was coated, this proportion increasing with decrease in temperature and reduction in particle size so that the effect of diffusion became progressively greater and could not be ignored. (See Section 3.3.)

In the initial stages of dissolution, the specific reaction rate is directly related to the actual reaction rate, since there is negligible change in the total concentration of reactants and the formula below may be employed ;

$$\log \left(\frac{k_2}{k_1}\right) = \frac{E}{R \times 2.303} \left(\frac{T_2 - T_1}{T_1 T_2}\right) \qquad (62)$$

Where k_1 and k_2 are the rates of reaction obtained by slope measurement of the curves in figs, (3) and (4) for temperatures T_1 and T_2 ^{o}K respectively and E is the Activation energy for the reaction.

Initial reaction rates obtained by slope measurement are tabulated below; expressed as SO_4" (g) produced per min.

Table VI.

Pyrite	Temperature ^{o}C						
	60	70	80	90	100	120	150
Rio Tinto	.011	.024	.036	.053	.075	.129	.284
Cassandra	-	-	.018	.031	.046	.080	.170

Arrhenius plots, using the above values, are shown in fig (5), in which (K) is the rate of sulphate produced per minute and (T) is the absolute temperature. The linear variation indicates that the reaction inhibiting coating had not developed an effective thickness. The greater reactivity of the Rio Tinto pyrite is clearly shown by the displacement of the line well to the right of the Arrhenius plot for the Cassandra pyrite.

The activation energies (or strictly, critical increments) for the two minerals are identical within the limits of experimental error ;

Rio Tinto pyrite : 8.7 $\pm$ 0.8. kcal/mole

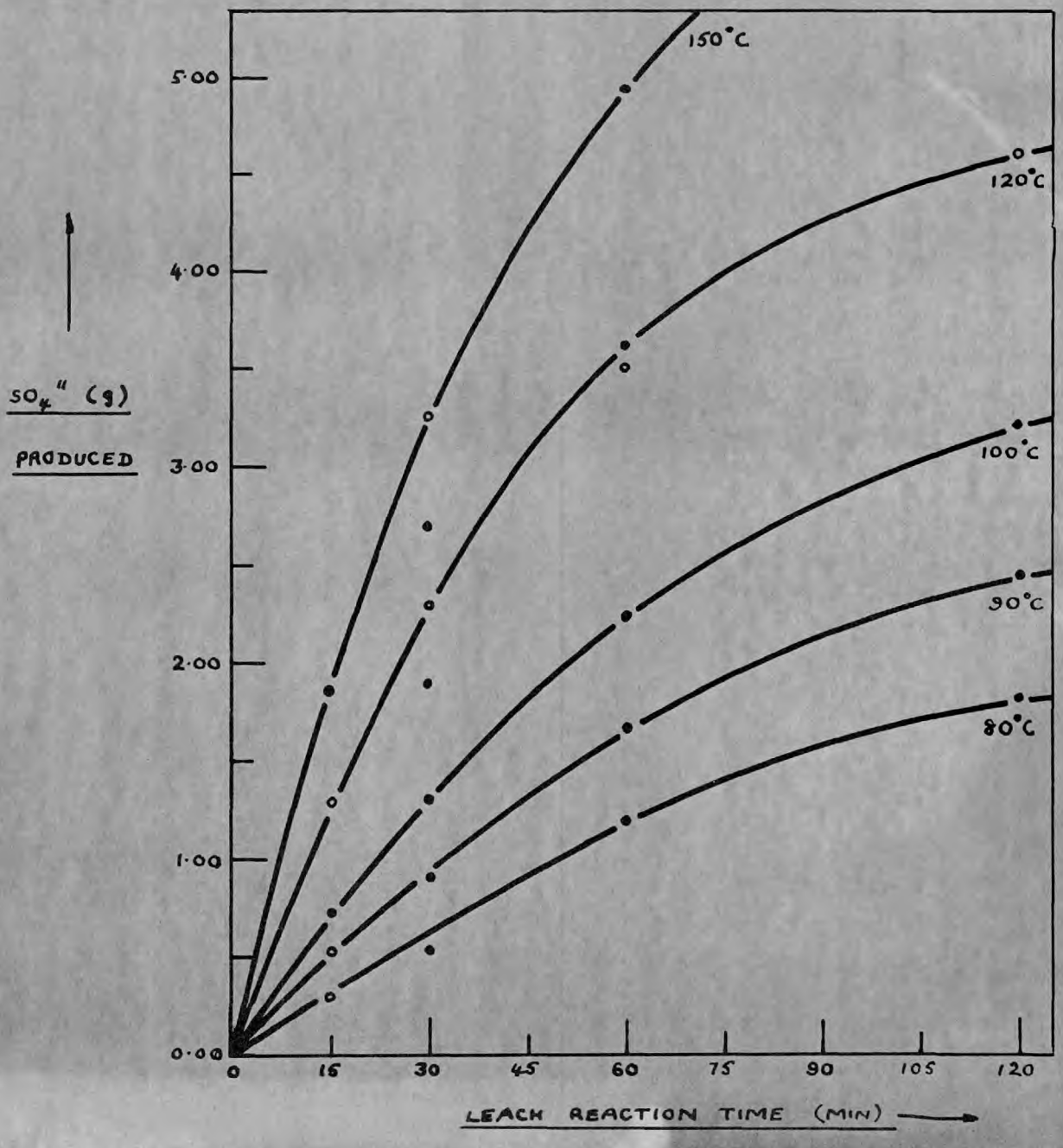
Cassandra pyrite : 9.3 $\pm$ 0.5 kcal/mole

The greater relative reaction rate of the Rio Tinto pyrite indicates a greater preponderance of reaction nucleating sites due to lattice defects caused by impurities or vacancies and to the greater effective surface area caused by the finely grained structure of the mineral.

Fig 3.

EFFECT OF LEACH REACTION TIME ON PYRITE DISSOLUTION

SOURCE : CASSANDRA



RESULTS BY EXPERIMENT: ●

RESULTS BY INTERPOLATION: o

Fig 4.

EFFECT OF LEACH REACTION TIME ON PYRITE DISSOLUTION

SOURCE: RIO TINTO

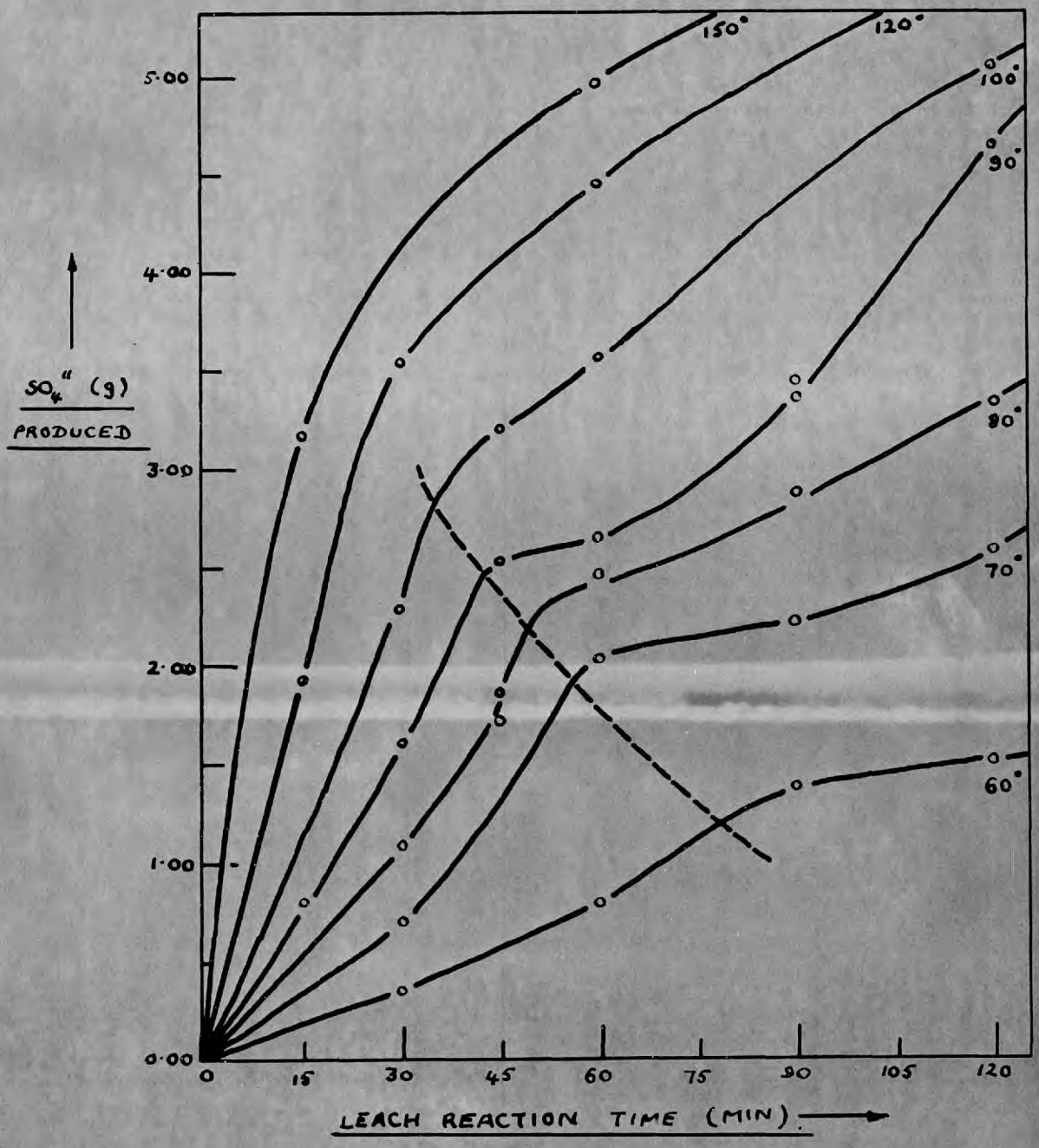
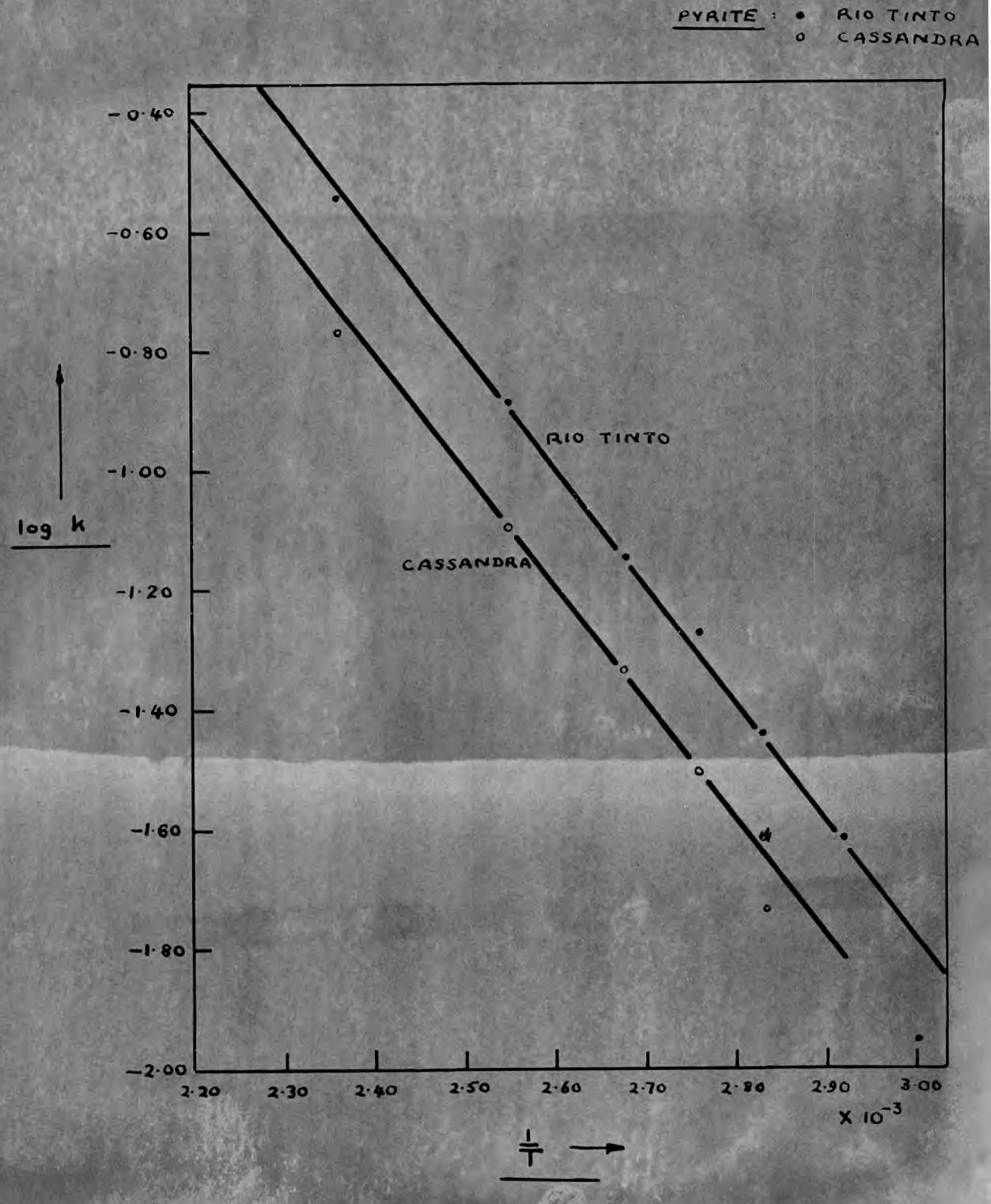


Fig 5.

ARRHENIUS PLOT FOR INITIAL RATES OF PYRITE DISSOLUTION



3.1.3. Effect of air pressure with temperature variation.

In order to reduce both the effects of extensive reactant ion penetration into the mineral particle and the rate of change of retained pyrite surface area during the reaction, a coarser grade of ore, viz. 48 - 100 mesh, Tyler screen size, was used for this series. The extent of reaction was kept at a low value by only allowing the reaction to proceed for 30 minutes. By so doing, the total extent of mineral dissolution was never higher than 27%.

A. Cassandra and Premier pyrite.

A uniform variation in plots of air pressure against sulphate ions produced is shown in figure 6. The residual pyrite retained much of the high degree of lustre and colour of the unleached mineral as was observed earlier, indicating a predominantly non-adherent product.

The crushed crystals of pyrite from the Premier diamond mine, although of the same high degree of pyrity as the Cassandra crystals, are shown to be somewhat more reactive and similar results were obtained for the Premier pyrite at 110°C as for the Cassandra pyrite at 120°C, allother leach conditions being the same. This greater reactivity no doubt depends on the history of formation of the mineral; the Premier pyrite had been formed under high pressures, (page 53) whereas the Cassandra ore was highly uniform and apparently formed under stress free conditions.

Experimental results are tabulated below for 5.000 g ore leached for 30 min in 750 cc 0.5 N sodium hydroxide solution.

Table VII.

Run	Temperature °C	Air pressure p.s.i.	SO_4"(g) produced.	Time taken for production of 1.4 g SO_4" (min)
Cassandra				
174	120	100	0.73	28
171	120	200	1.19	16
170	120	400	1.42	14
175	100	100	0.40	48
169	100	200	0.62	33
167	100	600	0.82	24
173	90	200	0.38	48
176	90	400	0.47	43
176	90	600	0.52	38
Premier				
216	120	100	0.99	20
213	120	200	1.55	12
212	120	400	2.06	11
203	120	600	2.25	10
217	110	100	0.69	27
214	110	200	1.08	17
215	110	600	1.55	13
179	100	200	0.52	40
178	100	400	0.73	17
177	100	600	0.91	19

Kinetic Measurements: For the determination of the order of reaction with respect to oxygen concentration, i.e. oxygen partial pressure, it was necessary that corrections be made for the effect of surface area change during the course of reaction. It was therefore assumed that, for a constant value of sulphate produced with mineral decomposition, the effective surface area was independent of the leach conditions. This correction was made by estimating from fig (3), the necessary time for a given proportion (1.4 g) of sulphate to be produced. Since the results for the rate curves were obtained using a 200 to 100 mesh size fraction of ore, a further correction had to be made from the values obtained in table VII by correcting for particle surface area using the results obtained in fig (13). It was found that the surface area of the 100 to 200 mesh size fraction remained almost double the area of the 48 - 100 mesh size fraction within the range of the experimental results.

The time (t) taken for the production of 1.4 g sulphate ions (i.e. c 17% mineral dissolution) was used in the general formula ;

$$\log \frac{t_1}{t_2} = -n \log \frac{C_1}{C_2} \qquad \ldots.(63)$$

Where n is the order of reaction with respect to reactant C and t_1 and t_2 , the times taken for a given degree of dissolution to be reached at a given temperature for oxygen concentrations of C_1 and C_2

Fig 6.

EFFECT OF OXYGEN PRESSURE ON PYRITE DISSOLUTION

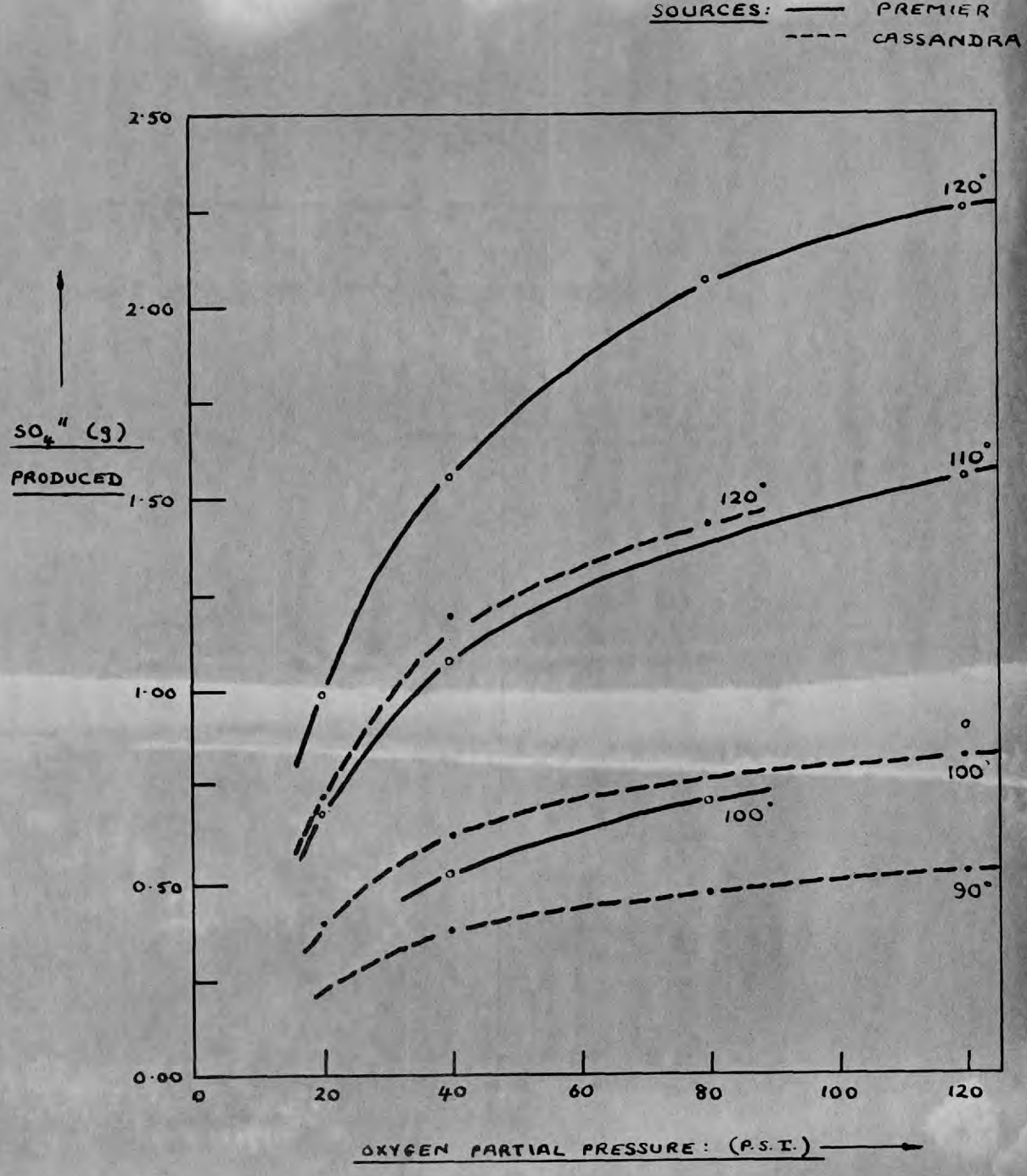
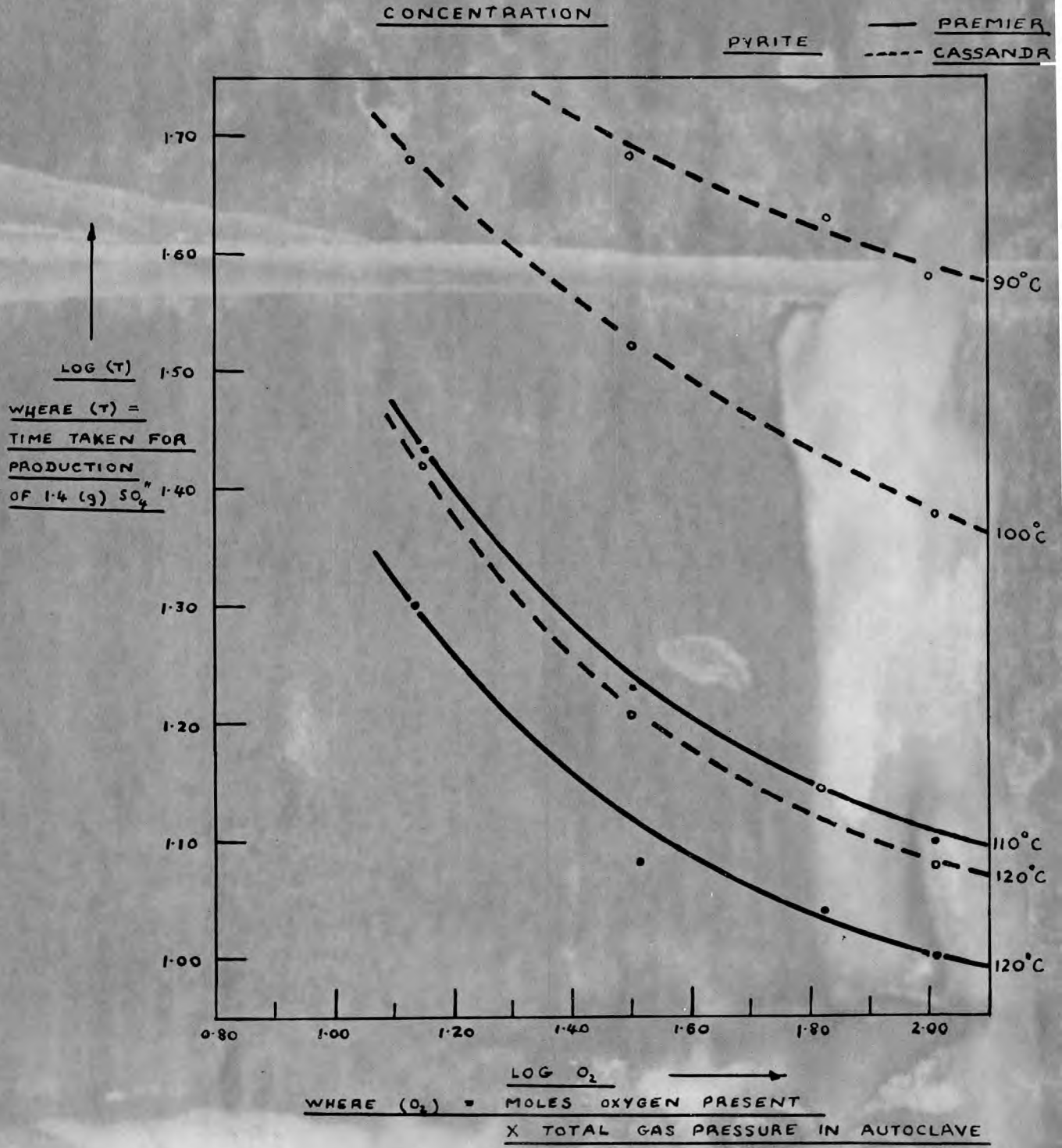


Fig 7.

RELATION BETWEEN LOG TIME TO COMPLETE 17% PYRITE DISSOLUTION AND LOG OXYGEN CONCENTRATION



respectively.

The slopes of the curves indicate a value for the order of reaction with respect to oxygen concentration which tends to zero order at high oxygen pressures. At oxygen pressures less than 20 p.s.i. the rate of reaction tends to first order and a dependence on the rate of transport of oxygen to the mineral surface.

B. Rio Tinto Pyrite.

In a manner related to the induction period shown by the Rio Tinto pyrite in fig 4, there was an abrupt change in the amount of sulphate produced after a constant time with variation of air pressure as shown in fig (8).

As indicated by the broken lines the period change of rate becomes narrower with increase in temperature and would probably not be noticed above 100°C. It occurs at higher pressures and is evident over an indeterminate range of pressure variation at 70°C. The behaviour is similar to that due to the induction period shown in fig 4, viz; that the oxide coating which is deposited pseudomorphically undergoes a change, apparently with oxidation. Thus, the transformation of the insoluble product takes place more rapidly at lower concentrations of oxygen and high temperatures and is sluggish at high concentrations of oxygen when the temperature is comparatively low at 70°C. By plotting variations of oxygen pressure against temperature, fig 9 the effect of the abrupt change in reaction rate during oxide transformation is clearly shown for

progressive variations in the amount of sulphate produced.

The partially leached residues appeared to have retained the shape and size of the unleached mineral and there was a progressive increase in redness (hematitic nature) with increments of both oxygen pressure and temperature.

Kinetic measurements: Using the same procedure as that employed for the Cassandra and Premier pyrite above, the order of reaction with respect to oxygen has been determined. However, as seen in fig 4, reaction rates were uniform at the early stages of dissolution and therefore within that range, the rate of sulphate production was assumed to be constant. The plot of log (t) against log (C) is shown in fig (10) .

The linear variation shown, indicates an order of reaction with respect to oxygen of 0.5 before the abrupt change in dissolution rate. The values of ca0.6, obtained by slope measurement of the lines to the right of the broken line, are unreliable, as no correction could be made for the period of time taken for the change in porosity of the insoluble product with the temporary ceasing of the dissolution rate.

The values of 0.5 obtained for the order of reaction with respect to oxygen are in agreement with observations made by Stenhouse and Armstrong (69). This indicates that the rate controlling step in the dissolution process involves dissociated oxygen molecules at the particle surface, irrespective of whether a stable insoluble product has been deposited on the mineral or a weakly adherent one which is readily removed from the particles during leaching.

Experimental results are tabulated below for 5.000 g of ore leached for 30 min in 750 cc, 0.5 N sodium hydroxide solution.

Table VIII

Run	Temperature °C	Air pressure p.s.i.	SO_4" (g) produced.	Time taken for production of 1.4 g SO_4" min
193	100	50	0.39	108
190	100	100	0.61	69
195	100	150	0.90	47
230	100	175	0.80	52
181	100	200	0.84	50
197	100	300	1.16	36
180	100	400	1.38	30
192	90	100	0.49	-
196	90	150	0.54	-
184	90	200	0.52	81
198	90	300	0.75	56
183	90	400	0.88	48
182	90	600	1.13	37
191	80	100	0.28	-
200	80	150	0.34	-
186	80	200	0.39	-
199	80	300	0.44	95
186	80	400	0.56	75
189	70	200	0.29	-
188	70	400	0.335	-
187	70	600	0.36	-

Fig 8.

EFFECT OF OXYGEN PARTIAL PRESSURE ON PYRITE DISSOLUTION

SOURCE : RIO TINTO

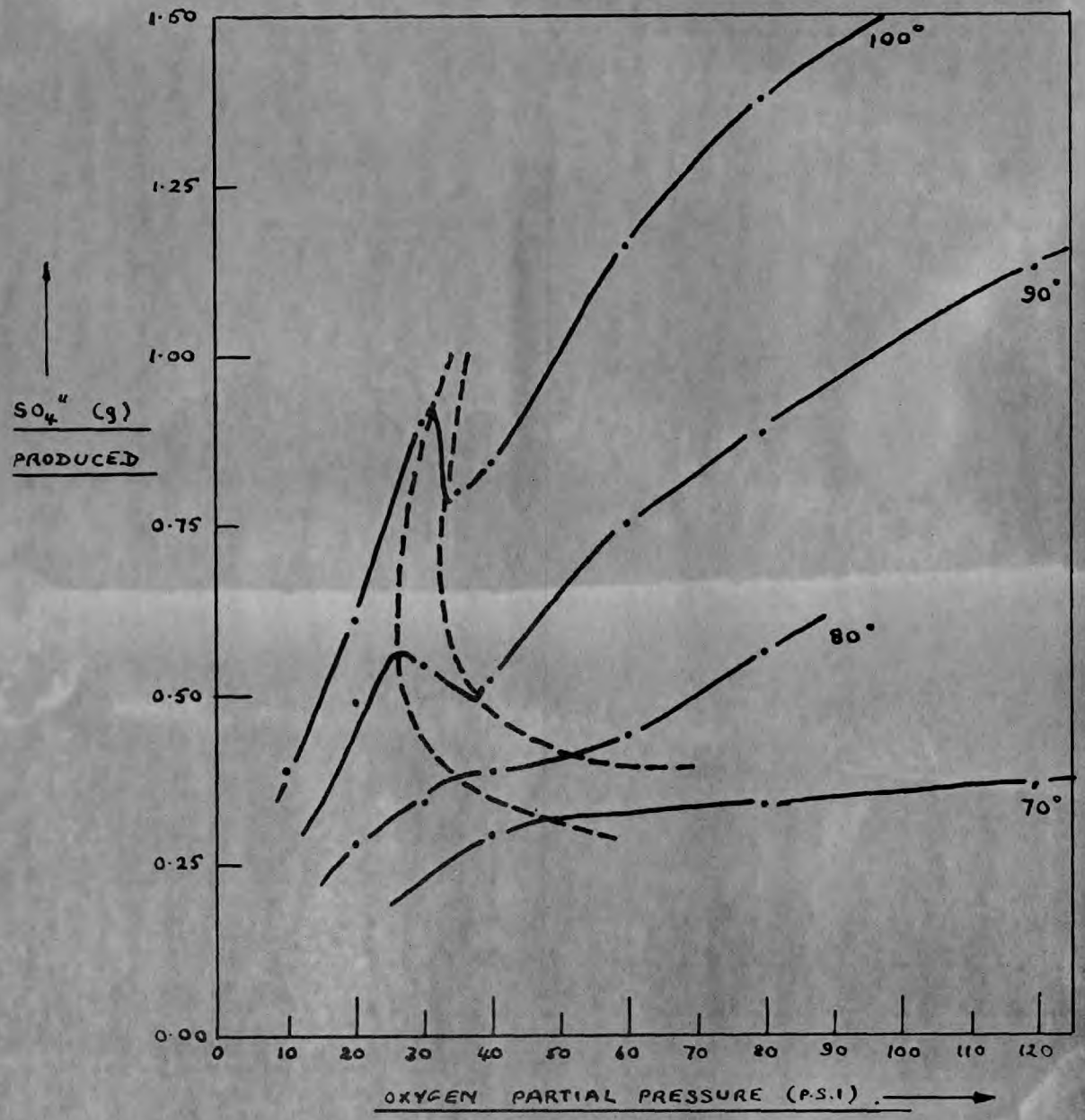


Fig 9.

RELATION BETWEEN OXYGEN PRESSURE AND TEMPERATUR

FOR INCREMENTS OF SULPHATE PRODUCED

SOURCE : RIO TINTO

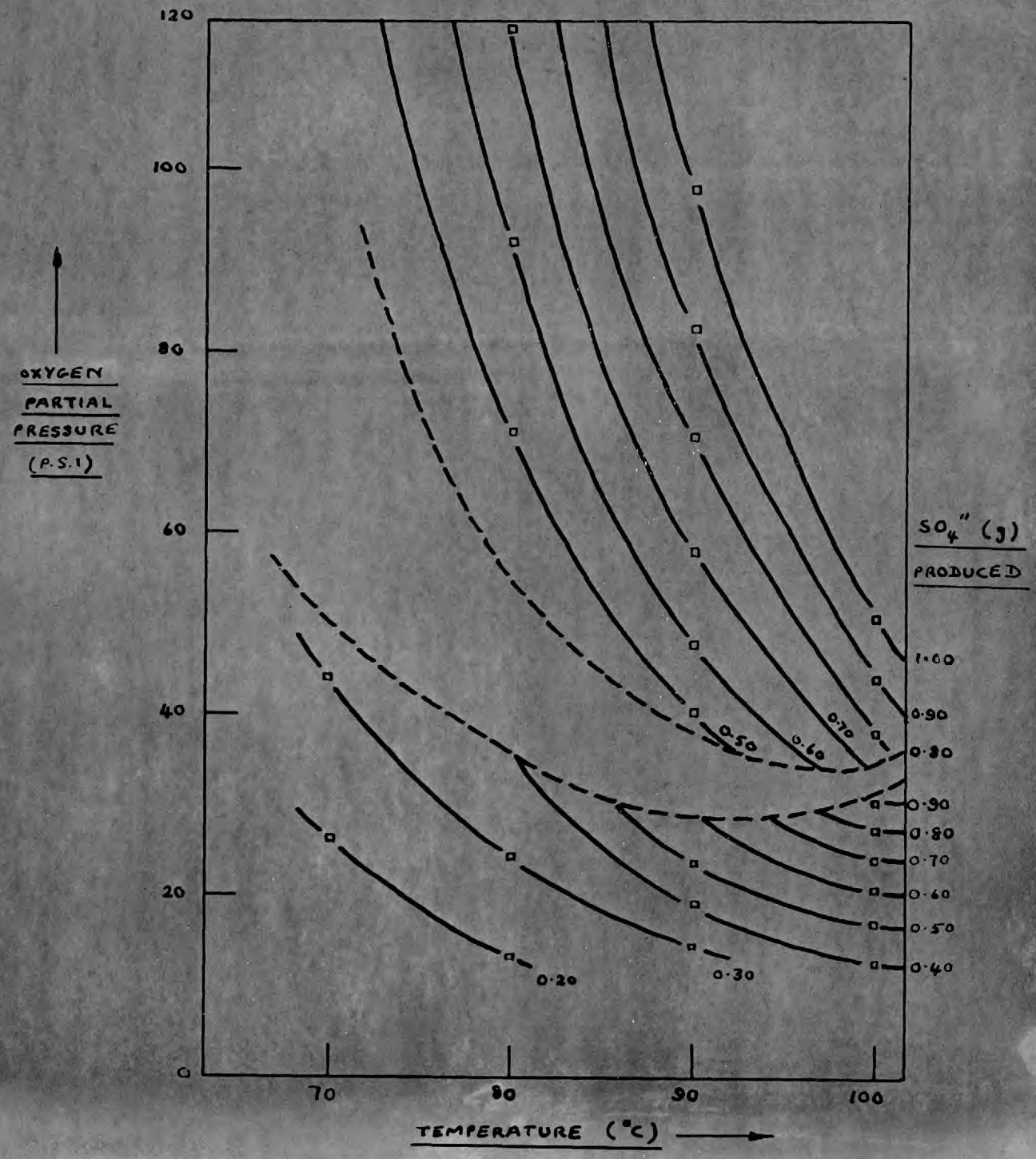
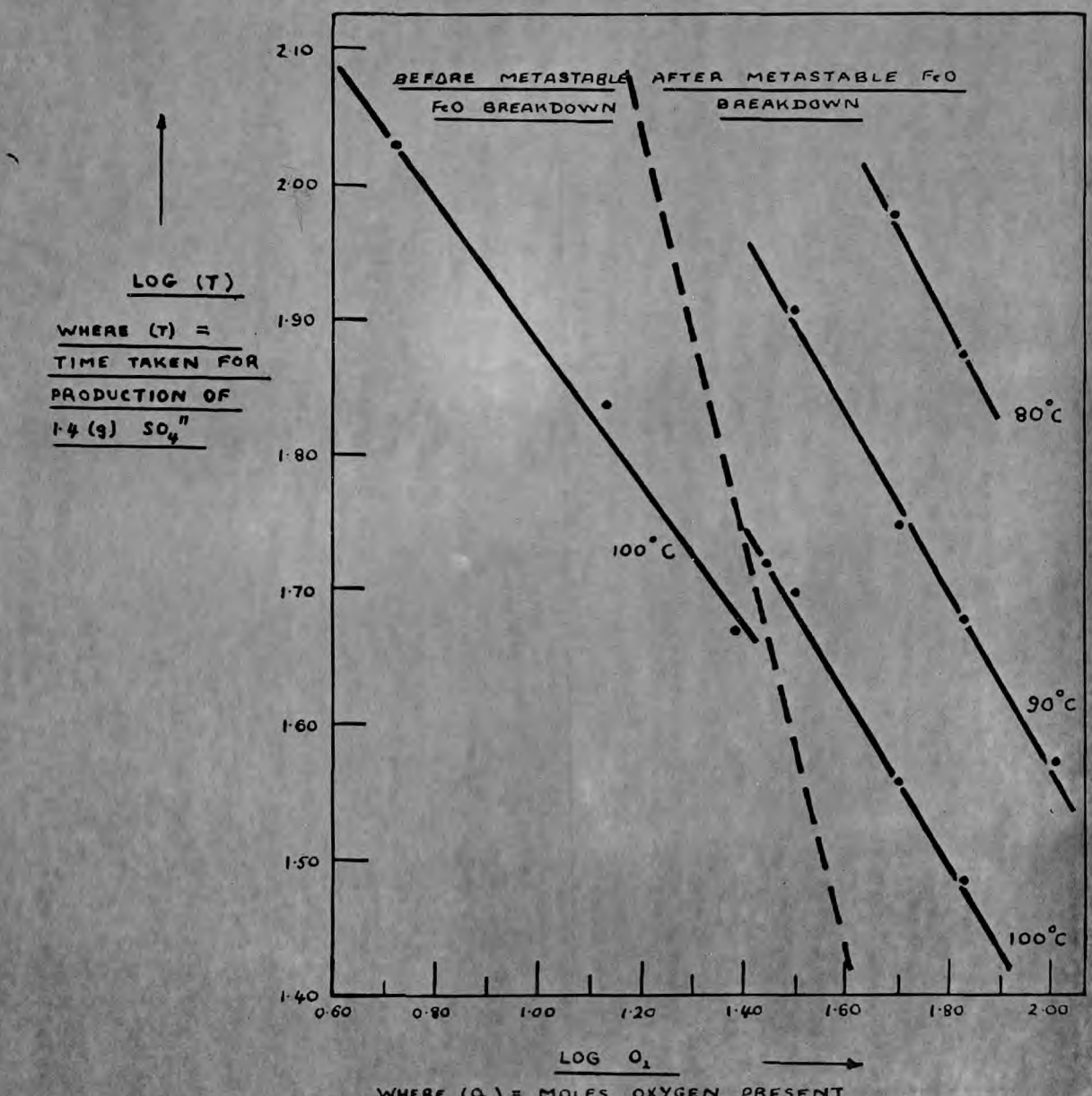


Fig 10.

RELATION BETWEEN LOG TIME TO COMPLETE 17 % PYRITE DISSOLUTION AND LOG OXYGEN CONCENTRATION

PYRITE : RIO TINTO



3.1.4. Effect of air pressure with sodium hydroxide variation.

As shown on page (64) the rate of reaction is of zero order with respect to sodium hydroxide concentration with alkali concentration greater than 0.50 N. The variation, with regard to oxygen partial pressure, when a non-adherent oxide is formed, as with Cassandra and Premier pyrite, would not be expected to show much change, provided that sufficiently high solution agitation rates are maintained. However, the increase in sodium hydroxide concentration plays an important part in stabilising the initial structure of the insoluble product formed on the Rio Tinto pyrite, as shown in fig. 11. The amount of sulphate produced has been plotted against oxygen partial pressure for concentrations of sodium hydroxide varying from 0.50 to 4.00 N, and reactions at 90^{c} and 30 min leach reaction time. Increments of sodium hydroxide concentration from 2.00 to 4.00 N show hardly any variation and the position of change in structure of the oxide product, between 60 and 80 p.s.i. oxygen partial pressure, is unaltered. The initial oxide product was substantially stabilised and had attained a 30% greater thickness before its alteration. Ferrous hydroxide has shown a similar behaviour by being more resistant to oxidation in the presence of sodium hydroxide solutions (54)

Experimental results for 5.000 gm ore at 48 - 100 mesh particle size are :

Table IX

Run	NaOH concentration N.	Air press. p.s.i.	SO_4"(g) produced
209	4.00	100	0.32
207	4.00	200	0.55
211	4.00	300	0.75
208	4.00	400	0.78
206	4.00	600	1.02
205	2.00	100	0.38
202	2.00	200	0.57
210	2.00	300	0.80
204	2.00	400	0.77
201	2.00	600	0.99

For runs at 0.50 N sodium hydroxide concentration see table (VIII)

In fig. 12, the results plotted in fig. 11 have been redrawn to show the variation of sodium hydroxide concentration with air pressure for progressive degrees of pyrite dissolution. The elevation of the range during which the iron oxide coating undergoes change is clearly shown between the concentrations of 0.50 and 2.00 N sodium hydroxide.

3.1.5. Effect of Particle Size.

In fig. 13 the variation in extent of mineral dissolution with particle size is shown and indicates the dependence of reaction on particle surface area. The Cassandra pyrite is less reactive and is displaced to the right. The lack of related trend with the two grades of Rio Tinto pyrite is due to the change of porosity of the insoluble product during leaching and to the reater extent of reactant ion penetration into the smaller particles of pyrite. In the regions of experimental work, the Cassandra pyrite showed a linear variation with change of temperature

Fig 11.

RELATION BETWEEN OXYGEN PRESSURE AND PYRITE DISSOLUTION FOR CHANGES IN SODIUM HYDROXIDE CONCENTRATION

PYRITE : RIO TINTO

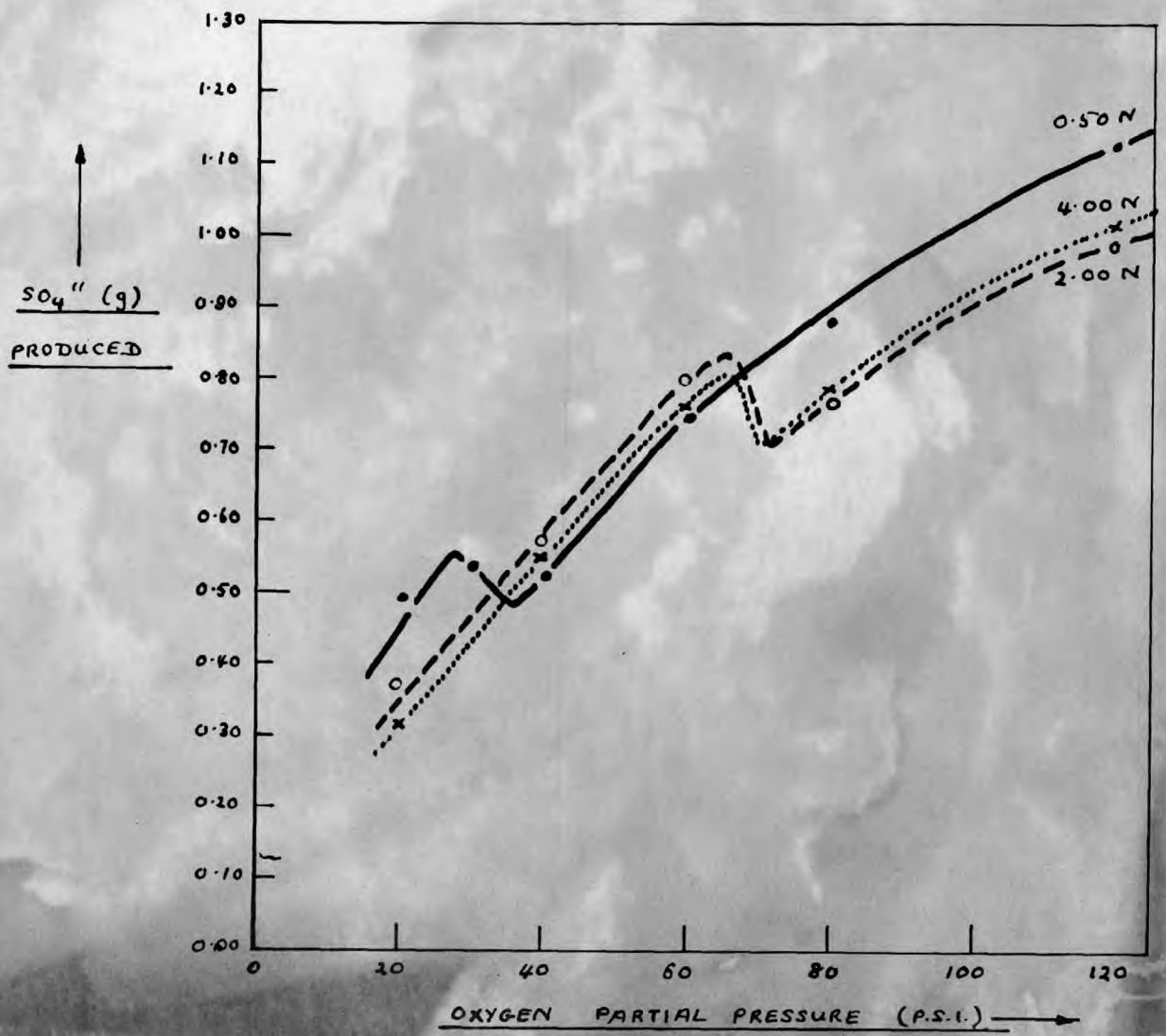


Fig 12.

STABILISATION OF INITIAL OXIDE PRODUCT BY INCREMENTS OF SODIUM HYDROXIDE CONCENTRATION

PYRITE : RIO TINTO

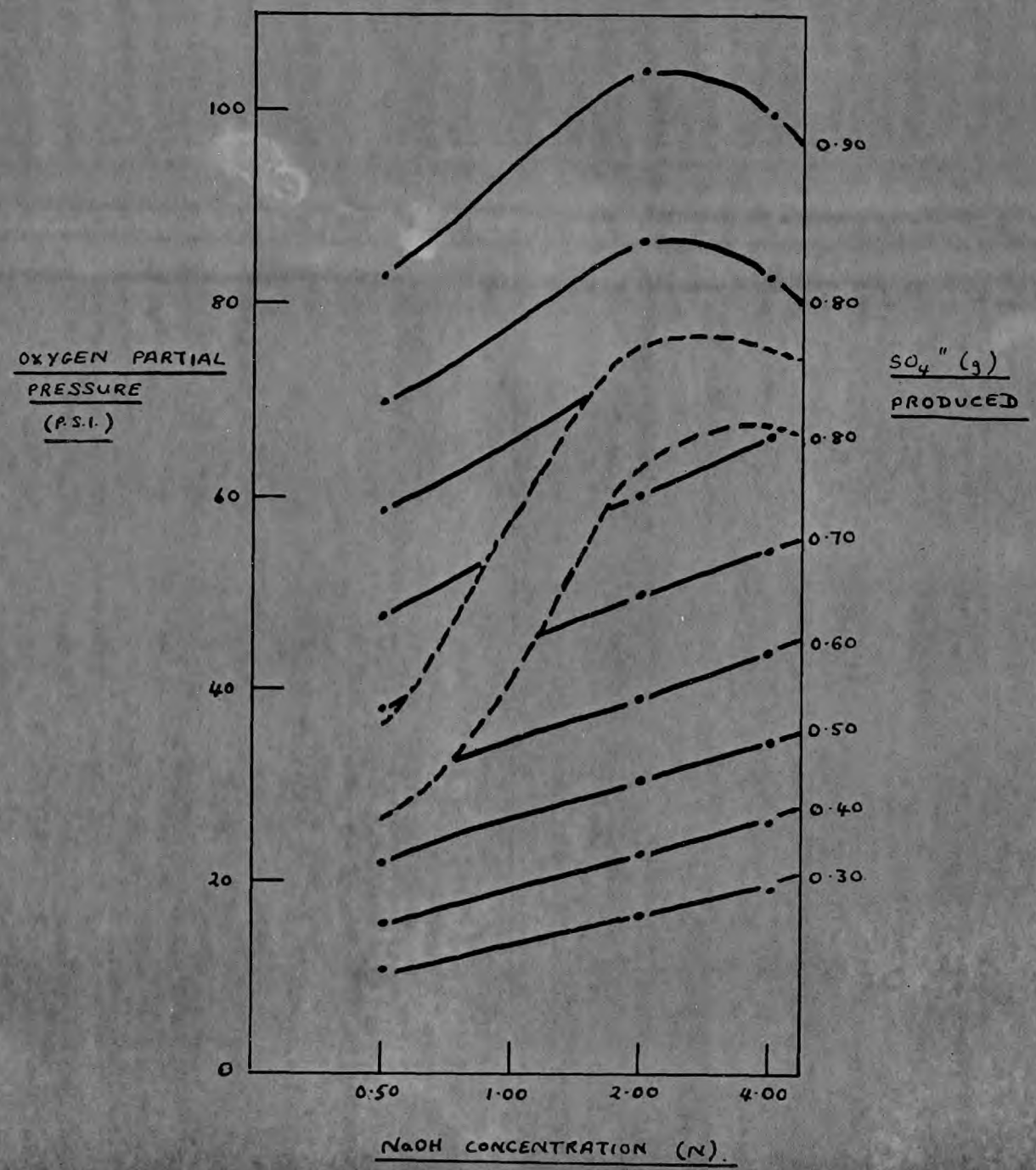
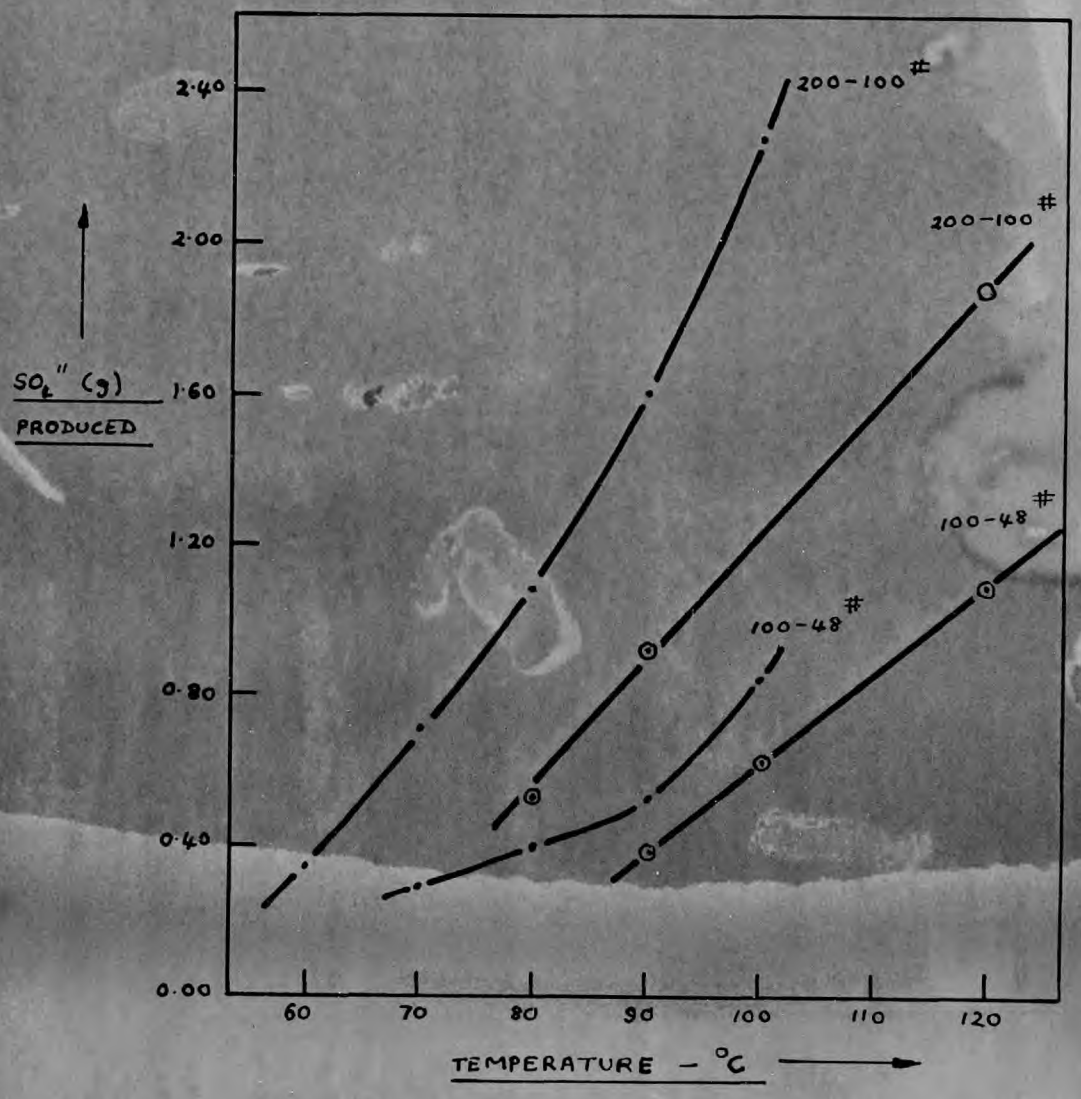


Fig 13.

RELATION BETWEEN PARTICLE SIZE AND PYRITE DISSOLUTION

SOURCE : ⊙ : CASSANDRA
• : RIO TINTO



3.2. Reagent Consumption.

The ratio of mineral decomposed to alkali consumed was constant and independent of the experimental conditions, see fig 14. The number of moles of sodium hydroxide used per mole of pyrite decomposed was :

Cassandra pyrite: Limits in 13 runs, 3.3-4.0, Ave. 3.7

Rio Tinto pyrite: " " 31 " 3.7-4.7, Ave. 4.3

Oxygen consumption could not be measured accurately due to slight leakages in the autoclave gas space and the relative insensitivity of the pressure gauge to small changes in pressure. However, under conditions which minimised the oxidation of ferrous oxide (or hydroxide) and when the whole of the oxygen was consumed during leaching, it was found that about 5 molecules of O_2 were required for each FeS_2 molecule decomposed. Utilisation of values shown in fig. 1, at 150°C, give a result of the same order

The following equation covers the stoichiometry of the reaction:

$$4\ FeS_2 + 16\ NaOH + 15O_2 = 2Fe_2O_3 + 8Na_2SO_4 + 8\ H_2O \quad ..(64)$$

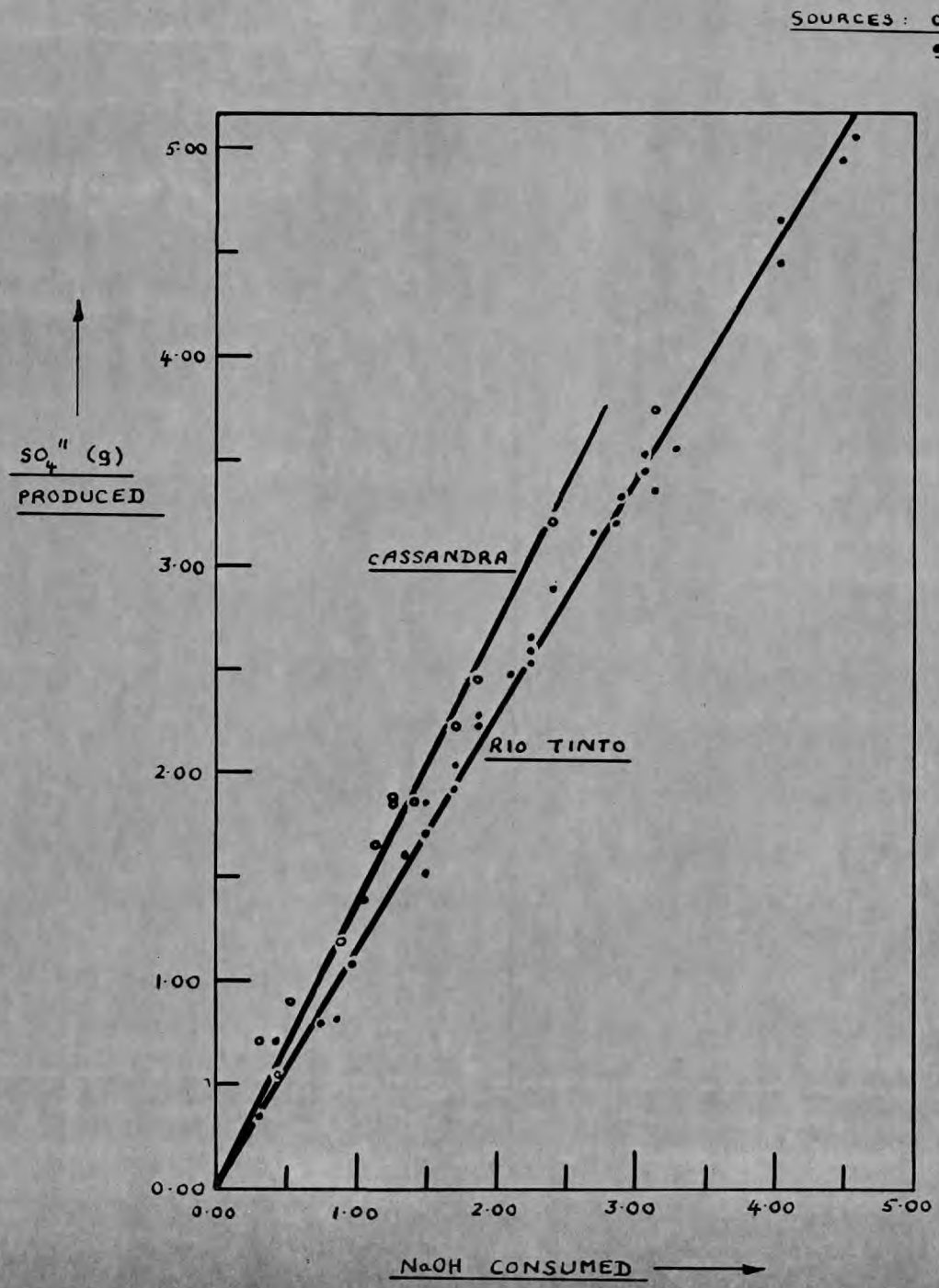
This is in close agreement with the experimental alkali consumption and the oxygen consumption is in reasonable agreement considering the experimental error involved. Sulphate is the only thermodynamically stable anion containing sulphur under the experimental conditions. The proposed mechanism of oxidation is discussed on page (164). For the determination of the oxygen consumption, 20 g Cassandra pyrite, were leached for 240 min. at 120°C in a 0.50 N sodium hydroxide solution at 200 p.s.i. air pressure. This gave 19.04 g SO_4" in solution. The volume of air in the autoclave gas space was measured at cal800 cc.

As mentioned on page (49), pyrite in nature seldom conforms exactly to the stoichiometric formula $FeS_{2.0}$ and the sulphur may, in fact be appreciably lower than the expected value. The value obtained of 4.3 moles of NaOH per mole of FeS_2 for the Rio Tinto pyrite is high due to the consumption of the reagent by the other metal sulphides present, viz; sulphides of copper, zinc, lead and arsenic. The value suggests that they constitute ca 8 mole % of metal atoms present in the system, on the assumption that the rate of oxidation of these impurities is the same as that of the pyrite. This of course would only be strictly true, if these mineral impurities were present in the pyrite in a finely disseminated state.

These observations show that, although the sodium hydroxide concentration is not rate controlling, it plays a prominent part in the dissolution process being directly related to the quantity of mineral dissolved.

Fig 14.

RELATION BETWEEN PYRITE DISSOLUTION AND SODIUM HYDROXIDE USED BY REACTION



3.3. Relation between particle surface area and extent of Mineral dissolution.

In order to calculate the reaction rates per constant surface area for the dissolution of Cassandra pyrite, in which the oxide product is largely non-adherent about the retained pyrite (see fig.3) the distribution of particles into respective size fractions was determined by microscopic particle size counting of the mean particle diameters of the graded ore prior to leaching. The analyses made from determinations of the number of particles of respective mean diameters are plotted in fig. 15, expressed as a weight percentage (i.e. volume percentage) of size fractions measured in microns. In fig. 16 the progressive change in particle weight and surface area is plotted for increments of mean particle diameters.

The variation of particle weight loss during leaching, with surface area loss was determined by assuming that all particles were reduced in diameter during leaching arithmetically until the particle diameter was zero for the given size fraction so that, at a given moment, all particles would have been reduced in diameter by the same length. Assuming then that the effective volume obeyed a cubic function of the diameter and the surface area a squared function, the surface area loss was found to increase more rapidly than the weight loss for a given degree of dissolution. A maximum variance was found at 50 - 60% weight loss. The curve shown in fig. 17 applies to the 100-200 mesh size fraction but the coarser fraction would be

roughly similar in shape. The formulae derived below were used for the construction of fig. 17.

If (x) is the initial particle mean diameter and n_1, n_2, n_3... and x_1, x_2, x_3... the number of particles of given mean diameter respectively at zero time, then the total initial particle volume may be expressed as ;

$$K\ (n_1 x_1^{\,3} + n_2 x_2^{\,3} + \ldots)$$ where K is a constant value.

If (a) is the mean particle diameter after leaching for time (t) and n_1, n_2, n_3... and a_1, a_2, a_3... the number of particles of remaining mean diameter respectively, then the particle surface area after time (t) is ;

$$K\ (n_1 a_1^{\,3} + n_2 a_2^{\,3} + \ldots)$$

The remaining volume, (R_v) therefore, expressed as a percentage of the initial volume, after time (t) is ;

$$R_v = \left(\frac{n_1 a_1^{\,3} + n_2 a_2^{\,3} + \ldots}{n_1 x_1^{\,3} + n_2 x_2^{\,3} + \ldots}\right) 100 \qquad (65)$$

The assumption has been made that uniform dissolution took place, so that $(x_1 - a_1) = (x_2 - a_2) = \ldots$

Similarly the remaining surface area (R_a) as percentage of initial surface area after time (t) would be ;

$$R_a = \left(\frac{n_1 a_1^2 + n_2 a_2^2 + \ldots}{n_1 x_1^2 + n_2 x_2^2 + \ldots}\right) 100 \qquad (66)$$

Thus fig 17. provides a means of determining the change of surface area for a given reduction in volume. The assumptions, of course are only true if particles tend to be spherical in shape and if uniform particle size reduction has occurred without penetration at more reactive sites on the particle surfaces. The degree of error in this determination will be discussed.

By measuring the slope of the curves for different degrees of dissolution, in fig 3, i.e. the rate of sulphate produced per unit time, and compensating for the reduction in surface area using fig 17, the relative rate of sulphate produced per unit time per initial surface area at each respective temperature was determined and plotted for each time of leaching in fig 18. The curves show a reduction in relative rate with time and hence reduction in particle surface area. This indicates one of three possibilities :

i) The system of particle size counting is grossly inaccurate.

ii) Only a fraction of the actual surface, after a given time of leaching, is available for heterogeneous reaction between pyrite and solution

iii) The reaction slows down due to products of reaction in solution or a smaller number of reaction nucleating sites at the free pyrite surface.

The third possibility seems highly unlikely due to the high degree of dilution of the solution and the high purity of the Cassandra pyrite in the first instance. This is substantiated by the fact that, for constant percentages of sulphate produced, the deviation from the straight line of the Arrhenius plot for the initial reaction rates becomes progressively greater, as shown in fig 19.

To verify factors i) and ii), the effective particle surface area, assuming constant reaction rates per unit surface area at all times, was calculated by measuring the curve slopes after different times of leaching in fig 3, and using the relation ;

$$S = \frac{R_t}{R_o} \cdot 100$$

where R_t is the rate of pyrite dissolution, expressed as sulphate produced per minute at time, t, and R_o is the initial reaction rate. Thus S is the effective surface area remaining at time, t, expressed as a percentage of the initial surface area.

Calculated values were ;

Table X

Reaction time (min)	Temperature 80		90		100		120		150	
	S	R_t	S	R_t	S	R_t	S	R_t	S	R_t
0	100	.024*1	100	.031	100	.046	100	.080	100	.070
15	84*2	-	80.5*2	-	75.5	.036	74*2	.059	67	.114
30	70	.017	66	.0205	65	.030	55*2	-	46.5*2	-
60	50	.012	47	.0145	43.5	.020	33	0.026	23	.039
120	29	.007	27.5	.0085	24	.011	17*2	-	7*2	-

*1 R_o as 80°C was obtained by extrapolation from the Arrhenius plot in fig 5.

*2 Values of S obtained by interpolation from fig. 21.

These values are plotted in fig.(20)with variation of the remaining surface area expressed as a percentage of the initial surface area for changes in the percentage of mineral dissolution. The thick broken line shows the change determined by particle size counting which can be compared with the values obtained from experimental results for varying times at each temperature from 80° to 150°, The curves show, that the deviation from the line obtained by measurement becomes greater the lower the temperature and the longer the reaction time.

Fig(20)thus shows that the utilisation of values obtained by particle size counting can provide a reliable guide. The apparent slowing down of reaction must therefore be due to an increase in the effective surface area by the adherent oxide coating, this effect becoming greater at lower temperatures, and the smaller particle sizes. These points serve to indicate that the coating on high purity pyrite, when present, is probably held physically by its formation along cracks or defects and about jagged edges of particles.

The deviation between effective remaining surface area and calculated remaining surface area obtained from figs., (17) and (20) is shown in fig (21) for variations in extent of pyrite dissolution.

These values only give an approximate indication of the actual proportion of residual mineral covered by adherent coating and serves rather to show the progressive trend in coating stability with variations of time and temperature. The actual remaining surface area would be somewhat less, due to the fact that curves have been

calculated for "effective" surface area which would include reaction taking place at the mineral-oxide interface after diffusion of reactants through the adherent insoluble product, where present.

With the Rio Tinto pyrite, in which a highly stable oxide coating is produced, this procedure could not be adopted; firstly because reaction soon becomes entirely diffusion controlled and secondly because the surface area changes considerably owing to its fine-grained structure and the consequent extensive reactant ion penetration along grain boundaries.

3.3.1. Actual reaction rates per unit surface area.

The relative reaction rates with respect to initial particle surface area have been discussed above.

On the assumption that particles tended to be spherical, a value has been obtained for the actual surface area using the measurements made during the particle size counting of the mean particle diameter. Since particle shapes are haphazard this assumption can only provide an approximate indication of the reaction rate per unit surface area.

In fig. (16) the integrated weight percentages and surface area percentages for increments of particle diameters are shown, and the mean diameter was obtained by measurement from fig. (16) of the particle diameter responsible for 50% surface area, the value found being 78 microns.

A formula was determined as :

$$\text{Actual surface area} = \frac{w\ a.}{g\ v.}\ cm^2 \qquad (68)$$

where w is the weight of pyrite used, g is the density of pyrite taken at 5.0 g/cc and a and v. the mean particle area and volume respectively.

Hence the calculated value for the total surface area was 7.68×10^2 cm^2 for 5.000 gm of the 100 - 200 # size fraction of pyrite. The actual reaction rates at different temperatures could thus be determined from table VI ;

Table XI.

	Temperature °C				
	80°	90°	100°	120°	150°
Initial rate of sulphate (g) produced per min. per cm^2 surface area $\times 10^5$	2.3	4.1	6.0	10.4	22.1

Fig 15. PARTICLE SIZE DISTRIBUTION

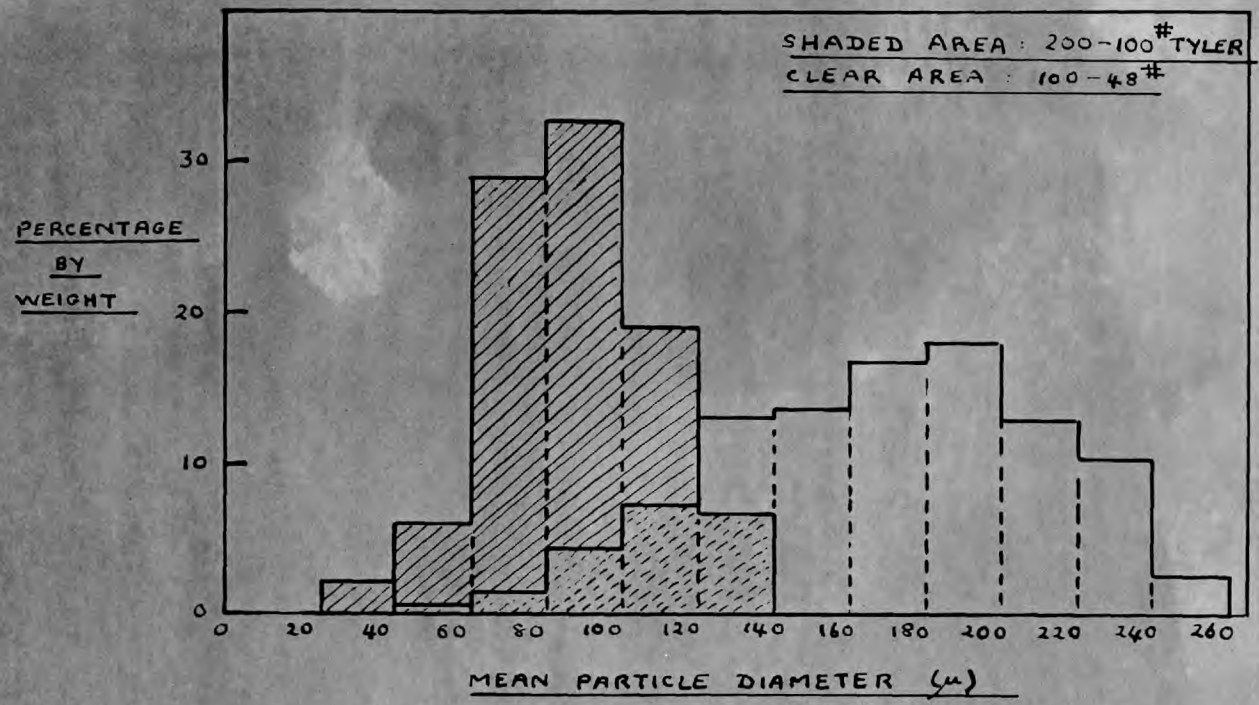


Fig 16. RELATION BETWEEN PARTICLE WEIGHT AND SURFACE AREA (PROGRESSIVE)

200-100# SIZE FRACTION

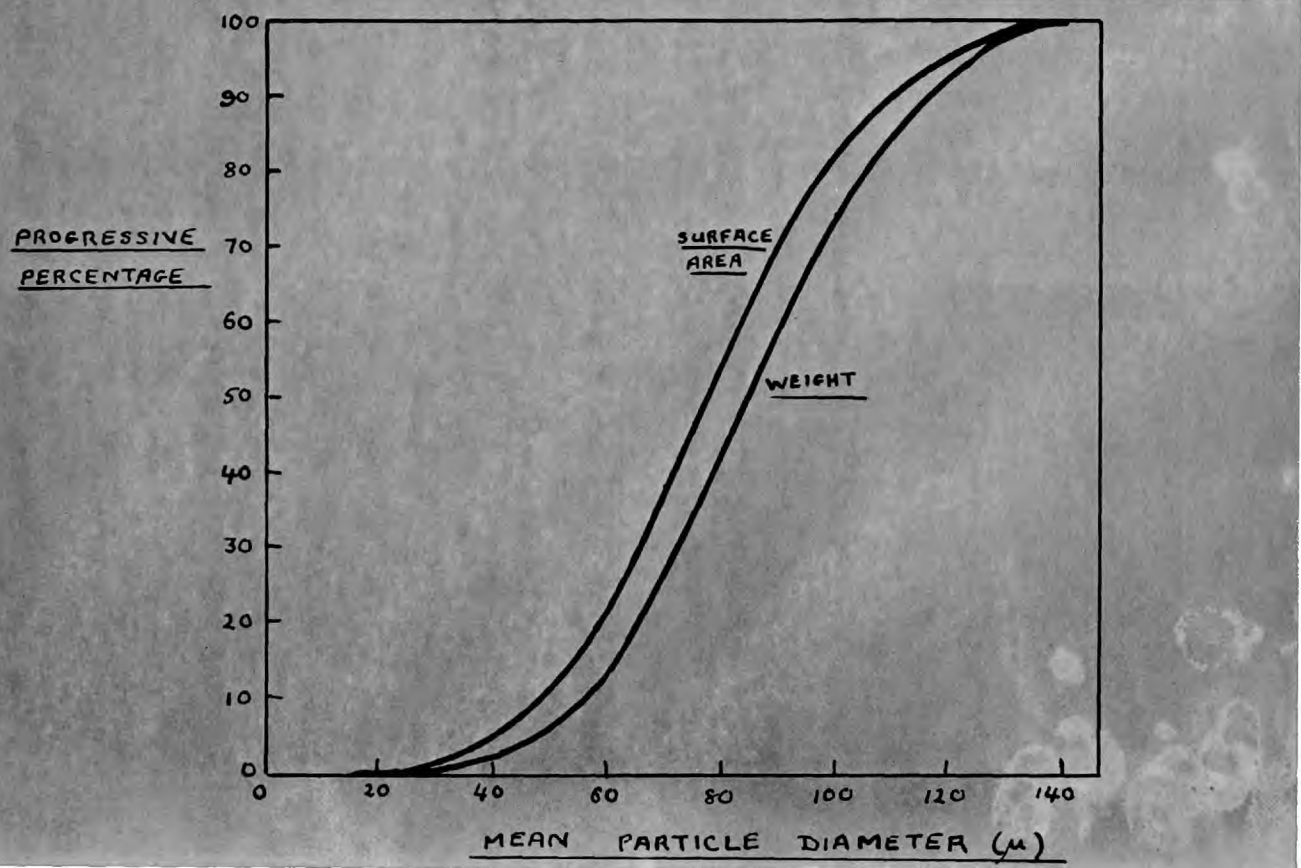


Fig 17. RELATION BETWEEN WEIGHT LOSS AND SURFACE AREA LOSS DURING REACTION

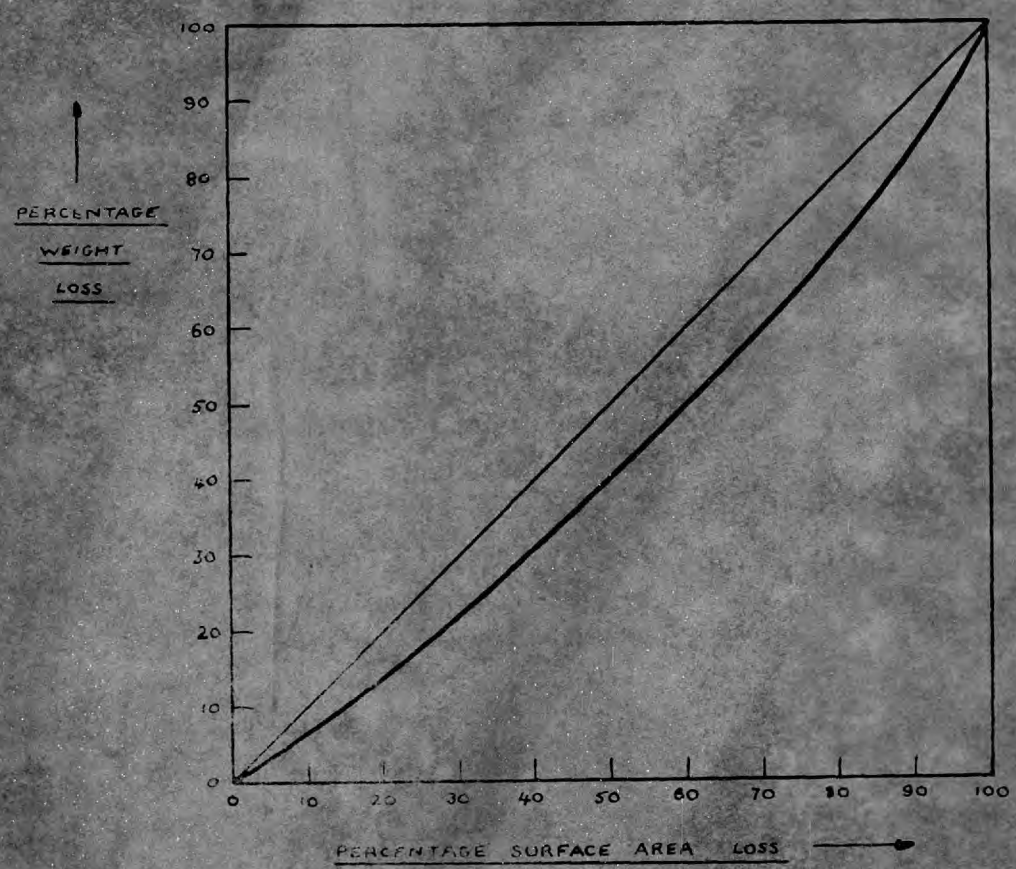


Fig 18. APPARENT REDUCTION IN REACTION RATE WITH TIME

PYRITE : CASSANDRA.

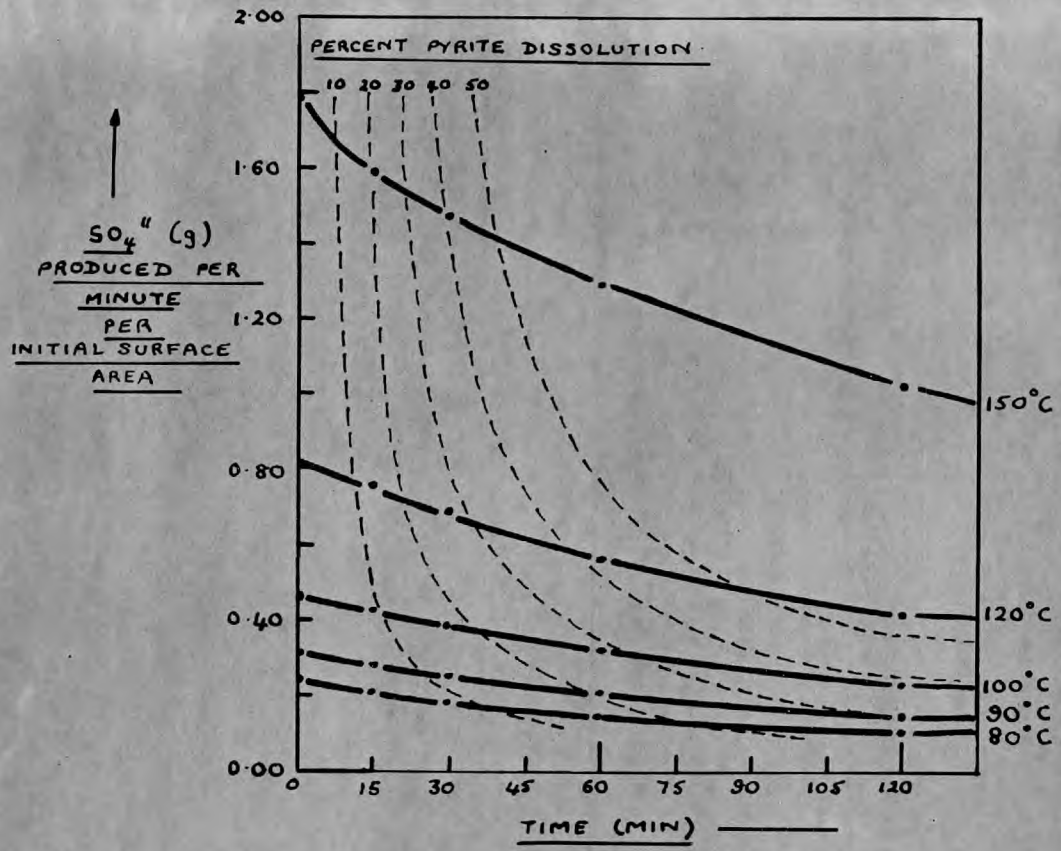


Fig 19. DEVIATIONS FROM ARRHENIUS PLOTS USING ABOVE VALUES

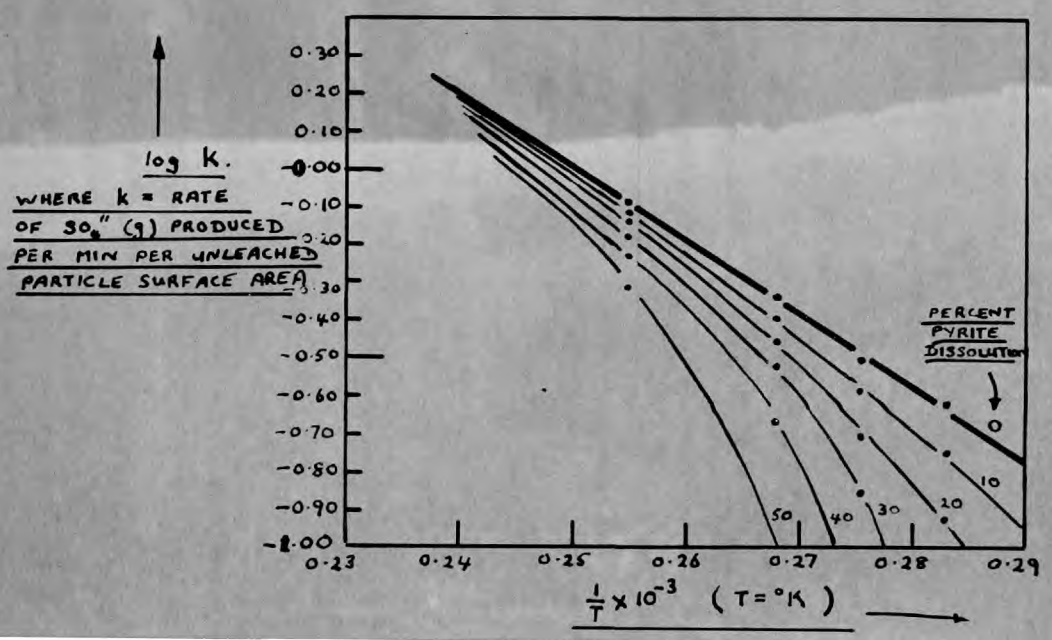


Fig 20.

SURFACE AREA IN RELATION TO PERCENTAGE PYRITE DISSOLUTION

PYRITE : CASSANDRA

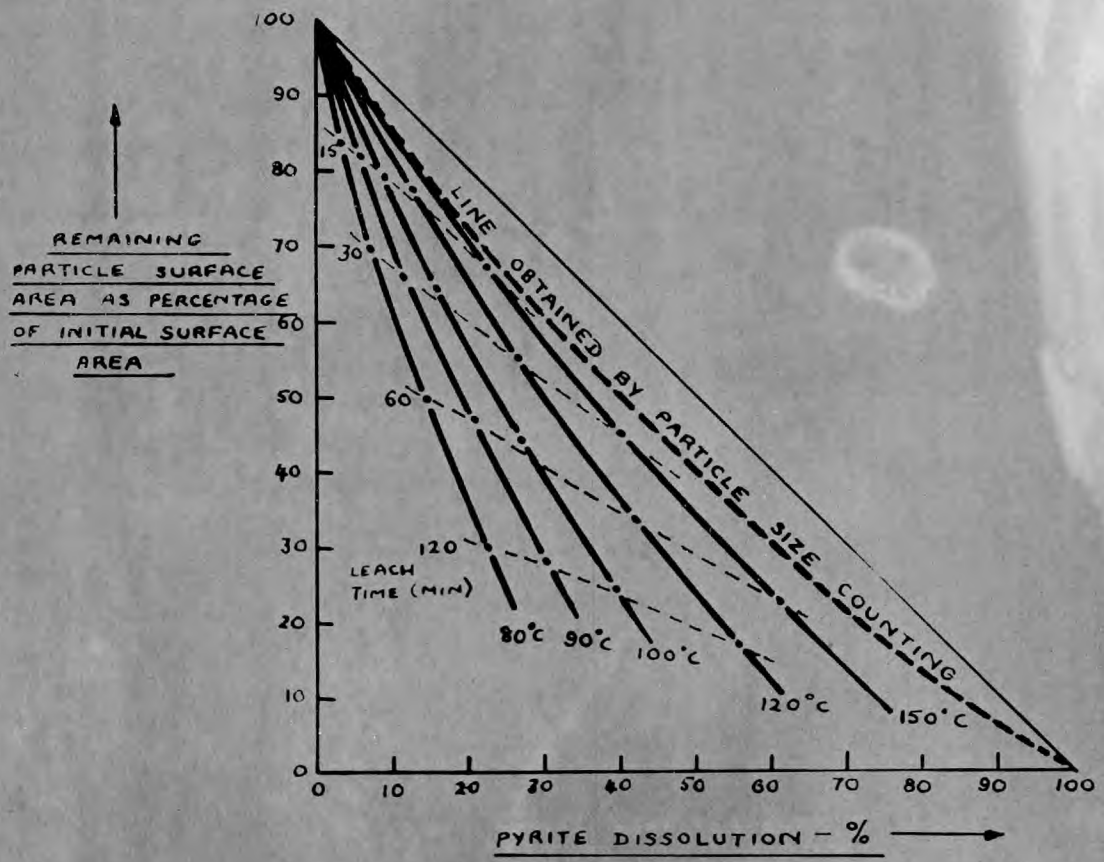
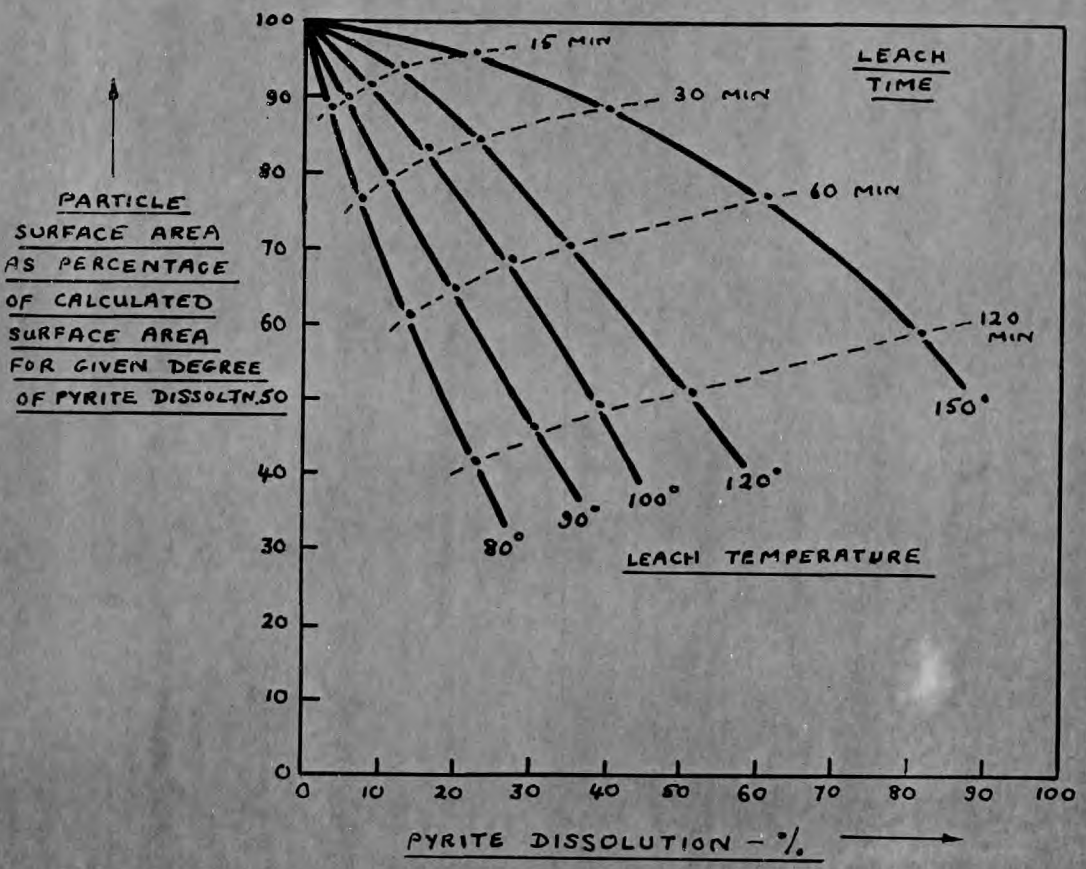


Fig 21. SURFACE AREA IN RELATION TO PERCENTAGE PYRITE DISSOLUTION

PYRITE: CASSANDRA



3.4. Study of Leach Residues.

3.4.1. Microscopic Examination.

Observations made by microscopic examination of polished cross-sections of residual particles, after leaching, have provided valuable evidence in elucidating the mechanism of oxide formation and mineral dissolution. After leaching, the residue was dried and residual traces of adherent oil removed by washing with ethanol. The residue was then cast in a rapid setting resin ("Ceemar" - see page 187) and abraded, to produce a highly polished surface, with a 0-0.5 micron diamond paste as the final stage in polishing. Pyrite is very hard and oxide products somewhat softer so that with relief effects and colour differences, the oxide phases were clearly visible and no etchant was required.

A. Cassandra pyrite: As mentioned earlier, the outward appearance of the leach residue showed, predominantly, particles free from any adherent coating. This was confirmed by microscopic examination and it was found that an adherent coating existed only about particles with jagged edges or along faults in the crystal structure. This is in agreement with the conclusions made earlier, that the coating appeared to be physically held in contact with the pyrite, at least after cooling and preparation for microscopic examination.

In figs. 22 - 25, photomicrographs show where the coating has been formed about particle edges, and examples of penetrations along crystal defects where extensive pyrite dissolution by reactant ions has taken

place into the body of the crystal. These penetrations are quite common and were found in about 20% of the particles examined. In fig. 22, which is an example of the adherent coating about a jagged edge at 1800 X magnification, the coating appears to have broken away from the surface and exhibits a thick dense blue layer facing the mineral and a thin red layer on the outside. This breakaway of oxide almost certainly occurred when the residue had attained the appreciable thickness shown, as the coarsely crystalline blue iron oxide layer could not have been precipitated from solution as such, owing to the extreme insolubility of iron oxides. (The solubility products of ferrous and ferric hydroxides are 1.0×10^{-14} and 1.1×10^{-36} respectively).

Further evidence for this will be dealt with later when the large-scale penetration of reactants into Rio Tinto pyrite is discussed.

Figs. 23 - 25 show examples of penetrations into the body of the crystals with fig. 23 showing an outer edge as well. The oxide along the line of penetration consists of the same dense blue oxide and a finely grained product between the mineral and the oxide, also blue in colour, the red outer layer being only found about the exposed particle outer edge. These penetrations are formed about holes in the crystal, usually in a straight line along a plane in the crystal, and frequently deviate as in fig. 24 where it appears to have forked out in two directions. These penetrations show how the advance of reactant ions took place on a roughly even front conforming with the crystallographic configuration.

B. Premier pyrite. This mineral exhibited the same behaviour as the Cassandra pyrite with, however, a greater number of penetrations into the mineral. Fig 25 is a particle shown with exposed surface and a number of penetrations into the crystal.

C. Rio Tinto pyrite. Microscopic examination of this ore has shown extensive penetration into the crystal both along defects as above and over selected areas of the mineral. Figs. 26 - 28 show colour photomicrographs of the partially leached residue. In fig. 26 the inward growth of oxide product is clearly shown pseudomorphic with the original pyrite surface, the original pyrite edge being well defined. The dense blue oxide has largely broken down at the pyrite-oxide interface. This is a comparatively rare case in which the Rio Tinto pyrite was observed to shown a distinctly crystalline outer edge.

In fig. 27, large areas have been replaced by oxide and, as in all cases, the breakdown, between dense oxide and retained pyrite at the oxide-pyrite interface, to a fine grained structure is shown. Similar behaviour is shown in fig. 28, together with an example of grain penetration in the centre of the picture similar to that noted for the Cassandra and Premier particles described above.

As mentioned earlier, so coarsely crystalline a product would not have been deposited from solution. The dense blue oxide product therefore provides evidence that oxidation takes place by a topotactic transformation from the parent pyrite mineral structure to that of the oxidation product. Based on this conclusion, the fine-grained material

between dense oxide product and pyrite must have been caused on cooling after leaching, when the crystallographic continuity at the interface, between pyrite and final product, had been disrupted.

Possible explanations for the mechanism of formation at restricted sites can be based on ;

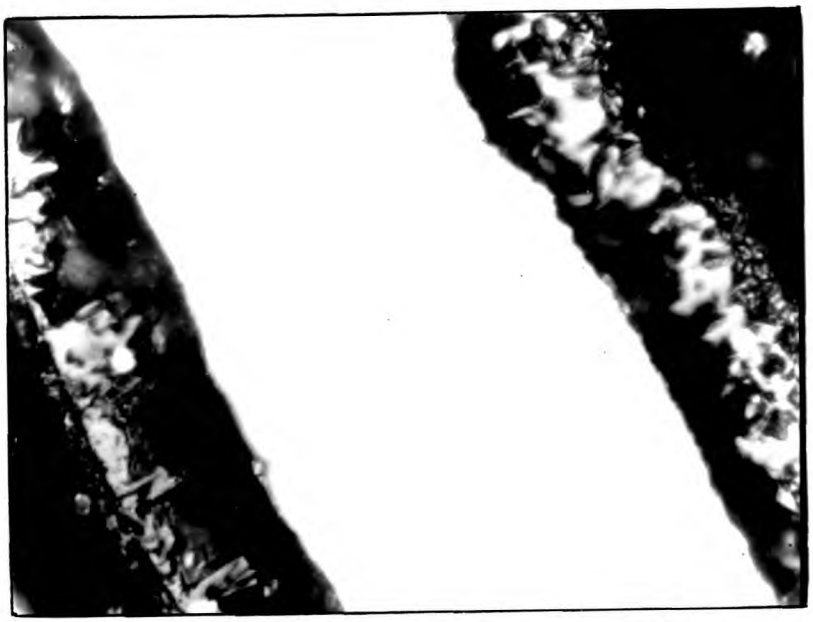
i) A lattice distortion caused by the presence of foreign metal ions.

ii) Vacancies in the lattice caused by a deficiency of sulphur atoms in the halide structure of the pyrite.

iii) Concentrated replacement of more reactive foreign minerals in the structure and about grain boundaries.

These points will be discussed.

Pyrite: Cassandra.



1800 X

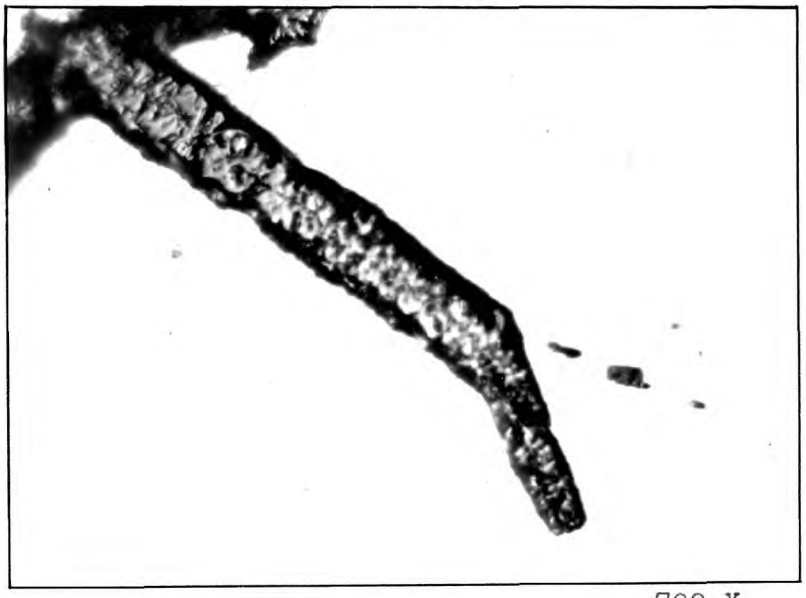
Fig 22. Weakly adherent coating on particle.



1000 X

Fig 23. Penetration along defect.

Pyrite: Cassandra.



700 X

Fig 24. Penetration along defect.

Pyrite: Premier.

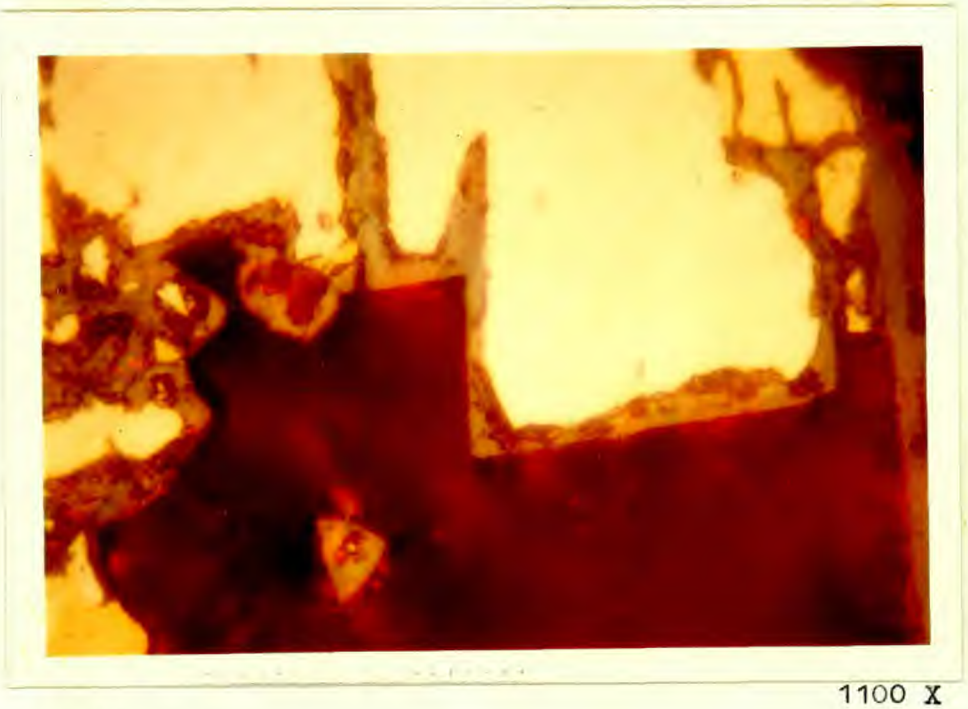


1000 X

Fig 25. Penetrations along defects.

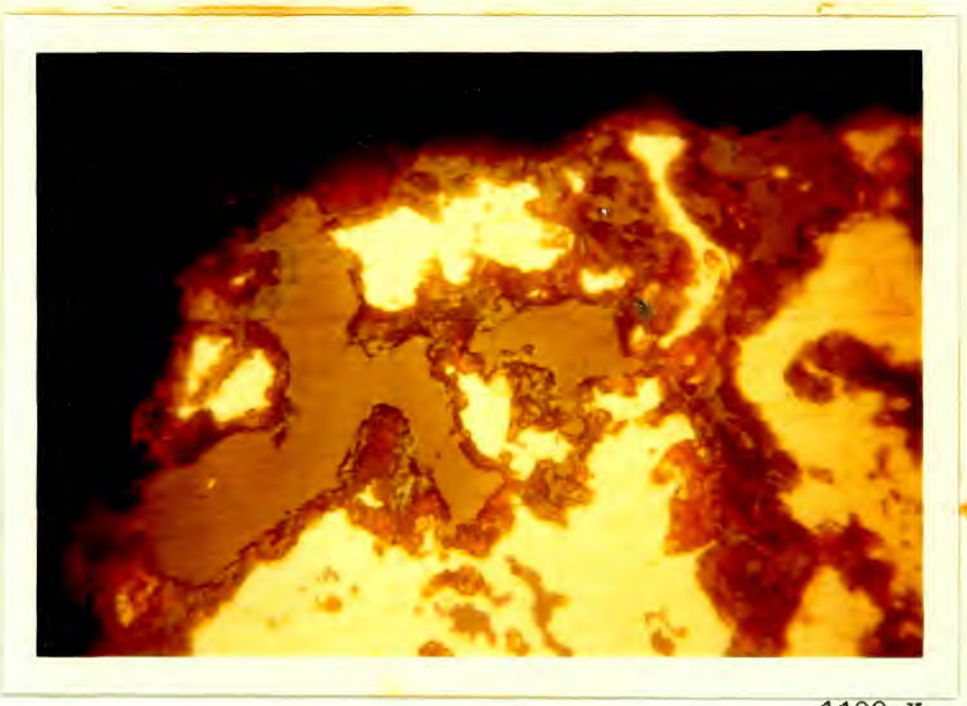
Replacement of pyrite by iron oxide.

Pyrite: Rio Tinto.



1100 X

Fig 26.

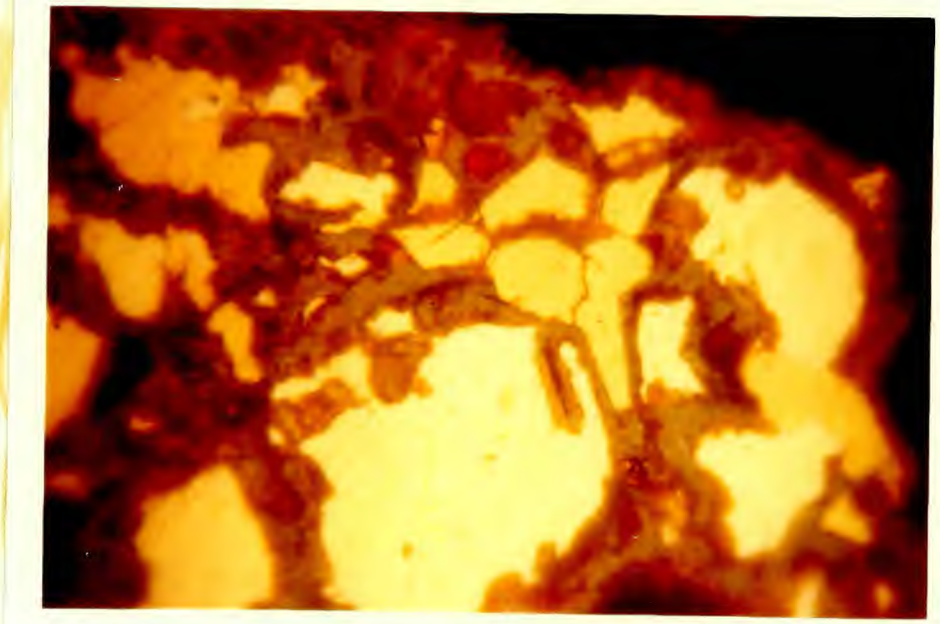


1100 X

Fig 27.

Replacement of pyrite by iron oxide

Pyrite: Rio Tinto.



1100 X

Fig 28.

3.4.2. Examination of leach residues using the Cambridge Microscan X-ray Analyser.

The polished specimens of the leach residues were examined using the Cambridge Microscan X-ray Analyser, after coating with a thin conduction film of aluminium. This instrument can provide the following information ; (53) ;

i) A picture of a surface can be obtained on a cathode ray screen based on the reflectance of the surface to electrons. The intensity of the picture depends on the atomic numbers of the elements present and the density of the atomic spacing in the surface.

ii) A similar picture can be obtained, based on the X-rays emitted by the electrons. The X-rays are passed through a monochronomator so that the distribution of any one of heavier elements in the surface can be seen pictorially.

iii) An electron beam less than 1 micron in diameter, can be made to scan along a line across the surface of the specimen. The X-rays produced by any element with atomic number greater than about 12, are separated and counted, giving a trace on the cathode ray screen. This gives a semi-quantitative estimate of the element concentration in the surface along that line.

iv) The electron beam may be left stationary and the X-rays, emitted from the spot counted to give a quantitative analysis at that spot.

A. Cassandra pyrite. Observations were made on a thin particle, similar to the photomicrograph shown in fig. 22. Photographs are shown in fig. 29 in which the retained pyrite is the uniform grey surface, surrounded by the oxide coating. The highly reflecting area in the top right hand corner is due to a small particle of galena. In figs. 29b and 29c, the iron and sulphur X-ray pictures are shown, and indicate, by the intensity of the characteristic X-ray emission, the relative concentration of the element in question, both in the mineral and in the coating. As shown, the iron is enriched in the coating and sulphur has been almost completely removed.

The iron X-ray scan across the pyrite and oxide surface, fig 29d, shows graphically the relative concentrations of iron in pyrite on the right, the depletion of iron in the area of oxide breakaway from the surface, the higher concentration of iron in the blue dense oxide coating and the lowering of iron in the more diffuse thin red outer layer.

Quantitative analyses using the X-rays produced by a stationary X-ray beam gave 70% and 47% iron in the inner and outer layers respectively. The possible products are $Fe(OH)_2$, 62.1%; FeOOH, 62.8%, Fe_2O_3, 70% Fe. It is most probable therefore, that the blue oxide compound is Fe_2O_3 or tends to that composition, and the outer red coating, an oxidation product, which has broken up leaving small spaces containing no solid, so that the iron seen by the electron beam occupies only part of the beam area, giving a low value for the iron

content. The product after leaching under all conditions, was ferromagnetic.

An example of penetration along defects, as shown in figs. 23 - 25, has been analysed using this instrument and observations are shown in fig. 30 with the enriched iron concentration and complete absence of sulphur in the penetration product clearly shown. The line of scan is shown as the white line across the electron image.

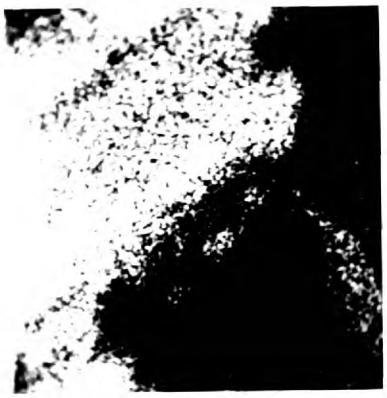
B. Rio Tinto pyrite. A particle magnified 700 times is shown in fig. 31a, in which the iron oxide products are present as large areas similar to the photomicrographs, fig 27. Oxide products were difficult to distinguish from retained pyrite areas owing to the almost similar degree of electron reflectivity of both compounds, but do show clearly in fig. 31c, the sulphur X-ray picture, that this element is absent in the oxidised area of the particle. Changes in composition are not clearly distinguishable in the iron X-ray picture, fig. 31. The area in which iron is absent in fig. 31 near the bottom edge of the particle was found to be occupied by the mineral sphalerite as an inclusion in the grain.

An iron and sulphur distribution scan from left to right across the particle is shown in fig. 31d, with the iron enriched areas in the oxide shown and the complete absence of sulphur in the same area.

Fig 29.
PRESSURE LEACHING OF PYRITE (CASSANDRA)



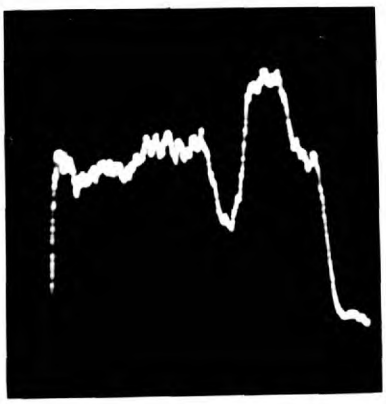
a. ELECTRON IMAGE



b. Fe X-RAY IMAGE



c. S X-RAY IMAGE



d. Fe X-RAY SCAN

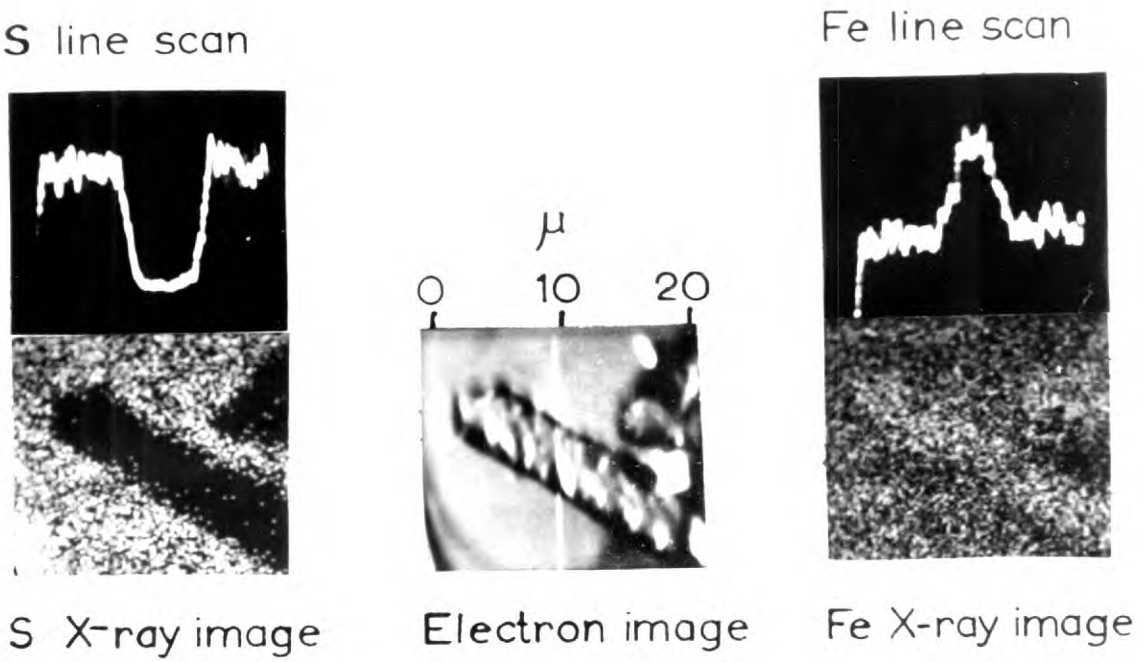


Fig 30. Penetration along defect.

Pyrite: Cassandra.

In the series of observations shown in fig. 32, a section of a leached particle has been magnified 2500 X and shows an area of retained pyrite surrounded by a halo of the uniform blue oxide product mentioned above. As before, the sulphur rich pyrite areas can only be distinguished from the oxide in the sulphur distribution X-ray picture, fig 32b. No variation in iron distribution can be seen in fig. 32c. However, in the X-ray scans across the large retained pyrite area in the upper left hand corner, shown in figs. 33d and 33e, the iron concentration is slightly higher in the immediate surrounding area and the sulphur content drops abruptly.

By counting the emission excited by the characteristic iron and sulphur X-ray values at progressive points along the same line of scan, the distribution of each element could be plotted on a quantitative basis. These plots show in fig. 33, the enrichment of iron at the expense of sulphur and the replacement of sulphur by oxide (or hydroxide), toward the edge and across the area of oxide breakdown. The electron beam was approximately 1 micron in diameter so that some overlap between oxide and pyrite would be expected with the change more abrupt than indicated by the graph. However, an impoverishment of sulphur is shown in the retained pyrite crystal, approaching the edge, and in the area of oxide breakdown, there is a narrow diffusion gradient as the sulphur becomes rapidly lower in concentration.

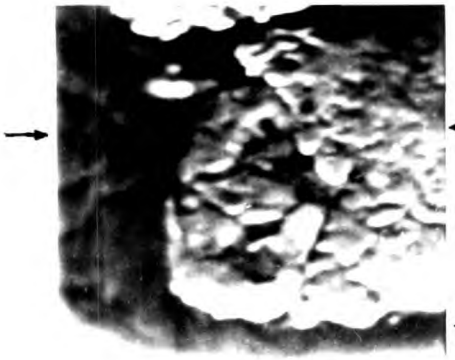
When a series of iron and sulphur counts was made over a number of retained pyrite areas, the mean sulphur count was of the order of 53%, iron making up the difference, whereas a number of random

sulphur counts made on the unleached ore (Rio Tinto) showed a considerable variation in sulphur content with 53% as a maximum value. This value of 53% is the same as found for the Cassandra pyrite but there was a very consistent correlation of sulphur counts selected at random over a surface of the unleached ore. This lowering of sulphur concentration in some areas is evidently due to impoverishment of sulphur atoms in the co-ordinately bonded S_2 sites of the halide structure of pyrite, as no other element was found to make up the deficiency. This therefore indicates that pyrite is more reactive in areas lower in sulphur and replacement of sulphur by reactant ions was more rapid in these areas. Similarly, this is probably the case where grain penetration has taken place in Cassandra and Premier crystals at sites in the pyrite lattice deficient in sulphur.

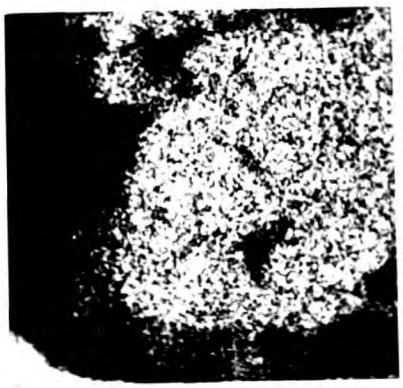
Therefore, in consideration of the possible reasons for the acceleration of reaction at restricted areas, given on page 115, a deficiency of sulphur provides the most probable explanation. The presence of foreign metal impurities as the corresponding sulphides tends to discount possibility (1) since the pyrite always gave a negative count for the foreign metals found to be present in the ore, though their presence in microscopic quantities at grain boundaries as a possibility, cannot be eliminated. The possibility of more reactive foreign minerals, cited in point (iii), may also be discarded, as the product of dissolution only showed iron as being present with atomic weight greater than 12.

Fig 31

PRESSURE LEACHING OF PYRITE (RIO TINTO)



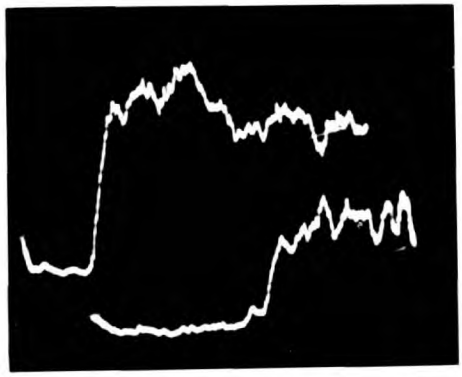
a. ELECTRON IMAGE



b. Fe X-RAY IMAGE



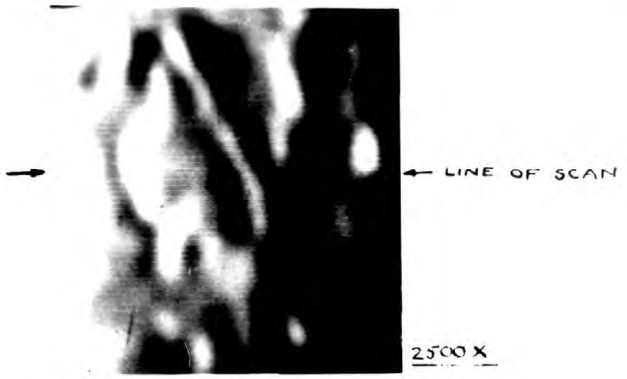
c. S X-RAY IMAGE



d. Fe AND S X-RAY SCAN

Fig 32

PRESSURE LEACHING OF PYRITE (RIO TINTO)



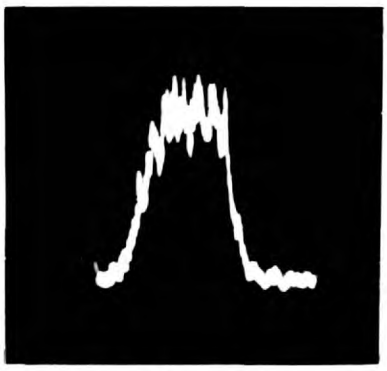
a. ELECTRON IMAGE



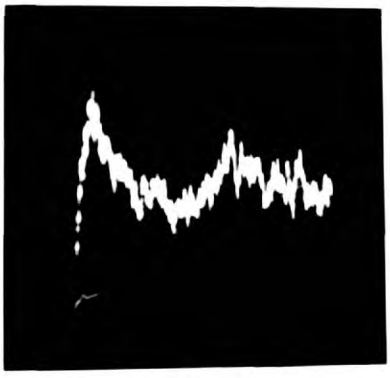
b. S X-RAY IMAGE



c. Fe X-RAY IMAGE



d. S X-RAY SCAN



e. Fe X-RAY SCAN

Fig 33 -

DISTRIBUTION IRON AND SULPHUR IN PYRITE AND ADJACENT OXIDE COATING

PYRITE RIO TINTO

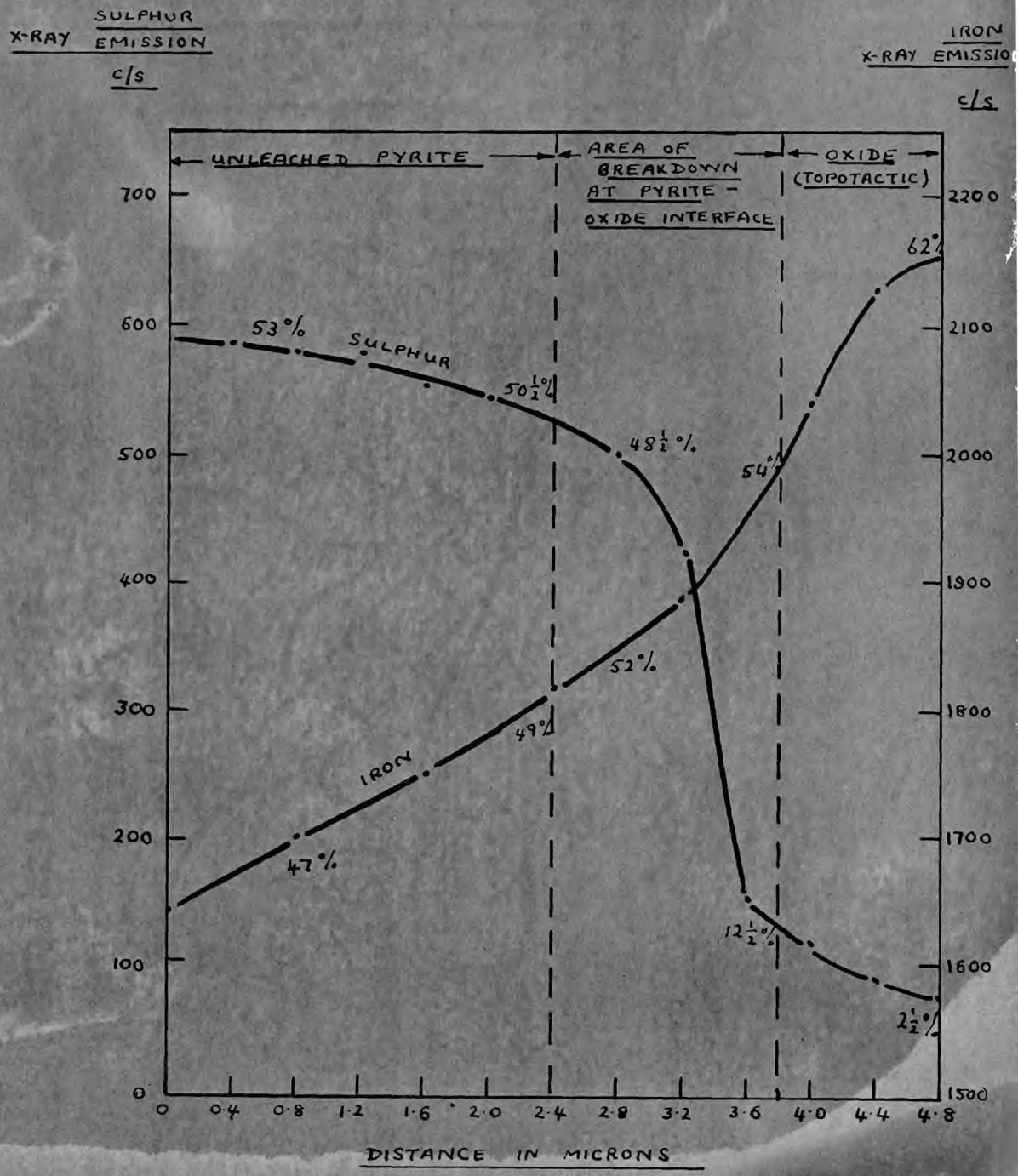
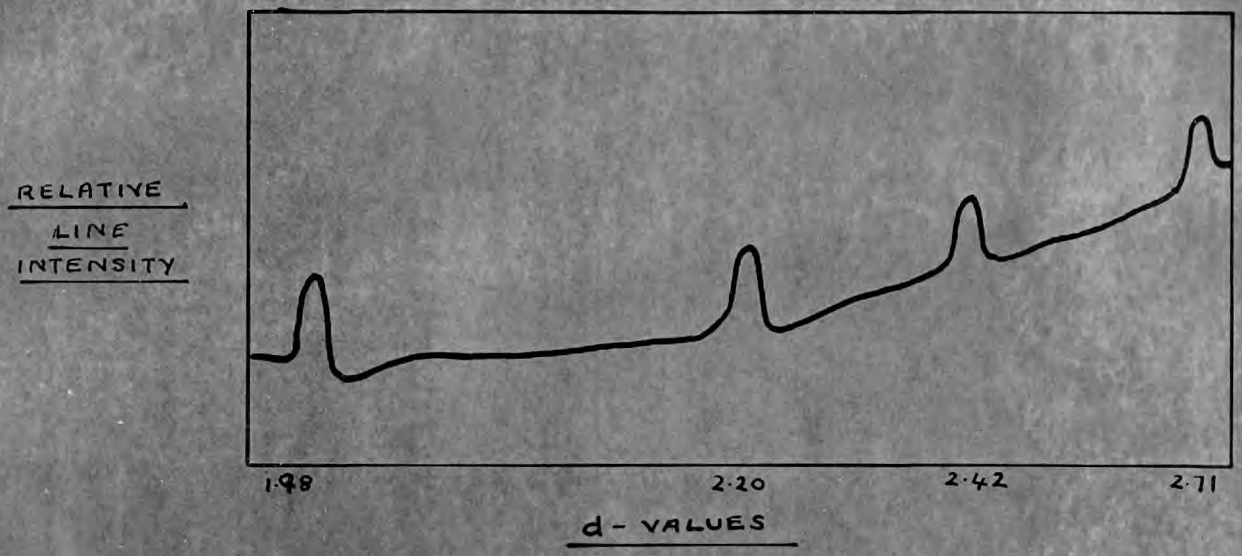


Fig 34.

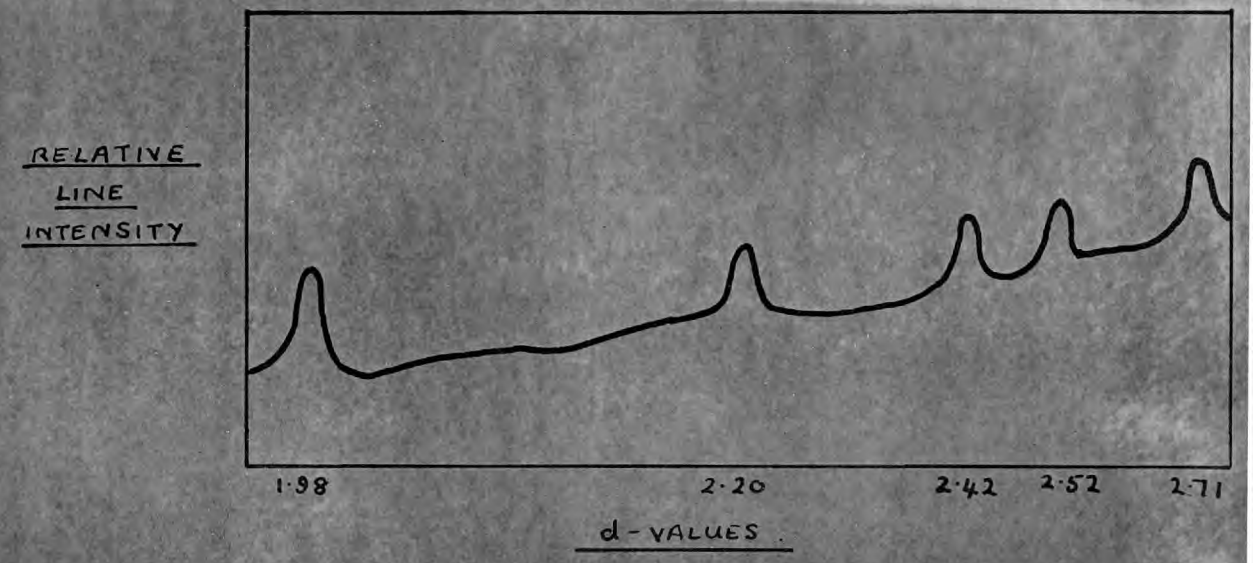
RELATIVE LINE INTENSITIES FROM X-RAY POWDER DIFFRACTION PHOTOGRAPH

PYRITE : RIO TINTO

UNLEACHED PYRITE



PARTIALLY LEACHED PYRITE



3.4.3. X-ray powder photographs

X-ray powder photographs were made, using a cobalt target, to ascertain the nature of the coarse blue oxidation product. Generally, iron oxidation products, when deposited in alkaline solutions, are so fine grained that it is seldom possible to obtain any X-ray diffraction pictures owing to the considerable amount of absorption and scatter that takes place. However, with the partially leached Rio Tinto pyrite (ca 50% dissolution) a definite, line was obtained with d-value of 2.52A which was not found in the unleached pyrite, in which the characteristic pyrite lines in order of density, 1.63A, 2.71A, and 2.42A, were found. The 2.52A value as shown in fig. 34 indicates an intensity about the same as the 2.42A pyrite value. This was the only finite line found, apart from the pyrite lines, after leaching, in the range of d-values from 0.9 to about 4 A. Good pictures were comparatively difficult to obtain owing to the large degree of scatter by the fine iron oxide product and the coarseness of the ore (200 - 100 mesh) used.

The pyrite lines are in perfect agreement with values cited in the ASTM index of X-ray Diffraction Data series (4). A series of ASTM values for iron oxides and hydrated oxides is given in table XII. From the values given, only the oxide, γFe_2O_3, gives its most prominent line at 2.52A and the other lines in order of intensity are considerably

weaker at 53% at 1.48A and 34% at 2.95A compared with the strongest line. This indicates that the oxide product had passed through a series of transformations terminating as the coarse blue oxide, maghemite; (Although the ferric oxides normally appear reddish in colour, they are blue when coarse grains are examined under the microscope).

The densities D, of iron oxide products, relative to that of pyrite, taken as unity have been calculated using the relation ;

$$D = \frac{Z.M}{a^3} \qquad (68)$$

where, Z is the number of formula units per unit cell with cell length, a, obtained from table I, and M is the molecular weight of the mineral.

Hence, the relative densities of FeO, Fe_3O_4 and γFe_2O_3 are: 1.18, 1.03 and 0.98 respectively.

Table XII

A.S.T.M. d-values obtained by X-ray powder diffraction studies (4)

Composition	Most prominent d-values			Relative line density		
* FeO	2.15	2.49	1.52	100	80	60
* γFe_2O_3	2.52	1.48	2.95	100	53	34
δFe_2O_3	2.19	1.69	2.53	100	100	80
Fe_3O_4	2.53	1.48	1.61	100	80	64
$\alpha Fe_2O_3H_2O$	4.18	2.45	2.69	100	80	80
β FeOOH	3.33	2.55	7.40	100	75	63
* $\beta Fe_2O_3H_2O$	3.33	7.6	2.55	100	85	80
* $\gamma Fe_2O_3H_2O$	3.27	7.3	2.56	100	90	80
$Fe(OH)_2$	2.42	4.61	2.82	100	80	50
* FeS_2	1.63	2.71	2.42	100	84	66

SECTION 3 cont.

LEACHING OF WOLFRAMITE

The behaviour of Wolframite $(Fe,Mn)WO_4$ has been studied when leached in 0.50 N sodium hydroxide and sodium carbonate solutions at temperatures from 100 to 150°C and at air pressures from zero to 250 p.s.i. Leach reaction times varied from 30 to 240 min. In contrast with the pyrite system, appreciable reaction took place when trace amounts of oxygen were present in the system, and the reaction rate increased rapidly with increase of sodium hydroxide concentration from 0.50 M to 2.50 M. at 50 p.s.i. air pressure. Because of this dependence on alkali concentration, the leaching of wolframite, in industrial practice, is carried out with concentrations of alkali as high as 10 to 12.5 N at the solution boiling point, the alkali being either sodium hydroxide or sodium carbonate (68) (40) (15). Such drastic conditions were not suited to this investigation since the increased solubility of iron and manganese oxidation products of reaction preventing their being precipitated as an adherent coating on unleached wolframite. The deposition of these oxides away from the surface as the amorphous hydrated oxide does not inhibit the reaction as would an adherent coating which controls the diffusion of reactant ions through it. The employment of 0.50 N solutions of both sodium hydroxide and sodium carbonate has enabled studies to be made of the

behaviour of the coating deposited, in situ, on unleached wolframite, particularly with respect to the marked change in porosity of the oxide product with change of oxygen partial pressure. This has necessitated the use of high rates of solution agitation throughout the series of experiments in order to prevent diffusion from the liquid-gas to the solid-liquid interface being rate controlling. The same reaction vessel was used as in the pyrite system.

Analyses, for determining the extent of mineral decomposition, were made by weighing the amount of tungstate produced in solution as the trioxide, WO_3, after precipitation from the leach liquor with cinchonine (See section 5.3.2.)

As in the pyrite system, the expected heterogeneous behaviour of the mineral during leaching necessitated the employment of a graded ore after grinding, the size fractions used in this investigation being 100-200 mesh, Tyler and 200-325 mesh Tyler. Either 5.000 or 10.000 g of ore was used and the solution volume was maintained at 750 cc. Due to the considerable degree of reaction that took place when oxygen was present in the system in very small quantities (less that 3 p.s.i.), the reaction times could not be as accurately controlled as for the pyrite system. Reaction was unavoidable during heating and cooling to and from the required experimental temperature. To reduce this effect to a minimum, the autoclave was heated to the operating temperature as quickly as possible, (ca 10 min to 150°) and the times of heating and cooling were maintained

constant throughout the series at the required temperature. The leach residues, in all cases, were found to be strongly ferromagnetic.

The experimental results are discussed below ;

3.5. Leach Reaction Variables

3.5.1. Effect of particle surface area.

The extent of mineral dissolution is directly related to the surface area of the mineral particles. The following results were obtained using different weights of the same size fraction of wolframite and equal weights of mineral of different size fractions. The relative surface areas of the samples were measured by microscopic particle size counting, (see page 99), an approximate method.

Table XIII

Run	Particle size Mesh Tyler	Weight of ore (g)	WO_3 produced (g)	Relative surface area Experimental	Calculated
48	200 - 325	5.000	1.86	5.0	5.0
49	200 - 325	10.000	3.70	10.0	10.0
50	100 - 200	10.000	2.60	7.0	6.3

These experiments were carried out at 150° using 750 cc of 0.50 N sodium hydroxide solution and 50 p.s.i. air pressure the leach [illegible] time being 240 min.

The results indicate the direct dependence on mineral surface area s as would be expected for a heterogeneous reaction.

3.5.2. Effect of NaOH Concentration

The effects of changing the sodium hydroxide concentration from 0.50 N to 2.50 N have been investigated under the experimental conditions of 150°C and 50 p.s.i. air pressure, a leach reaction time of 120 min, and using 10.000 g wolframite in a sodium hydroxide solution of 750 cc. The results are plotted in fig . 35 and indicate a direct dependence on sodium hydroxide concentration if allowance is made for reduction in leached wolframite surface area. (92% of the mineral was decomposed at 2.50 N sodium hydroxide concentration.) Since virtually complete dissolution of wolframite in too short a time was not desired, later runs were carried out using 0.50 N sodium hydroxide solutions.

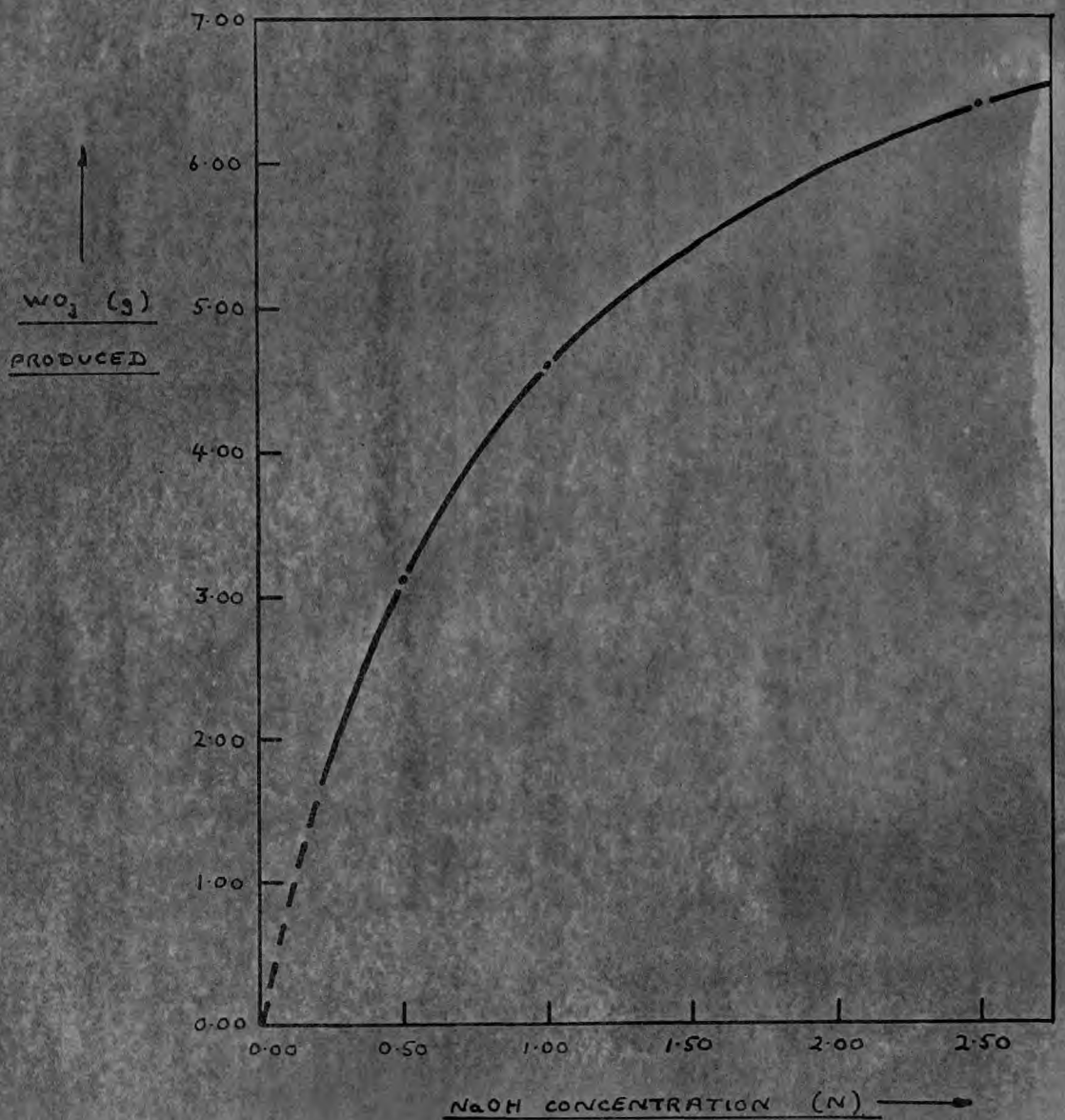
Results are tabulated below :

Table XIV

Run	NaOH Concentration N	WO_3 (g) produced
10	0.50	3.10
13	1.00	4.60
1	2.50	6.43

Fig 35

EFFECT OF SODIUM HYDROXIDE CONCENTRATION ON WOLFRAMITE DISSOLUTION



Calculations to establish the change of surface area with degree of wolframite decomposition, could not be made with any degree of accuracy, because of the substantial change in effective surface area during the reaction, caused by extensive reactant ion penetration along the cleavage planes of the mineral. Thus the same difficulty was encountered as that caused by the extensive penetration of Rio Tinto pyrite at more reactive sites. However, results do indicate that the rate of reaction is dependent on the sodium hydroxide concentration, and, as will be shown later, is not accelerated in any way be increase of oxygen partial pressure beyond very low concentrations.

3.5.3. Effect of air pressure with temperature variations.

The effect of oxygen partial pressure on the extent of reaction is complex and is shown in figs. 36 and 37 for solutions of sodium hydroxide and sodium carbonate, respectively. The curves are not comparable quantitatively since a 325 - 200 mesh grading of wolframite was used for the sodium hydroxide system and a 200 - 100 mesh grading of ore for the other, but do indicate that sodium carbonate reacted somewhat more readily with wolframite than did the hydroxide. In both cases at 150°C, there was a considerable lowering of the extent of reaction when the air pressure was greater than 15 p.s.i. and the presence of small quantities of oxygen produced very high degrees of mineral dissolution.

The results for the South Crofty wolframite are shown in fig. 38 and show a similar trend in behaviour though the lowering of the extent of mineral dissolution was not evident at 120 min leach reaction

time. However, at 120°, the extent of mineral decomposition did not increase much after 3 p.s.i. oxygen partial pressure, since further increases of oxygen pressures served only to oxidise the coating. In the absence of oxygen, i.e. leaching in an atmosphere of oxygen-free nitrogen, there was negligible decomposition by hydroxyl ions. This indicates that the wolframite used for the main body of experimental work was probably slightly oxidised before leaching, and, when leaching was carried out in the absence of oxygen, a sufficiently high oxygen potential was retained at the particle surface to maintain the reaction. The restricted quantity of South Crofty wolframite available, prevented a more detailed study being made but the results given do suffice to show the general trend of behaviour.

Hence, conclusions made were ;

i) The presence of small amounts of oxygen were essential in maintaining reaction. It would seem that oxygen used in the reaction was regenerated and behaved as a catalyst, since, in relation to the amount of oxide produced by the reaction, all oxygen would have been consumed at an early stage of the decomposition had it remained with the oxidation product after leaching.

ii) With increase of oxygen concentration, the large amount of excess oxygen reacted with the insoluble product of dissolution surrounding the unleached wolframite causing it to become practically impervious. This prevented further access to the unleached wolframite

surface by reactant ions when the coating had reached a substantial thickness. This reaction inhibiting effect became progressively greater, the higher the oxygen partial pressure of the autoclave gas space, (after 120 min the extent of wolframite dissolution was reduced from 71% at $1\frac{1}{2}$ p.s.i. oxygen to 32% at 50 p.s.i. oxygen pressure.) This depressing effect by oxygen became less marked at the lower temperatures and was not noticed at 100° .

Experimental results are tabulated below for the leach conditions of 0.50 N alkali concentration in 750 cc solution, 10.000 g wolframite being leached for 120 min. For the South Crofty wolframite 5.000 g of the 100 - 200 mesh mineral was used, other conditions being the same. The results of the latter have been multiplied by two for the sake of comparison.

Table XV

Temp. °C	O_2 pressure p.s.i.	WO_3 (g) produced			
		NaOH	Values corrected for 100 - 200 size fraction from fig. 43 NaOH	Na_2CO_3	South Crofty NaOH
180	10	5.08	3.8	-	-
150	50	2.2	1.2	2.55	5.8
150	10	3.10	1.9	3.54	-
150	3	4.70	3.4	4.90	4.8
150	0	2.75	1.65	2.63	-
120	50	-	-	0.98	3.4
120	10	2.06	1.2	1.06	3.4
120	3	2.0	1.2	1.55	3.2
120	0	1.29	0.6	0.80	0.2
100	50	0.87	0.4	--	-
100	10	0.88	0.4	0.40	-
100	3	0.67	0.35	0.57	-
100	0	-	-	0.39	-

When the values obtained for the sodium hydroxide series are corrected using fig. 43 for the 200 - 100 mesh size fraction the values obtained in table XV can be directly compared.*. Comparison shows that the South Crofty wolframite was a good deal more reactive. This explains the reduced inhibiting effect of the insoluble reaction product since the ratio of rate of oxidation of the coating to rate of mineral decomposed would have been much smaller.

---

* This is an approximate method and assumes constant change of surface area with percentage of mineral dissolution.

Fig 36. EFFECT OF OXYGEN PRESSURE ON WOLFRAMITE DISSOLUTION

SOLUTION: 0·50N SODIUM HYDROXIDE

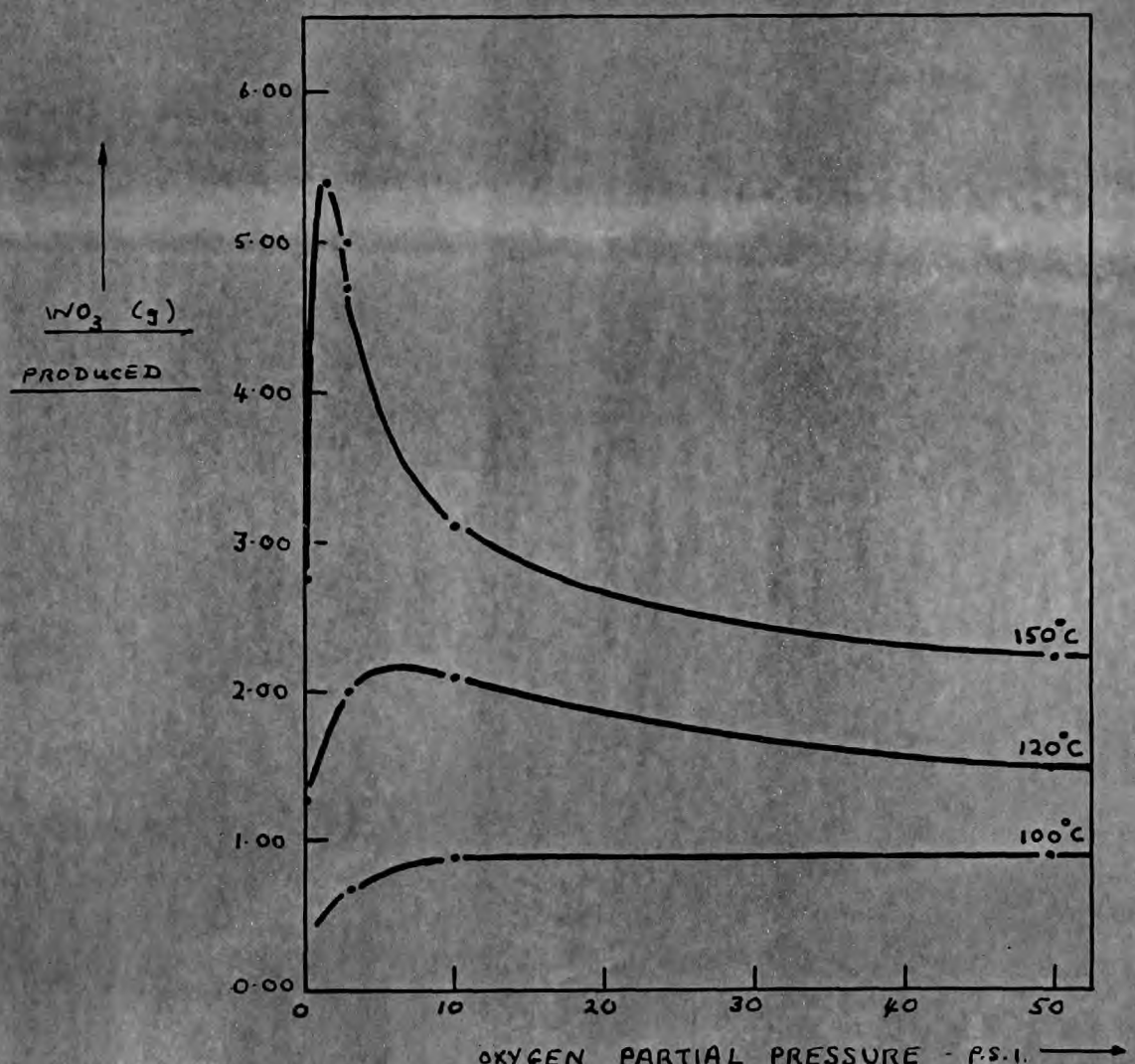


Fig 37. EFFECT OF OXYGEN PRESSURE ON WOLFRAMITE DISSOLUTION

SOLUTION: 0·50N SODIUM CARBONATE

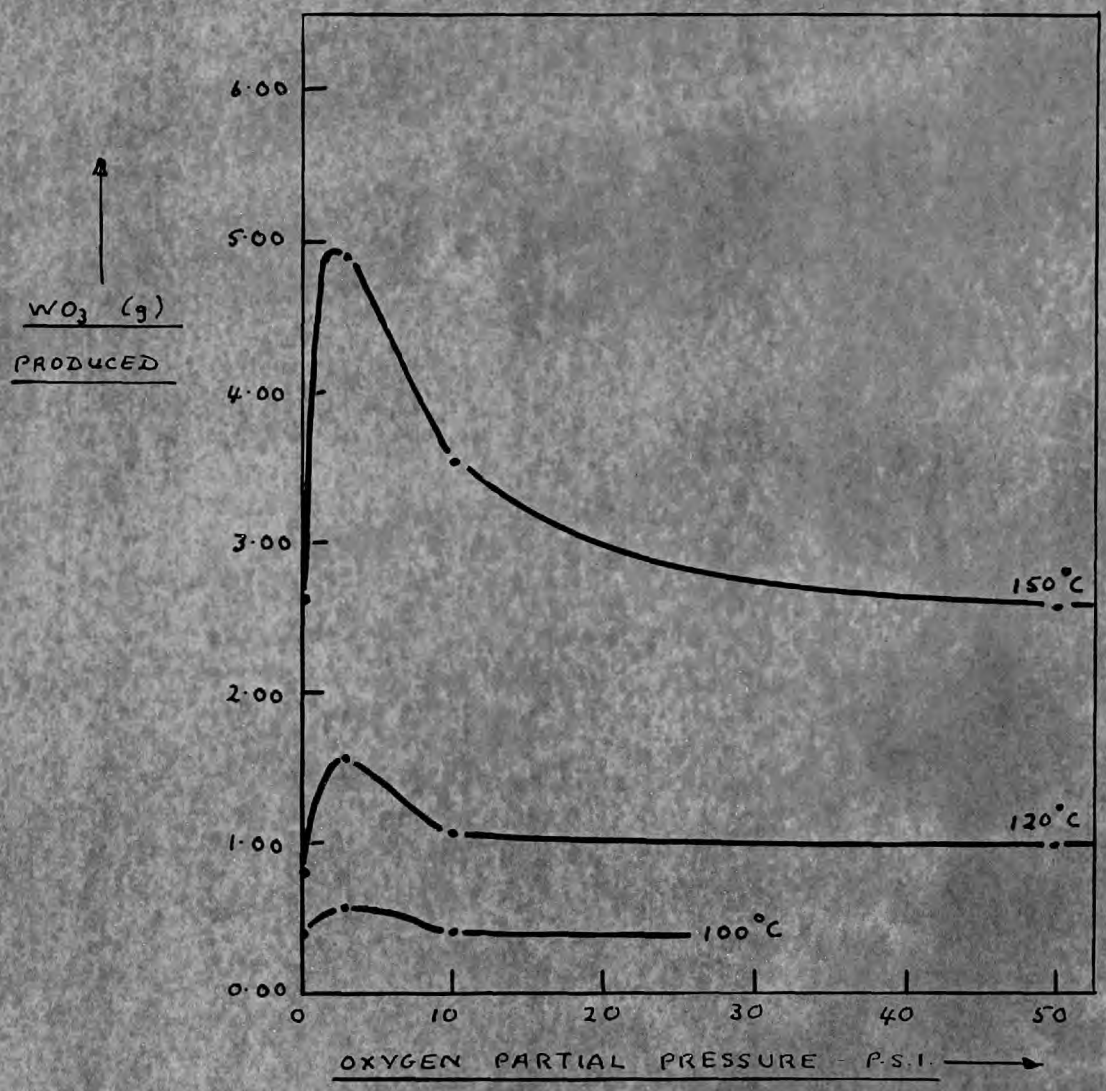


Fig 38. SOUTH CROFTY WOLFRAMITE

EFFECT OF OXYGEN PRESSURE

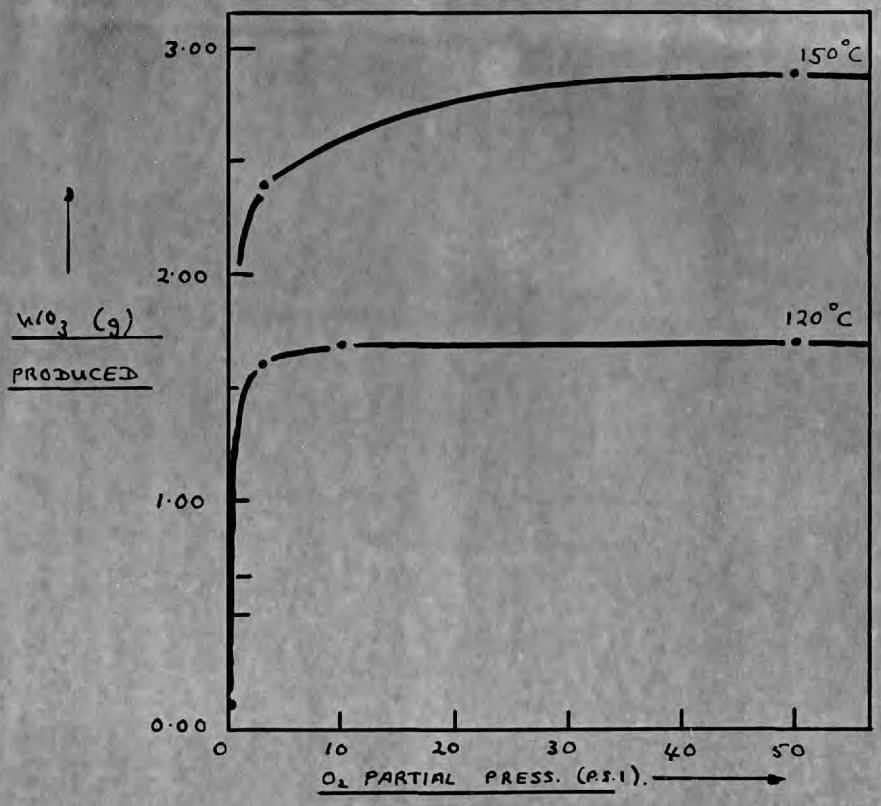


Fig 39. EFFECT OF REACTION TIME

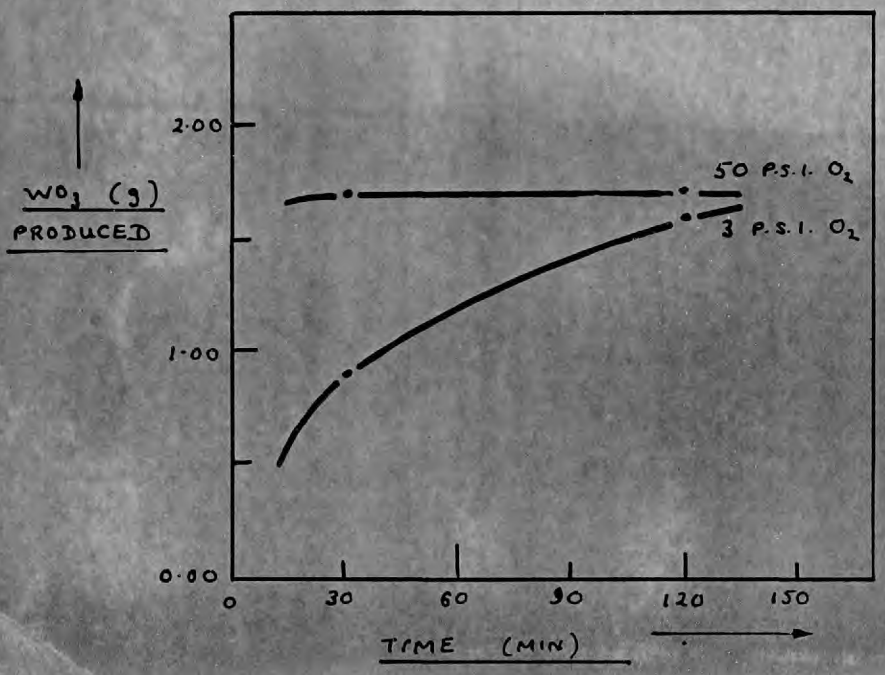
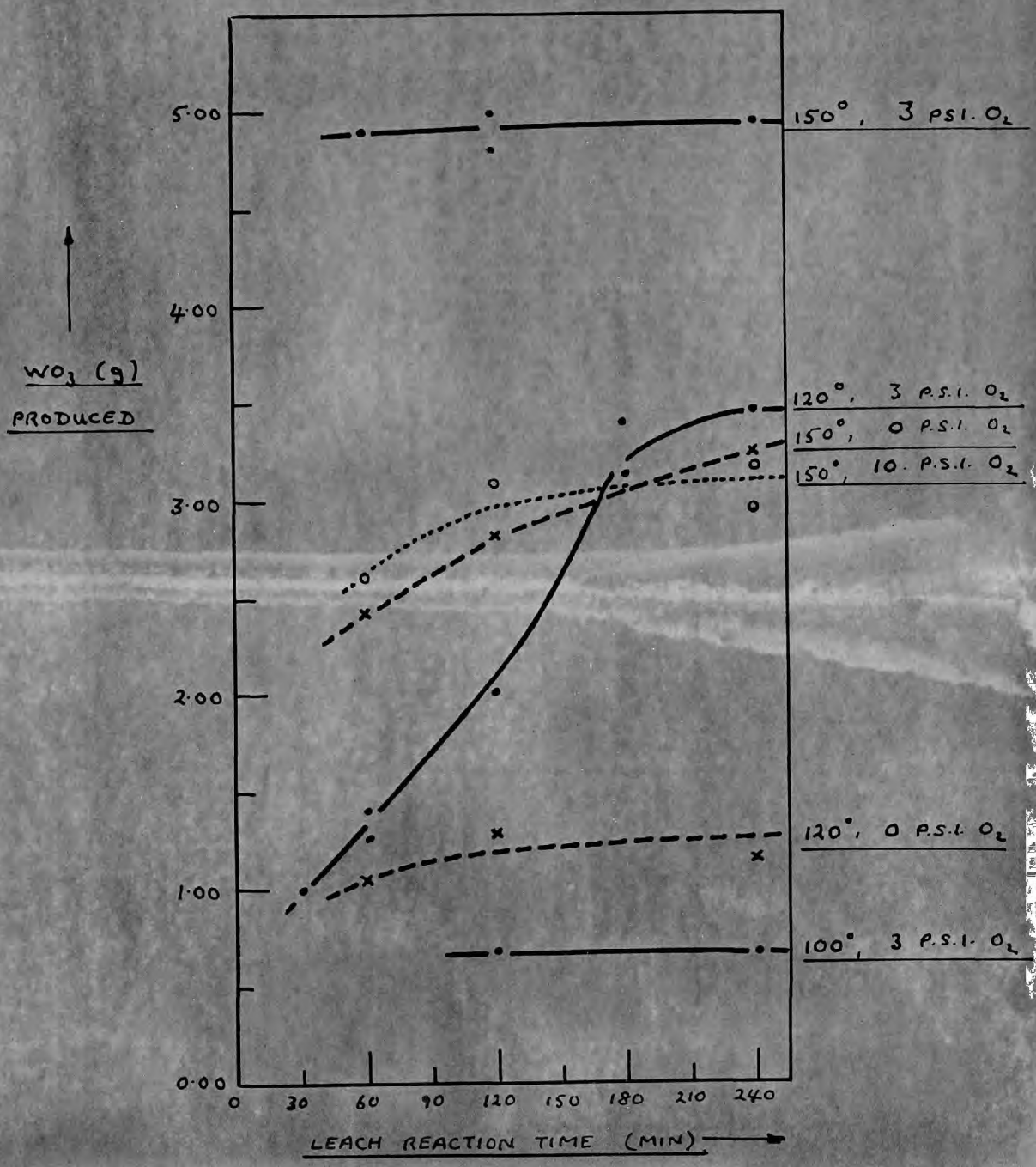


Fig 40. EFFECT OF REACTION TIME ON WOLFRAMITE DISSOLUTION



3.5.4. Effect of Reaction Time with Temperature variation

Experimental results plotted in figs. 39. and 40. show that the reaction between wolframite and reactant ions at the wolframite surface is very rapid and cannot be determined under the experimental conditions, since it would have been effectively inhibited by the insoluble product within the first few minutes of leaching. The reaction stopped almost completely at 150° except for slow increments in the absence of oxygen. However, at 120° and 3 p.s.i. oxygen pressure there was a progressive increase in the degree of dissolution for at least 180 min of leach reaction time. At the lower temperature, the slowing down of oxidation of hydroxide product of dissolution apparently caused the dense product to be more dispersed throughout the oxide, thus the formation of a uniform reaction inhibiting layer was prevented and diffusion of hydroxyl ions through the oxide was not stopped as at the higher temperature. (A similar effect was noticed for the sodium carbonate system which has not been shown graphically.)

A related behaviour is shown with the South Crofty wolframite at 120°, the reaction having stopped completely at 150° within the first 30 minutes of leach reaction time.

Experimental results are tabulated below, leach condition being 10.000 g wolframite leached in 750 cc 0.50 N alkali solution. 5.000 g of South Crofty wolframite were used.

Results at 120 min. leach reaction time are given in table XV.

Table XVI

Temp. °C	O_2 pressure p.s.i.	Time min	WO_3 (g) produced per 10 g ore		
			NaOH	Na_2CO_3	South Crofty NaOH
150	10	60	2.60	3.25	-
		180	3.02	-	-
		240	2.95/3.20	4.05	-
150	3	60	4.90	4.21	-
		180	-	-	-
		240	4.95	4.93	-
150	0	60	2.41	-	-
		180	-	-	-
		240	3.24	2.44	-
120	50	30	-	-	3.4
120	3	30	1.00	-	1.8
		60	1.40/1.26	-	-
		180	3.45/3.15	-	-
		240	3.47	2.86	-
120	0	60	1.03	-	-
		240	1.14	-	-
100	3	240	0.66	-	-

By introducing air before heating, reaction was unavoidable during the times of heating and cooling of the autoclave and the extent of error caused by so doing, prevented runs for durations of time less than 30 min. It was therefore not possible to do any kinetic studies on the behaviour of the mineral.

3.5.5. Agitation Rate.

Since only small quantities of oxygen are soluble in water, continuous transfer from the gas must occur when oxygen is removed from solution by reaction with the solid. The rate of transfer therefore depends on the rate of agitation. Two experiments were carried out using 10.000 g of wolframite, 750 cc of 0.50 N sodium hydroxide solution and 10 p.s.i. oxygen at 150°C, for 240 min. In one, a low rate of agitation was employed and in the other, a high rate.

Actual rates of agitation could not be measured since minor fluctuations took place with changes in compressed air pressure. In all experimental work, therefore, a vigorous agitation rate was employed to diminish the effects of these fluctuations.

Table XVII

Run	Agitation	WO_3(g) produced
47	Slight	3.94
50	Vigorous	2.60

Results show a high dissolution rate with slight agitation due to the reduced rate of oxygen supply to the mineral particles and the resultant decrease of coating porosity with oxidation.

3.6. Reagent Consumption

As in the pyrite system, the amount of sodium hydroxide consumed with decomposition of wolframite was proportional to the amount of sodium tungstate produced and was independent of the experimental conditions, shown in fig. 41. The number of moles of sodium hydroxide required per mole of wolframite decomposed varied from 1.81 to 2.07, the average value being 1.92.

This is a value in good agreement with that expected in the general equation ;

$$(Fe,Mn)WO_4 + 2NaOH = (Fe,Mn)(OH)_2 + Na_2WO_4 \qquad (69)$$

This equation does not require any oxygen in the overall reaction and is in agreement with the observation that small quantities of oxygen are essential for the maintenance of reaction, and apparently not consumed by reaction. Furthermore, the divalent metal hydroxide, $(Fe,Mn)(OH)_2$ is readily oxidised, which explains the marked dependence of oxide coating porosity on oxygen partial pressure.

3.7. Promotion of reaction using a Chelating agent.

If the oxide can be removed or prevented from forming, reaction of the wolframite should go to completion. This was confirmed by using the proprietary material, "Detarex C" (F.W. Berk and Co., Ltd., London) which is diaminoethane tetra acetic acid "modified with a buffering agent". This material is particularly effective in dissolving iron in alkaline solutions.

Two experiments were carried out using 5.000 g wolframite and 750 cc of 0.50 N sodium hydroxide, containing just sufficient Detarex C to combine with all of the iron in the mineral, as determined experimentally. Oxygen partial pressure was 10 p.s.i. and leaching was carried out for 120 min at 120°C and 150°C, respectively. In each case almost complete decomposition of the wolframite was achieved.

Fig 41. RELATION BETWEEN WOLFRAMITE DISSOLUTION AND SODIUM HYDROXIDE USED BY REACTION

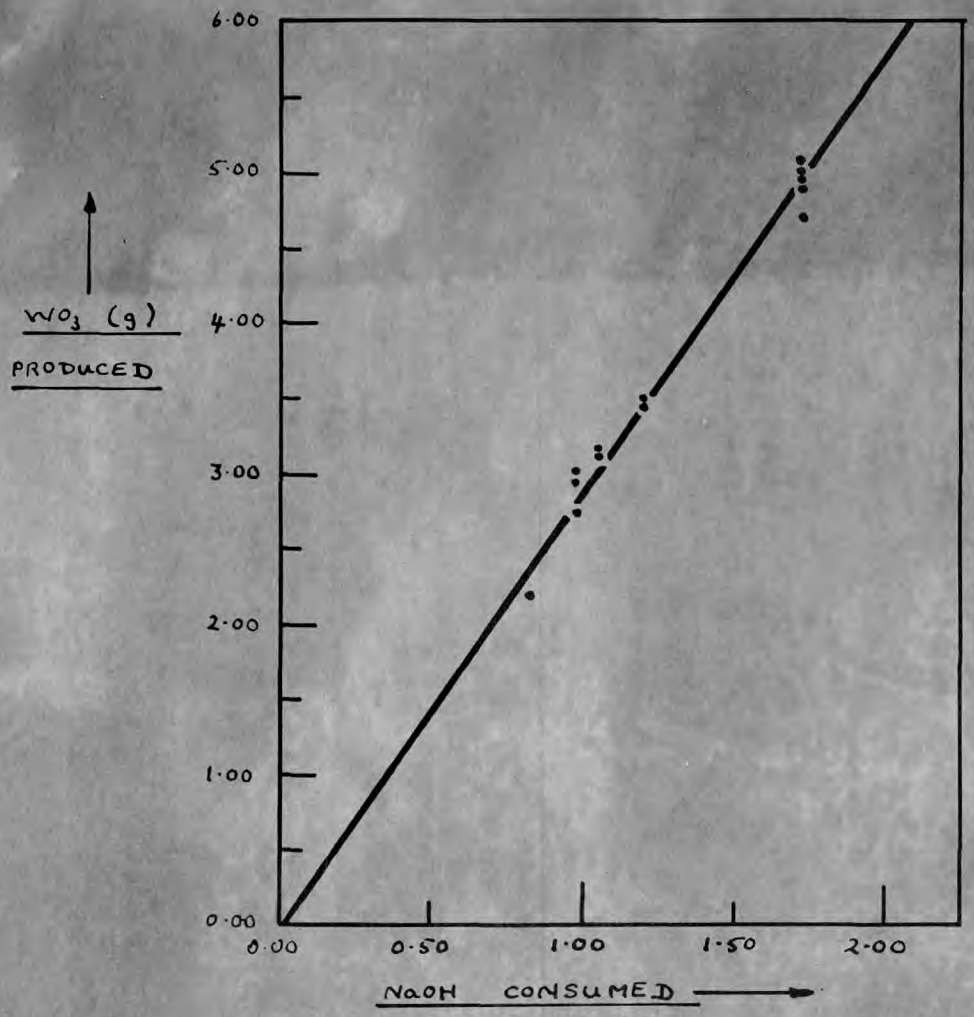


Table XVIII

Run	Temperature °C	WO_3(g) produced
52	120	3.16
53	150	3.16

3.8. Relation between particle size and reduction in Surface area.

By the same method of particle size counting employed in the pyrite leaching series,(page100),a distribution of percentage by weight of each size fraction, measured in microns, was determined, fig. 42. Each size fraction is displaced to the left of the Tyler screen size apertures. This is partly due to the fact that in the measurement of particle diameters, an estimation of the mean diameter was made. Assuming, in the heterogeneous reaction, that uniform increases in effective coating thickness were produced during leaching, the variation in percentage dissolution for each size fraction was determined using equations (65) and (66). The results are plotted in fig. 43. Of course, this would only be strictly true if the extent of reactant ion penetration along cleavage planes and cracks was of the same order in both cases. This does however, provide a rough means of comparing figs. 36. and 37, the corrected values from fig. 36. with respect to the carbonate series, fig 37, being given in table XII.

Fig 42. PARTICLE GRAIN SIZE DISTRIBUTION

SHADED AREA: 325-200# TYLER
CLEAR AREA : 200 100#

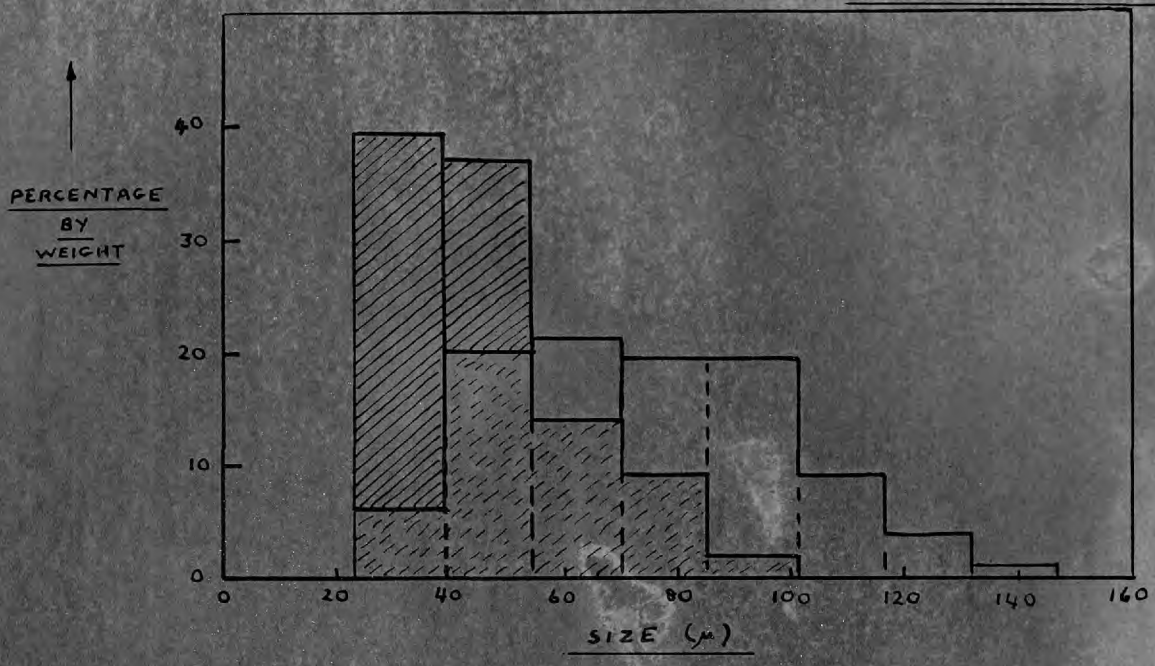
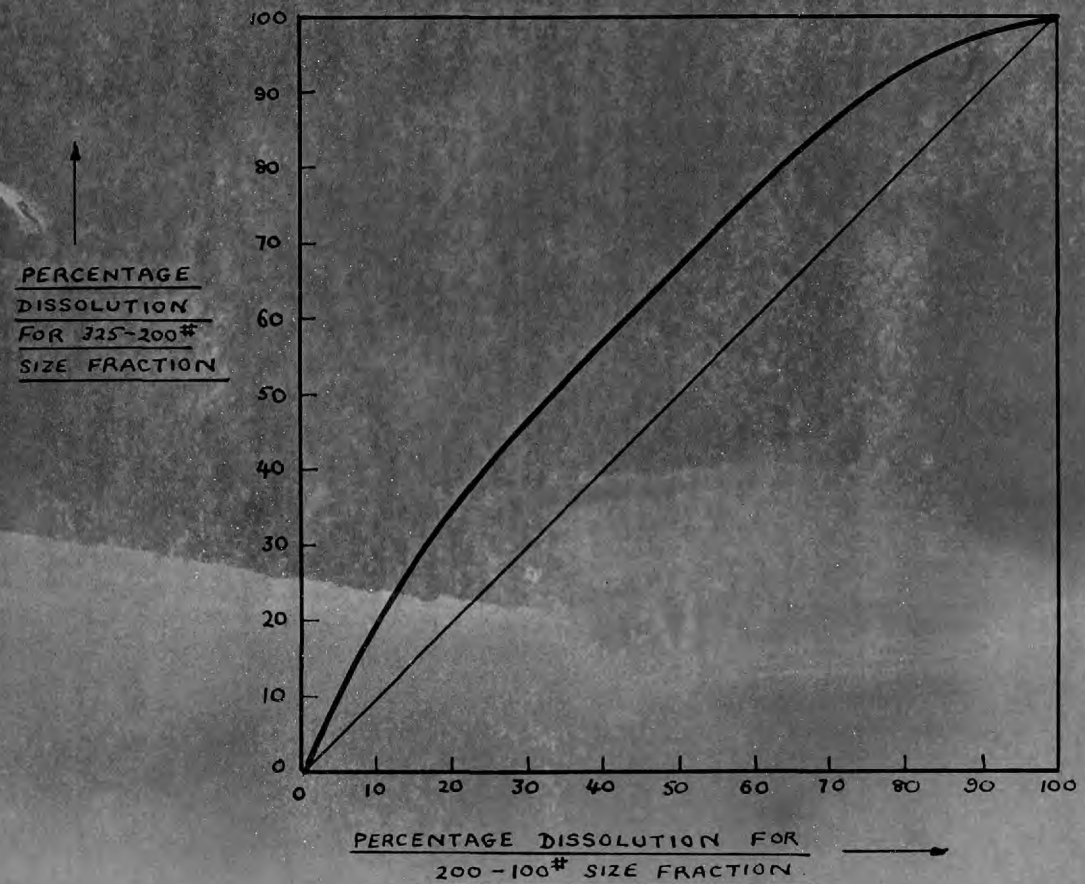


Fig 43. RELATION BETWEEN ABOVE SIZE FRACTIONS



3.9. Study of Leach Residues.

3.9.1. Microscopic examination.

Polished sections of the partially leached residues were prepared in a manner similar to that mentioned in the pyrite system, page Photomicrographs are shown in figs. 44 - 47. The oxide products in this system were colourless, the dense white bands of oxidation product being almost as hard as the unleached wolframite.

In fig. 45, a particle of wolframite, leached in sodium hydroxide, is shown at 1000 times magnification. The large uniform white areas are unleached wolframite and the finely grained dense white areas indicate sites where reaction was initiated, both at the outer edge of the particle and along cleavage planes running parallel with the edge. In the presence of 50 p.s.i. oxygen pressure, the dense white product is absent at the outer edge exposed to leach liquor. Wolframite areas can be distinguished from dense white oxidation product by the greater hardness and consequent higher relief on polishing. In fig 44, dissolution has been concentrated along parallel cleavage planes.

That the dense white products of oxidation were absent about the edges, when the mineral was leached at high oxygen pressures, indicated that this product had broken down or was more dispersed through the oxide coating.

A similar behaviour is shown in figs. 46 and 47, of particles of leached South Crofty wolframite. The particle shown in fig. 46 was leached at 120° in 3 p.s.i. oxygen partial pressure and that in fig. 48 at 50 p.s.i. oxygen pressure. Both figures show particles magnified 2800 X. In fig. 46, a coating about a narrow particle is shown, the dense white product being deposited about the leached wolframite. In fig 47, which shows a penetration inside a particle, the same dense white product is clearly shown having a comparatively coarse grained structure. As in fig. 45, this dense white product had broken down about the exposed edges where it would have been readily oxidised at the high oxygen pressure of leaching.

General observations made are given below ;

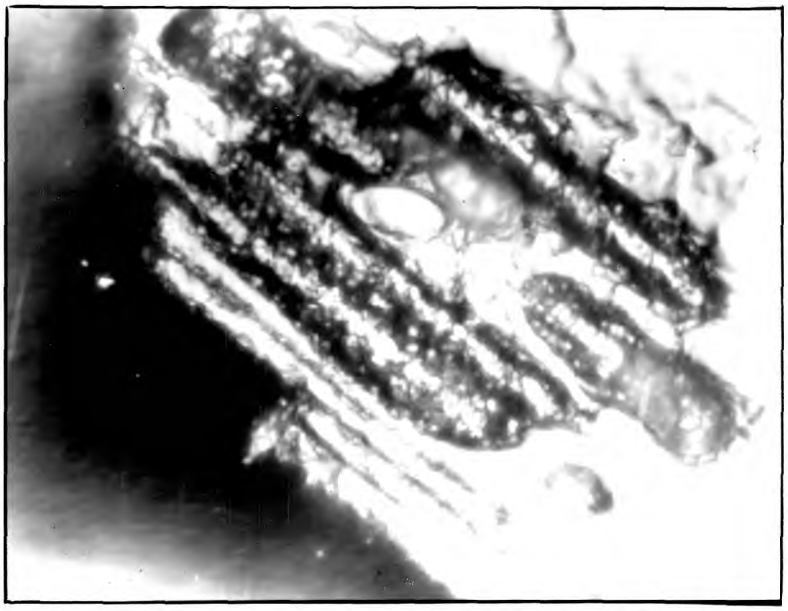
i) The initial product of dissolution was coarse grained and highly reflecting.

ii) The oxidised insoluble product of mineral composition was fine grained as was the coating in immediate contact with the unleached wolframite.

iii) The oxide product, after leaching at high oxygen pressures, was morecompact and more highly reflecting, whereas at low pressures, the product was less dense, except for the highly reflecting narrow oxide bands, and softer,being easily removed during abrading.

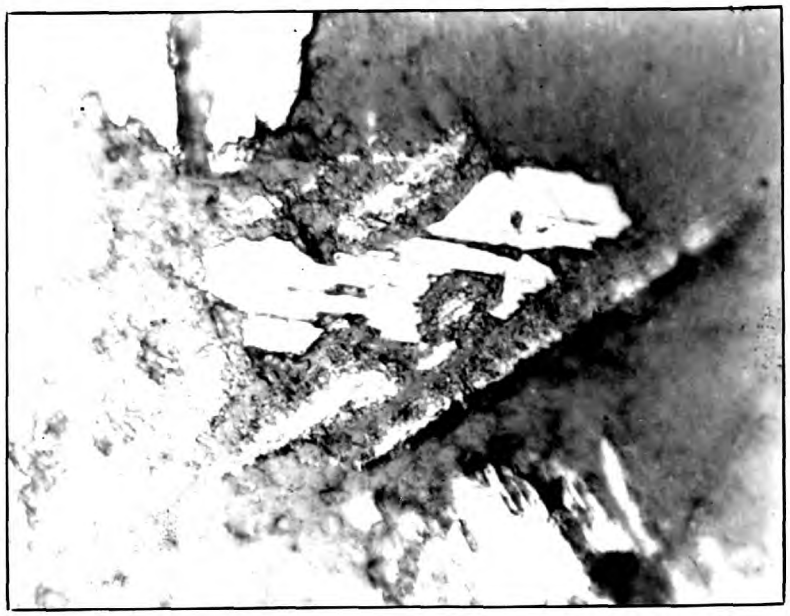
iv) Extensive penetration took place along mineral cleavage planes.

Wolframite.



2500 X

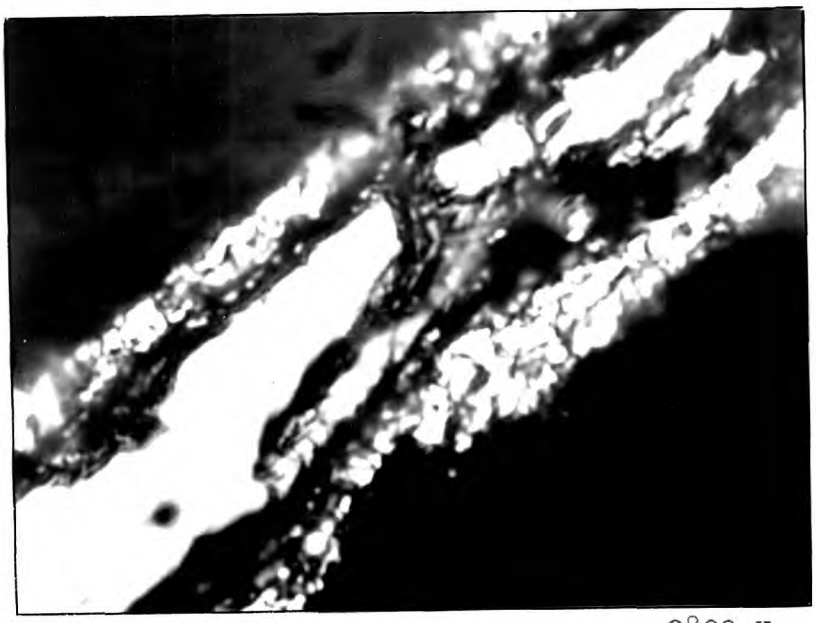
Fig 44. Penetration along cleavage planes.



1000 X

Fig 45. Replacement by insoluble product.

South Crofty wolframite.



2800 X

Fig 46. Insoluble coating on mineral.



2800 X

Fig 47. Penetration in particle.

3.9.2. Examination of leach residues using the Cambridge Microscan X-ray analyser.

The Cambridge Microscan X-ray Analyser has produced valuable evidence in elucidating the relation between iron and manganese in the soluble oxidation product and eliminating the possibility that intermediate tungstate products had been deposited with the iron and manganese oxides. The usefulness of this instrument is described on page 120.

In fig. 48, a series of photomicrographs is shown at 1000 X magnification for a particle leached in 750 cc 0.50 N sodium hydroxide solution, at 3 p.s.i. oxygen pressure, for 120 minutes at 150°C. In the electron image, fig. 48a, the intermediate dense product is shown as the area of highly reflecting material surrounding the large body of unleached wolframite. In figs. 48c and 48d are shown the relative increases in iron and manganese concentrations in this highly reflecting layer, and, in fig. 48b, the virtually complete removal of tungsten in the surrounding coating.

Quantitative determinations of the metal contents in both wolframite and oxidation product were ;

Wolframite: 55.5% W, 11.5% Mn, 13.0% Fe, Ratio Mn:Fe=1.0:1.13

Coating : 4% W, 20.5% Mn, 24 % Fe, Ratio Mn:Fe=1.0:1.17

As indicated on page 101 these results are not reliable when expressed on this quantitive basis, but they do show that the elements, manganese and iron, were not separated into their respective oxidation products during leaching but apparently remained together as the combined metal oxidation product.

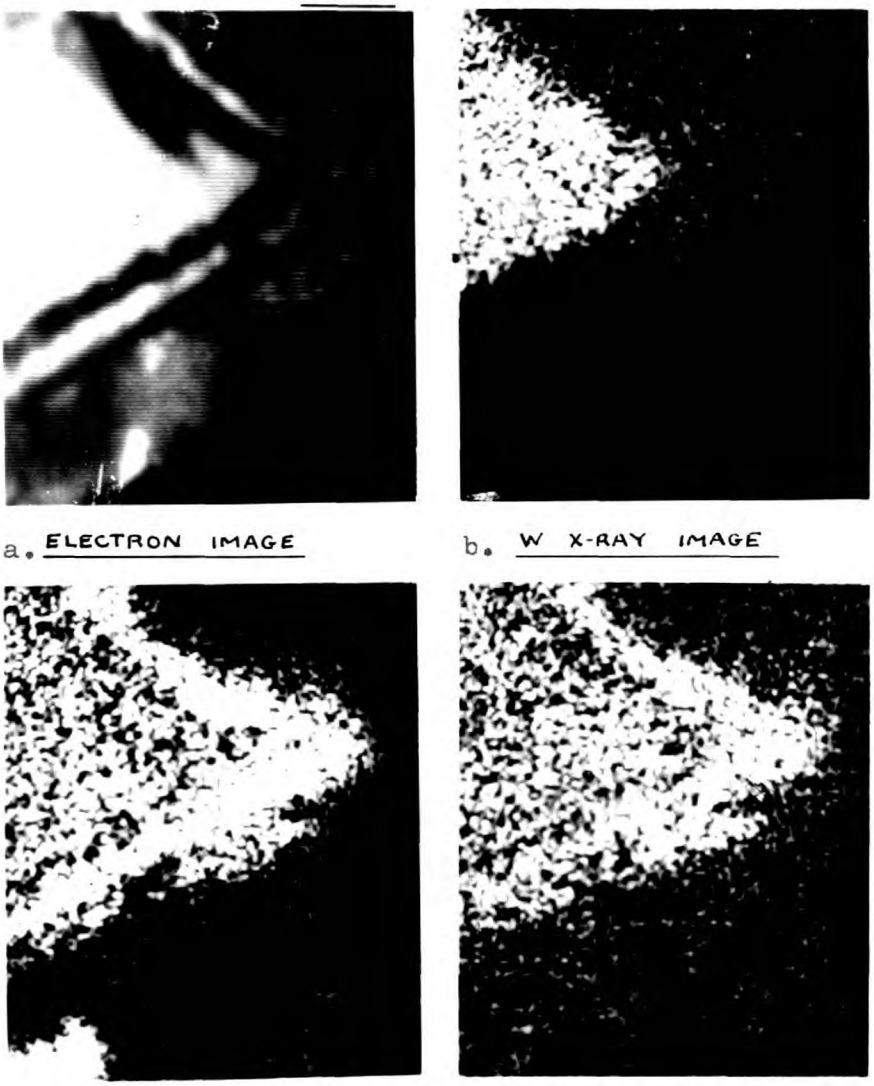
The large scale elimination of tungsten in the coating shows that no intermediate insoluble tungstates were deposited with the iron and manganese product.

In fig. 49, pictures are shown for a particle leached in 0.50 N sodium carbonate at 50 p.s.i. oxygen partial pressure for 120 min at 150°C and 850 X magnification. The pseudomorphic oxidation product is shown as the uniform finely grained product, and the dense, highly reflecting oxidation product shown in fig 48 is absent. Similarly, the iron and manganese constituents are seen to be increased in concentration in the oxide, and tungsten, practically absent.

Fig 48. PRESSURE LEACHING OF WOLFRAMITE

IN 0·5 M NaOH AT 3 PSI O_2 PRESSURE FOR 120 MIN AT 150°C

1500 X



a. ELECTRON IMAGE

b. W X-RAY IMAGE

c. Fe X-RAY IMAGE

d. Mn X-RAY IMAGE

Fig 49. PRESSURE LEACHING OF WOLFRAMITE

IN 0·5 M Na_2CO_3 AT 50 PSI O_2 PRESSURE FOR 120 MIN AT 150°C

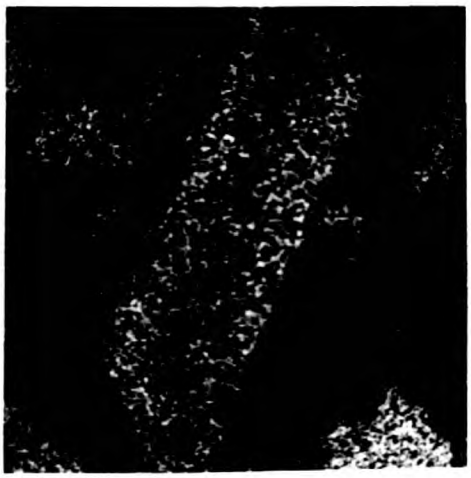
850×



a. ELECTRON IMAGE



b. W X-RAY IMAGE



c. Fe X-RAY IMAGE



d. Mn X-RAY IMAGE

3.9.3. X-ray powder diffraction studies.

In these studies, similar to those carried out with pyrite and described on page 131 no additional lines were detected in the leached mineral. This is probably due to the fact that the oxidation product was very finely crystalline except for the thin bands of highly reflecting material normally present along cleavage planes.

Pictures were difficult to obtain due to the very high degree of absorption and scatter by the finely crystalline product, and to the coarse-grained size fraction of mineral employed during leaching (100 - 200 mesh Tyler). Lines obtained for the unleached wolframite of unknown origin, and the wolframite from South Crofty, were identical, and indicated structure and constituent elements in similar proportion.

SECTION 4.

MECHANISMS OF REACTION

Experimental evidence has enabled the following theories to be evolved for the mechanisms of reaction of pyrite and wolframite and the formation of the insoluble products of reaction, during the leaching in sodium hydroxide solutions.

A summary of conclusions made in Section 3, is tabulated for each subsection, below.

4.1. Pyrite Section

4.1.1. Interaction at the pyrite-solution, or pyrite-insoluble product, interface.

i) Reaction was heterogeneous, and controlled by direct interaction between reactants and pyrite at the exposed pyrite surface, (page 92)

ii) Oxygen was essential to the reaction and was the rate controlling element (page 65). When an insoluble product effectively covered the pyrite surface, the order of reaction with respect to oxygen tended to the value 0.5, indicating dissociation of oxygen molecules prior to reaction(page 84)

When a loosely adherent coating was formed, which ineffectively covered the pyrite surface, (page 80), the order of reaction with respect to oxygen was 0.5 at oxygen partial pressures of about 20 p.s.i., this value tending progressively to zero order at oxygen pressures greater than 120 p.s.i. At oxygen pressures less than 20 p.s.i., the reaction tended to first order, as the rate of pyrite dissolution tended to become greater than the rate of oxygen supply to the particle surface.

iii) Concentrations of sodium hydroxide greater than 0.50 N resulted in little change in the rate of reaction, at least up to 4.00 N, so that the rate of mineral dissolution remained one of zero order with respect to sodium hydroxide concentration (pages 62 and 90)

iv) Temperature increments on the dissolution rate gave an energy of activation for the initial reaction of ca9 kcal/mole, (page 74).

v) Reaction was accelerated at areas showing a comparative deficiency of sulphur atoms in the pyrite crystallographic lattice. This sulphur deficiency was apparently not made up by foreign elements and was either due to the presence of elemental iron atoms or vacancies in the lattice (page 126).

vi) Four moles of sodium hydroxide and about five moles of oxygen were used in reaction per mole of pyrite decomposed. (page 96)

The following mechanism is proposed for the mineral dissolution process:

With sufficiently high oxygen pressures and solution agitation rates, the reaction was independent of the rate of transfer of oxygen to the particle surface.

Stages in the reaction involve ;

i) Dissolution of oxygen molecules at the gas/liquid interface.

ii) Transport of dissolved oxygen from the gas-solution to the solid-solution interface.

iii) Chemisorption of oxygen on the pyrite surface;

$$FeS_2 + O_{2\,(aq)} \xrightarrow{fast} FeS_2 \cdot O_2 \qquad \ldots(71)$$

iv) A proportion of oxygen molecules were dissociated at the pyrite surface, the fraction increasing with temperature;

$$O_{2\,(aq)} \xrightarrow{fast} 2O \qquad \ldots(72)$$

$$\text{and} \quad FeS_2 + O \xrightarrow{slow} FeS_2 \cdot O. \qquad \ldots(73)$$

The dissolution of pyrite was controlled by the complex formed with elemental oxygen, and involved heterogeneous interaction with replacement of two sulphur atoms, or as many as were present at the particular site in the pyrite lattice, by an oxygen atom. This effect was found to be more rapid at sulphur deficient sites where the mineral may have had only one or no sulphur atoms;

$$FeS._{-}. + O \xrightarrow{slow} FeS._{-}.O \quad \cdots(74)$$

As observed by Smith (1942) (67), the pyrite becomes more electrically conducting when a deficiency of sulphur is found in the lattice and it was assumed that iron atoms behave as elemental iron at sulphur deficient sites, so that there is an overall charge balance.

The cubic sodium chloride structure of the original pyrite would be retained in the transformation to a wustite configuration with a retained iron configuration in its lattice;

$$FeS._{-}.O \longrightarrow FeO + 2S^{\circ} \quad \cdots(75)$$

$$FeS_2.O \longrightarrow FeO + 2S^{\circ} \quad \cdots(76)$$

v) The sulphur was oxidised by oxygen and went into solution by interaction with sodium ions as sodium sulphate.

$$2S^{\circ} + 3O_2 + 4NaOH \xrightarrow{fast} 2Na_2SO_4 + 2H_2O. \quad \cdots(77)$$

The transformation to wustite represents a progressive reduction in unit cell size from 5.42 A for pyrite to 4.33 A for wustite. The topotactically transformed wustite remained in direct contact with unleached pyrite and outward diffusion of sulphur and inward diffusion of oxygen was required through the greatly expanded wustite lattice.

4.1.2. Behaviour of the insoluble iron oxide product of reaction.

It has been observed that;

i) When adherent to the unleached pyrite surface, the oxide coating produced was pseudomorphic with the original pyrite particle (page 68 and 112).

ii) An initially formed iron oxide product was metastable and transformed with oxidation, after a time depending on leach temperature (page 69) and oxygen partial pressure (page 83). The initial product was stabilised in the presence of increased alkali concentration. (page 90)

iii) The final product of oxidation apparently resulted from a series of topotactic transformations derived from the original pyrite structure as was observed by, (a) the coarsely grained structure of the product, its blue colouration and magnetic nature (page 114), (b) the line conforming with that of the mineral, maghemite (γ Fe_2O_3) as indicated by X-ray powder diffraction study (page 131) and (c) the iron composition of 70% by weight, as obtained by X-ray microscan analysis (page 121).

iv) The oxide was only adherent when the ore was relatively impure either stoichiometrically or chemically and penetration into the particle could be accelerated at more reactive sites, such as crystal imperfections

and grain boundaries within the particle. The oxide product adhered only loosely and with difficulty when the pyrite was a mineral of high purity and coarsely grained (page 68 and page 112). This adhesion was of a physical nature and became greater the lower the temperature and the longer the time of mineral decomposition (page 101).

v) Sulphur was absent in the oxide product with only a very small diffusion gradient at the pyrite-oxide interface, (page 121).

The extreme insolubility of iron oxides and hydroxides in water invariably results in their "in situ" precipitation as a pseudomorphic layer about the unleached mineral. The strong evidence in favour of the existence of maghemite as the final stage in the oxidation of the insoluble product shows that it has been formed through a series of topotactic transformations with a structure related to the original pyrite lattice, since no coarsely crystalline iron oxide can be precipitated from a relatively weakly alkaline solution.

It has been shown by previous workers, (section 1.6.1.) that certain iron oxides do form topotactically with an increased tendency for this type of reaction to take place when there is a correlation in crystal structure, particularly regarding the oxygen atom configuration in the lattice. It is therefore proposed that the initially formed metastable iron oxide is wustite (FeO) having the

having the same sodium chloride crystallographic structure as the original pyrite.

With the progress of reaction, the wustite phase grows topotactically on the pyrite with the inward diffusion of oxygen to the mineral and the outward diffusion of sulphur which is oxidised at the particle-solution interface to form sulphate ions.

So long as oxygen rapidly interacted with the pyrite, no breakdown of the wustite phase took place. However, when the metastable phase had attained sufficient thickness, depending on temperature and oxygen partial pressure in the autoclave gas space, oxygen was available for oxidation of the ferrous ions of the initial oxide phase by a regrouping of the iron atoms in the oxide lattice to form a magnetite of invariant composition and finally the maghemite phase in which only ferric ions exist dispersed in the retained cubic close packed oxygen lattice.

The abrupt transformation to magnetite, with metastable FeO breakdown, represents a rapid consumption of oxygen, so that supply of oxygen to the pyrite surface is temporarily stopped. This effect is shown by the induction periods in fig. 4. The oxidation of magnetite to maghemite is a slow step in the reaction. As shown on page (132), there are only slight differences in the relative densities of the minerals, pyrite, magnetite and maghemite. All stages of transformation will have taken place simultaneously during the leaching process.

It is thus assumed, that, in the first transformation from pyrite to wustite structure, the iron atom configuration was retained with the resultant replacement of sulphur by oxygen. The second stage of transformation resulted in a retention of oxygen atom configuration and a regrouping of iron atoms during the oxidation from the ferrous to ferric state.

The overall reaction has been written as :

$$4FeS_2 + 16NaOH + 15O_2 = 2\gamma Fe_2O_3 + 8Na_2SO_4 + 8H_2O$$

which incorporates the final oxidation state of the insoluble iron oxide and satisfies the experimental consumption of 4 moles of sodium hydroxide per mole of pyrite and an oxygen consumption of the same magnitude.

This is the first example of a hydrometallurgical leaching process being observed to take place through a series of topotactic transformations. The early observation made by Sullivan in (1933) (70) of the progressive removal of copper atoms in two stages from the chalcocite lattice and the retention of sulphur atoms when leaching in sulphuric acid medium was not explained, but it seems likely that a similar mechanism of dissolution existed.

4.2. Wolframite Section

4.2.1. Interaction at the wolframite-solution or wolframite-insoluble product interface.

Wolframite behaves in a different manner with the similar appearance of an insoluble pseudomorphic oxide product. Conclusions made in section 3 are tabulated below ;

i) Reaction was heterogeneous, being controlled by interaction at the exposed wolframite surface (page 136).

ii) Oxygen was essential to the reaction though the presence of a trace of oxygen was capable of causing extensive mineral decomposition and any increase in oxygen concentration above this low value resulted in an effectively reduced degree of mineral dissolution with the oxidation of the initially deposited mixed iron-manganese hydroxide. (page 139).

iii) Increased concentrations of sodium hydroxide enhanced the rate of mineral dissolution. (page 137).

iv) The extent of reaction increased with temperature. Quantitive determinations could not be made since the extent of dissolution was only related to the temperature insomuch as the reaction retarding influence of the insoluble hydroxide was decreased at higher temperatures. (page 139).

v.) Reaction was accelerated by penetration along cleavage planes in the mineral (page 155).

vi) Two moles of sodium hydroxide were used in reaction per mole of wolframite decomposed.(page 150).

vii) When an iron oxide dissolving chelating agent was used, virtual complete decomposition was obtained at 120°, because of the removal of the inhibiting effect of the insoluble product (page 151).

viii) Reactions were somewhat more extensive in sodium carbonate solutions. (page 142).

The following mechanism is proposed for the mineral dissolution process.

The importance of trace amounts of oxygen has been emphasised, particularly in the case of the South Crofty ore. The lesser importance of oxygen with the other ore is attributed to an oxidation of the surface of the mineral prior to leaching.

The initial stage of dissolution involves the adsorption of elemental oxygen on to the mineral surface, which initiates the reaction;

$$(Fe,Mn)WO_4 + O = \underset{\text{activated complex}}{(Fe,Mn)WO_4.O} \quad \ldots(78)$$

The activated complex produced reacts with sodium hydroxide as follows;

$$(Fe,Mn)WO_4 + (Fe,Mn)WO_4 \cdot O + 2NaOH = \begin{matrix}(Fe,Mn)(OH)_2 \\ | \\ O \\ | \\ (Fe,Mn)WO_4\end{matrix} + Na_2WO_4 \quad \cdots(79)$$

where $(Fe,Mn)WO_4$ signifies an immediate underlying wolframite "molecule" in the mineral lattice.

In this way there is produced a catalysing effect by oxygen with a progressive oxidation and reduction of metal atoms at the wolframite surface.

The overall reaction is shown by the reaction.

$$(Fe,Mn)WO_4 + 2NaOH = (Fe,Mn)(OH)_2 + Na_2WO_4 \quad \cdots(80)$$

which is in agreement with the calculated consumption of 1.92 moles of sodium hydroxide per mole of wolframite decomposed and shows the independence of oxygen concentration.

4.2.2. Behaviour of the insoluble product of reaction

It has been shown that :

i) The insoluble product of dissolution was pseudomorphic with the original wolframite particle (page 155).

ii) The initial hydroxide was oxidised in the presence of oxygen, when its concentration was greater than that required for the maintenance of reaction at the wolframite surface, the oxidised product broke down to the typically fine-grained material usually formed when iron and manganese oxides are precipitated in alkaline solutions. No X-ray powder diffraction lines could be obtained from the leach residues. This finely grained product was highly impervious to reactant ions and soluble products of reaction, the reaction ceasing when it had attained an effective thickness (page 163).

iii) The initial product of dissolution may have been formed topotactically from the parent wolframite, as shown by the highly reflecting coarsely grained product in figs. 46 and 47 (page 158).

iv) Iron and manganese remained together in the same concentration ratio throughout the dissolution process and tungsten was virtually absent in the insoluble product. This confirmed the assumption that tungsten did not form any intermediate insoluble tungstates and was liberated to the solution during reaction (page 160).

As shown by Bernal et al (9), ferrous hydroxide transforms non-topotactically to goethite (αFeOOH) in strongly alkaline solutions, non-topotactically to magnetite, (Fe_3O_4) and, with rapid oxidation, topotactically to δFeOOH. The experimental conditions favoured the formation of magnetite, which was confirmed by the strongly ferromagnetic properties of the material and its very finely grained structure indicative of a recrystallisation.

It is assumed in this work that the mixed iron-manganese compounds behaved in a similar manner.

Hence the mechanism may be summarised as follows ;

i) Reaction proceeded rapidly in the presence of trace amounts of oxygen with the deposition of the divalent metal hydroxide, $(Fe,Mn)(OH)_2$, which may have been formed topotactically.

ii) The rate of reaction was critically controlled by the rate of diffusion of reactant ions through the insoluble product and was drastically retarded when the hydroxide was oxidised to a magnetite configuration.

$$(Fe,Mn)(OH)_2 \longrightarrow (Fe,Mn)(O.OH) \longrightarrow (Fe,Mn)_3O_4$$

SECTION 5.

EXPERIMENTAL WORK.

5.1. Apparatus

The autoclave used in experimental work was a modified version of the design by B.T.K. Barry (5), capable of operating at pressures up to 2000 p.s.i.

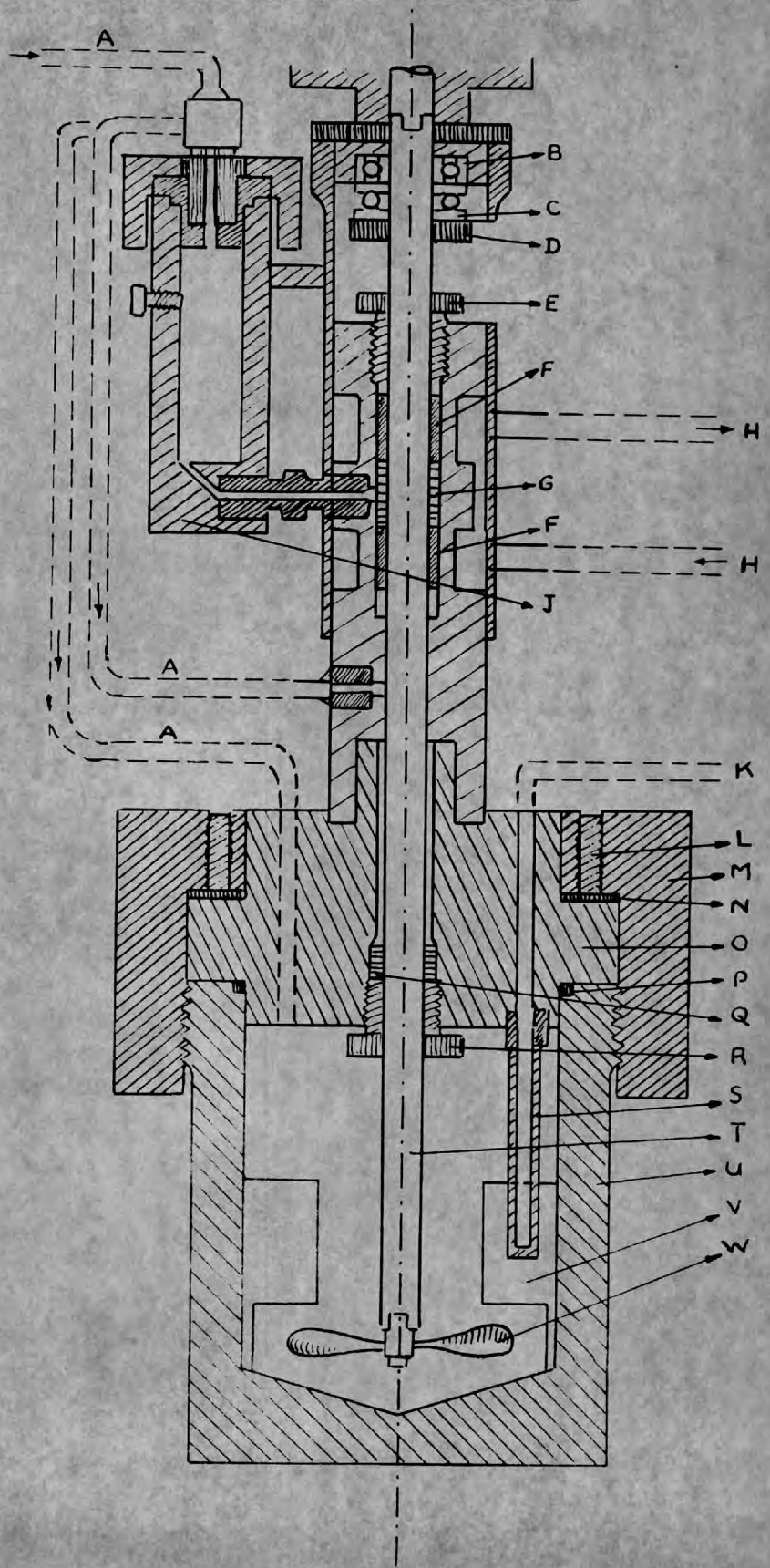
The autoclave had a capacity of $2\frac{1}{2}$ litres and agitation was provided by a compressed air motor externally mounted above the reaction vessel, the compressed air being supplied at about 100 p.s.i. The reaction vessel was heated externally by gas burners and instruments and attachments were provided for control of heating rate, temperature, and gas pressure.

The use of compressed air for agitation had the disadvantage that the solution agitation rate fluctuated somewhat with unavoidable variation in compressed air pressure.

A diagram of the autoclave is shown in fig. 50.

Leach Vessel: The body (U) and head (O) of the reaction vessel were made from a forged billet of SF 22 molybdenum stabilised stainless steel, effective sealing being provided by an enclosed "Klingerite" gasket (P) (A patented graphitic material supplied by Richard Klinger Ltd., Sidcup, Kent). The head fitted within the

Fig 50. DIAGRAM OF THE AUTOCLAVE



open end of the body locking by means of a mild steel collar (M) screwed on to the body of the autoclave, and which bore down on to the head through a steel ring (N). Eight Allen screws (L) were placed uniformly around the collar and bore on to the steel ring rendering the seal fully effective.

Gas (A) was introduced into the autoclave through a 0.1 inch hole drilled through the head and tapped at the outer end to accommodate the 3 mm bore pressure tubing.

Temperature was measured by means of a mercury-in-steel thermometer (K) placed in a $^{3}/_{8}$ inch diameter steel tube (S) passing through the head and enclosed at the lower end, which was in contact with the leach solution. More rapid heat transfer from the solution to the thermometer was provided by placing mercury in the pocket.

The stirring shaft, (T) with bearings and shaft sealing glands (E) and (R) was mounted on the head, sealing being effected by means of bearings (F), which supported the thrust imposed on the shaft by pressure from within the autoclave and prevented gas liberation.

Lubrication for the shaft bearings was introduced under pressure from an oil reservoir, (J) which was mounted alongside the shaft enabling the apparatus to be assembled and dismantled with minimum disturbance to pipe joints and glands. The pressure was the same as the operating pressure during leaching. The shaft was surrounded by a water cooled jacket. (H) The two bladed propeller (W) was mounted at the end of a $\frac{1}{2}$ inch diameter stainless steel stirring rod

(T) and was driven by the externally mounted turbine. Two sets of bearings supported the shaft both at the upper end where a ball race (B) backed by a thrust race (C) was mounted being held in position by the thrust pin (D), and, at the lower end, a bronze bearing was placed. A series of white metal bearings, (F) which acted as gland seals, supported the stirring rod at either end, the lower gland nut bearing through an asbestos ring (Q) which prevented lubricating oil from seeping into the reaction vessel. Lubrication of the upper white metal bearings was provided by oil forced upwards under pressure from the lantern ring (G), the resulting pressure loss in the autoclave being negligible with this escape of oil. Two baffles (Y) were placed in the body of the vessel.

Heating and Temperature Control; Heating was effected and controlled by a centrally placed gas jet beneath the autoclave and by booster jets placed about the sides of the reaction vessel. These booster jets were only employed in the initial stages of leaching to attain the required operating temperature as rapidly as possible. The mercury-in-steel temperature regulator was controlled by a magnetically operated valve fitted with a bypass to allow a pilot flame to remain burning after the main gas flow had been cut off. By using the booster jets, it was possible, with the wolframite series, to attain a constant temperature within 10 minutes.

The temperature was thermostatically controlled in the range of

$\pm 2^{\circ}$ at temperatures up to 150°. At temperatures below 100°, the above pilot burner, having too large a flame, was not employed,and therefore a small flame was introduced from an independent gas source.

Air and Nitrogen supply: The gases were supplied by compressed gas cylinders, the pressure being measured by a pressure gauge connected to the circuit by 3 mm bore pressure tubing.

5.2. Operation of Autoclave

Throughout the series of experiments, 750 cc of leach solution and either 5.000 or 10.000 g of mineral was used. The autoclave was charged with the reactants and assembled while cold.

5.2.1. Pyrite Series.

Since negligible reaction took place in the absence of oxygen, oxygen was evacuated from the vessel by two successive introductions of oxygen-free nitrogen at 600 p.s.i. and the solution agitated vigorously for 5 minutes. The nitrogen was then released to atmospheric pressure and the vessel sealed and heated to operating temperature. At temperature, air was introduced to the required pressure and the solution rapidly agitated for the required experimental time. Air was then eliminated and replaced by nitrogen. The abrupt cessation of reaction in the absence of oxygen enabled runs to be accurately

controlled and to be maintained at temperature with smaller fluctuations in temperature.

5.2.2. Wolframite series.

Trace amounts of oxygen caused appreciable reaction to take place, so that the above procedure could not be employed. Air was introduced at room temperature and the solution heated to the required temperature at a constant rate, and, after leaching, was rapidly cooled by a jet of compressed air. It took about 30 minutes to cool the autoclave from 150°to 80°C.

Gas pressures never exceeded 1000 p.s.i. and temperatures up to 200°C were employed. The autoclave was dismantled after cooling at the maximum temperatures of 60° for pyrite and 90° for wolframite and the charge siphoned out. The solution was immediately filtered. With the wolframite series, the solution frequently became turbid on standing.

5.3. Analytical

5.3.1. Pyrite series.

Mineral: The pyrite was digested in aqua regia for several hours, bromine being added to oxidise the small proportion of sulphur liberated in the free state. The solution was evaporated to dryness to render the silica insoluble. Iron was eliminated by double precipitation of ferric hydroxide with excess ammonia, and filtered off.

The solution was rendered slightly acidic with HCl and at 90 - 100° 10% excess of the calculated amount of Barium chloride solution was added. The Barium sulphate precipitated was separated with Gooch filter crucibles, calcined at ca. 800° and weighed.

Leach Liquor: As for the mineral, sulphur in solution was precipitated as barium sulphate. This is the most convenient method for sulphur determination. The solution was acidified with HCl, 5 cc added in excess to make the precipitate easier to filter and precipitation more selective. At 90 - 100°, 10% excess of $BaCl_2$ solution was added. An excess of $BaCl_2$ causes some barium chloride molecules to be adsorbed with the $BaSO_4$ precipitate. Fe(III), in particular, is carried down by the precipitate and had to be separated by double precipitation with ammonia. Generally the precision is

seldom very good because of the adsorbed impurities but good correlation and satisfactory results were obtained in this work. The precipitate was filtered through Gooch filter crucibles and washed with boiling water until chloride was absent from the filtrate, and then given a final wash with ethanol. The precipitate was heated to about 800° to eliminate chemically occluded water and the precipitate weighed and the sulphur determined as SO_4".

Sodium hydroxide concentration: The residual sodium hydroxide was determined by titration with sulphuric acid.

5.3.2. Wolframite series.

The most suitable method for the determination of tungsten from its ore is the gravimatric method (46) (41) in which tungsten is precipitated and weighed as the trioxide WO_3. The cinchonine method has been used, being the most reliable, though time consuming, method. A volumetric method may be used in the reduction of WO_3 to WO_2 with zinc followed by the reoxidation to WO_3 with a standard solution of potassium permanganate. However results are influenced by the presence of molybdenum and iron which are difficult to remove so that this method is not preferred for accurate determinations. Colorimetric methods are used for determinations of small amounts of

tungsten, a yellow colour being produced on the addition of thiocyanite and stannous chloride to an alkaline tungsten solution.

Cinchonine method for determination of tungsten in the ore.

1 g of finely pulverised ore was digested in 100cc conc. HCl at a low temperature and the volume reduced to 50 cc by slow evaporation, the contents being stirred at regular intervals to avoid crust formation. 40 cc conc. HCl and 15 cc conc HNO_3 were added and the contents again evaporated to 15 cc. 150 cc water was added and boiled for about 30 min. By this stage, the ore will have been virtually completely decomposed to the insoluble tungstic acid, H_2WO_4. The contents were filtered and washed with 10% HCl and 2 cc cinchonine solution were added to the filtrate which was set aside to ensure that precipitation was complete. (Ppt A).

Cinchonine solution consisted of 10 gm cinchonine in 75 cc water and 10 cc HCl.

To the residue, 25 cc hot water was added which was dissolved after addition of 5 cc NH_4OH. The solution was filtered and washed with hot 10% NH_4OH solution, the filtrate diluted and boiled to remove excess ammonia. Cinchonine solution was added and the solution stirred vigorously to coagulate the precipitate, (ppt B), containing the bulk of the tungsten. The insolubles from the last filtrate consisted predominantly of silica and a small percentage of undecomposed ore. This residue was mixed with 5 times its weight of sodium

carbonate and ignited in a nickel crucible. The ore was converted to the tungstate, Na_2WO_4, which was dissolved by lixiviation after fusion and filtration. To the filtrate, 5 cc HCl excess was added to acidify, and the solution boiled to expell CO_2 and 4 cc cinchonine solution added. The precipitate was reserved as ppt (C).

Under ideal conditions, no precipitate should be produced in cases A and C. All precipitates A, B, and C were filtered on ashless filter paper and washed with cinchonine wash solution. The paper and precipitate was transferred to a platinum crucible and ignited at less than 850° to avoid volatilisation of WO_3. During ignition, the cinchonine precipitate decomposes leaving the trioxide, which is subsequently weighed.

Leach Liquor: The above procedure was modified. 100 cc of leach solution containing excess sodium hydroxide or carbonate depending on leach conditions, was neutralised with HCl and acidified with 5 cc excess HCl. The solution was boiled to remove CO_2, and 4-8 cc cinchonine solution, depending on the degree of decomposition, were added and the hot solution stirred vigorously to coagulate the precipitate. It was allowed to stand overnight and then filtered and washed with cinchonine solution and ignited in a platinum crucible as described above.

Determination of alkali concentration: The residual sodium hydroxide and carbonate after leaching was determined by titration with sulphuric acid. The presence of sodium ions as hydroxide or carbonate were determined and found to agree with the calculated sodium ions remaining after leaching by determining the proportion of sodium ions required for the formation of sodium tungstate from the weight of WO_3 found after analysis.

pH measurements were made of the leach liquors after digestion with sodium carbonate but the small percentage of sodium carbonate used in reaction did not appreciably affect the pH which was found to drop from 11.4 for the 0.50 N solution before, to 10.4 after leaching, the pH being dependent on the degree of decomposition.

5.4. Preparation of Polished specimens for Microscopic Examination.

The residue after leaching, was washed, filtered, and dried with alcohol. Cross-sections of these leach residues were then prepared by mounting a sample of the residue in the patented embedding resin, "Ceemar" FR 264" (produced by E.M. Cromwell and Co., London). and the reagents FR 228 and FR 252 used as hardener and accelerator, respectively. This is a cold setting resin and

and had hardened sufficiently for polishing within 24 hours.

The mounted specimen was abraded with series of silicon carbide powders and alumina, and polished with a diamond paste down to 0 to 0.5 micron diameter.

Differences in colour and hardness of mineral and insoluble product enabled the different phases to be easily distinguished without using any etchants. To prevent oxidation of the surface, specimens were kept in a desiccator and the polished surface covered with a thin film of oil.

SECTION 6.

SUMMARY.

A study has been made of the behaviour of the minerals pyrite and wolframite when leached under conditions of elevated temperatures and pressures in sodium hydroxide solutions. Particular attention has been given to the formation of the insoluble iron oxide products which are invariably deposited on unleached iron bearing minerals during the course of the reaction. Most of the observations made are new and provide further contributions to the existing knowledge of hydrometallurgical processes involving the leaching of minerals.

6.1. Leaching of pyrite.

A relatively dilute caustic solution was used (0.5 N) for most of the work and temperatures up to 150°C and air pressures up to 600 p.s.i. allowed measurable mineral dissolution rates to be obtained, the temperatures being sufficiently low to enable the structuctural transformations of the insoluble oxide products to be observed. As in most hydrometallurgical leach processes, the presence of oxygen was essential to the reaction and the dependence of the reaction rate on oxygen partial pressure was determined.

The reaction was found to be of 0.5 order with respect to oxygen, which indicated a primary step in the dissolution involving oxygen atoms at the exposed mineral interface. The diffusion of oxygen atoms through the iron oxide coating when present as a coherent layer about unleached pyrite was rate controlling at an early stage of the dissolution process. This tendency for the formation of a continuous layer diminishes with increase in purity and particle grain size of the mineral. The coating may be formed as a weakly adherent layer of diminishing thickness in which case it is more effectively adherent at the lower temperatures with prolonged duration of reaction. This loosely adherent coating plays an increasingly important role in retarding oxygen supply to the mineral surface when particle sizes become progressively reduced during the course of mineral dissolution.

It was observed that the coherently stable coating is formed only when the particles consisted of an agglomeration of small crystals and/or an appreciable degree of lattice distortion has been caused by lattice vacancies or replaced impurities at the crystal boundaries. Coarse, high purity crystals tended to form the loosely adherent oxide product which was readily abraded with agitation of the solution unless physically held in contact with pyrite about jagged edges.

Microscopic examination of polished cross-sections of the mineral has revealed that the adherent oxide product retained the structure of the original pyrite, i.e. underwent topotactic transformation during reaction. This was caused by both the effects of extreme

insolubility of iron oxides in relatively dilute alkaline solutions and similarity in the cell structure of pyrite and iron oxides in which the cubic close packed configuration of oxygen is maintained. Rate curves at different temperatures have shown that a metastable, initial iron oxide product was formed whose stability was prolonged at the low temperatures, i.e. 90 min at 70° and was hardly noticeable at temperatures greater than 100°. This initial product has been assumed to be of wustite configuration in which the halide structure and crystal orientation of the parent pyrite had been retained. X-ray powder diffraction photographs have shown that the final oxidation state of the oxide during leaching is maghemite, the prominent line due to the presence of this mineral being easily detectable. Hence, a coherent coating formed during the sodium hydroxide pressure leaching of pyrite undergoes a series of topotactic transformations involving, initially, the replacement of sulphur by oxygen atoms to form wustite, and then the oxidation of the wustite with retention of the oxygen atom configuration to the formation of maghemite. The wustite phase was stabilised in the presence of increased alkali concentration.

The dissolution process was of zero order with respect to sodium hydroxide concentration and took place by heterogeneous interaction at the exposed pyrite interface. The number of molecules of alkali and oxygen required in the overall reaction has been determined and examination of partially leached pyrite using the Cambridge Microscan

X-ray Analyser has revealed that the deposition of a coherent coating during leaching is encouraged not only by preferential penetration of reactants along grain boundaries but also at sulphur deficient sites in the pyrite. X-ray analysis revealed that the final oxide product conformed with the expected stoichiometric proportion of iron in maghemite and that only a slight sulphur diffusion gradient, (less than 0.5 microns) was present, sulphur being virtually absent in the oxide product.

6.2. Leaching of Wolframite.

Wolframite was leached in solutions of sodium hydroxide (and sodium carbonate) of similar concentration (0.5 N) at temperatures up to 180°. The mechanism of dissolution and behaviour of the insoluble product was different from that of pyrite: In wolframite, the presence of oxygen is emphasised by the necessity for a molecular layer of ferric/manganic ions to be present at the mineral surface before the acceleration of reaction between minerals and leach solution can take place. Thus, although reaction was inhibited in its absence, trace quantities of oxygen were found to be adequate in ensuring extensive dissolution of the mineral at 150°C within 1 hour.

An adherent manganese-iron hydroxide coating was formed which tended to concentrate along the cleavage planes of the mineral. High oxygen pressures were detrimental to the dissolution process by causing reaction to be appreciably slowed down with oxidation of the initial divalent metal hydroxide product. This decreased the porosity so that diffusion of reactant ions to the mineral surface was practically stopped.

The dissolution of wolframite is accelerated by increase in alkali concentration and the reaction is heterogeneous at the mineral surface. The alkali requirement for the overall reaction has been determined and the reaction retarding influence of an insoluble produc emphasised by the immeasurably rapid rate of dissolution to completion in the presence of an iron oxide dissolving chelating agent.

Particles have been examined microscopically and the pseudomorphic, in situ, precipitation of the metal oxide product shown. X-ray powder diffraction studies revealed a considerable degree of scatter with no formation of lines indicative of iron or manganese oxides. This usually happens when very fine grained particles or iron oxides are deposited in alkali solutions. Analysis using the Cambridge X-ray Analyser has shown that the ratio of iron to manganese in mineral and oxide product is unchanged and that tungsten atoms were absent in the coating.

This is the first work in which cross-sections of the partially leached residues have been examined both microscopically and with the Cambridge Microscan X-ray analyser and in which the insoluble products of dissolution have been identified and their formation correlated through a series of topotactic transformation.

oOo

ACKNOWLEDGEMENTS.

The author wishes to express his sincere gratitude for the encouragement and useful suggestions given by Dr. A.R. Burkin.

Further thanks are due to Dr. A.P. Millman and Mr.T.K.Kelly for valuable assistance given with the Cambridge Microscan X-ray Analyser and to Dr. J. Cox for reading the proof.

The author is particularly indebted to the Johannesburg Consolidated Investment Co. Ltd., South Africa, for the financial assistance given and to the management of the Premier Diamond Mine, South Africa, and the Cassandra mine, Greece, for supplying minerals for this investigation.



Imperial College of Science and Technology,
Royal School of Mines,
Metallurgy Department,
London S.W.7.

LIST OF REFERENCES

1. A.E. Anderson, J. Halpern and C.S. Samis;
   Jour. Metals. A.I.M.E. Trans. 5 554-58 (1953)

2. Anon. Engng. Min. Jour. 6 89-91 (1958)

3. R.G. Arnold.
   Carnegie Inst. Washington. Ann. Rep.Div. Geophys. Lab. 57 218 (1958)

4. A.S.T.M.
   Alphabetical and Grouped Numerical Index of X-ray Diffraction Data.

5. B.T.K. Barry
   Thesis, R.S.M. (1955)

6. M.C. Ball and H.F.W. Taylor;
   Mineral Mag. 32 754 - 66 (1961)

7. J.D. Bernal
   Trans. Farad. Soc. 34 834 (1938)

8. J.D. Bernal, D.R. Dasgupta and A.L. Mackay,
   Nature. 180 645 - 647. (1957)

9. J.D. Bernal, D.R. Dasgupta and A.L. Mackay
   Clay Minerals Bull 4 15 - 30 (1959)

10. L.G. Berry and B. Mason
    Mineralogy, 327 - 332 (1959)

11. G.W. Brindley and J.O. Choe.
    Amer. Min. 46 771 - 85 (1961)

12 L.C. Bryner and R. Anderson
   Ind. Engng. Chem. 49 1721 - 24 (1957)

13 A.R. Burkin
   Personal Communication (1963)

14. A.R. Burkin
    Paper presented for Publication (1963)

15. B. Burwell ;
U.S. Pat. 2,394,362 (1946)

16. R.J. Cornelius and J.T. Woodcock;
Pro. Aust.Inst. Min. and Met. 185 109-33 (1958)

17. D.R. Dasgupta and A.L. Mackay;
Jour. Phys. Soc. Japan 14 932 (1959)

18. W.A. Deer, R.A. Howie and J. Zussman
Rock forming minerals. Vol. 5, 128-144 (1962)

19. G.A. Deitz and J. Halpern;
Jour. Metals. A.I.M.E. Trans. 5 1109-1116 (1953)

20. L.S. Dent Glasser, F.P. Glasser and H.F.W. Taylor;
Quatr. Reviews 16 343 - 60 (1962)

21. K.W. Downes and R.W. Bruce ;
Trans. Can. Inst. Min. Met. 58 77 (1955)

22. W.H. Dresher, M.E. Wadsworth and W.M. Fassell;
Jour. Metals, A.I.M.E. Trans, 8 794-800 (1956)

23. G. Ervin
Acta Crys. 5 103 - 8 (1952)

24 C.J. Farrow;
Thesis R.S.M. (1959)

25. G.M. Faulring, W.K. Zwicker and W.D. Forgeng;
Amer. Min. 45 946-59 (1960)

26. W. Feitnecht ;
Z. Electrochem. 63 34-43 (1959)

27. G.I. Finch and K.P. Sinha ;
Proc. Roy. Soc. A. 241 1 (1957)

28. M. Fleischer ;
Econ. Geol. 50th Anniv. Vol.Pt.II, 999-1008 (1955)

29. F.A. Forward and J. Halpern ;
J.Metals. A.I.M.E. Trans 7 463-66 (1955)

30. F.A. Forward, J. Halpern and E. Peters ;
Trans. Canad. Inst. Min. Met 56 354 (1953)

31. F.A. Forward and V.N. Mackiw ;
J. Metals. A.I.M.E. Trans 7 457-63 (1955)

32. M.H. Francombe and H.P. Rooksby ;
Clay Minerals Bull 4 1-14 (1959)

33. S. Glasstone, K.J. Laidler and H.Eyring ;
The Theory of Rate Processes N.Y. (1941)

34. A. Goswami and Y.N. Trehan;
Trans Farad. Soc. 52 358-62 (1956)

35. P.M.J. Gray;
Trans. Inst. Min.Met. 65 55-64(1955)

36. J.W. Greig, E.Posnjak, H.E. Merwin and R.B.Sosman ;
Amer. J. Sci. 30 239 - 316 (1935)

37. J.W. Gruner;
Econ. Geol 21 375-393 (1926)

38. J. Halpern;
Trans. Electrochem. Soc. 100 421 - 28 (1953)

39. J. Halpern and F.A. Forward;
Trans. Inst. Min. Metal 66 181 (1957)

40. H.W. Highriter and W.C. Lilliendahl;
U.S. Pat. 2316583 (1943)

41. Hillebrand and Lundell;
Applied Inorganic Analysis

42. V.Kudryk and H. Kellogg;
J. Metals. A.I.M.E. Trans 6 541-49

43. G. Kullerud and H.S. Yoder;
Econ. Geol 54 533-69 (1959)

44. B.G. Langston, R.D. Macdonald and F.M. Stephens;
J.Metals. A.I.M.E. Trans 9 752-56 (1957)

45. P.A.Laxen and M.G. Atmore;
Uranium in S. Africa Vol 1. 315-331 (1957)

46. K.C. Li and C.Y. Wang ;
Tungsten (1955)

47. vF. Liebau, F. Wodtcke and H. Bunge ;
Acta. Crys. 13 1016 (1960)

48. F.K. Lotgering;
J. Inorg. Nuclear Chem. 9 113-23 (1959)

49. A.L. Mackay;
Mineral Mag. 32 545-557 (1960)

50. D.R. McKay and J. Halpern;
Trans. Met. Soc. Amer. Inst. Min.Met Engrs.212 301-09 (1958)

51. R.W. Mancant elli and J.R. Woodward;
J. Metals A.I.M.E. Trans 7 751-55 (1955)

52. J.E.O. Mayne ;
Jour. Chem. Soc. 129 - 132 (1953)

53. D.A. Melford and P. Duncumb ;
Metallurgia 59 205 (1960)

54. J.W. Mellor ;
Treatise on Inorg. Chem. Vol. 13. 718

55. A.P. Millman ;
Personal Communication (1963)

56. I.M. Nelen and S.I. Sobol ;
Chem. Abs. 20731 b. (1960)

57. G.W. van Oosterhout ;
Acta. Crys 13 932-935 (1960)

58. H.M. Parker and W.J. Whitehouse ;
Phil. Mag. 7th ser. 14 936-960 (1932)

59. M.R. Piggott ;
Acta. Crys. 10 364 - 68 (1957)

60. I.N. Plaskin and A.A. Masurova;
Chem. Abs. 8513 b (1960)

61. H. Remy ;
Treatise on Inorganic Chemistry Vol II 756

62. H.P. Rooksby and C.J.M. Rooymans;
Clay Minerals Bull. 4 234-38 (1961)

63. D.P.Seraphim and C.S. Samis;
J. Metals A.I.M.E. Trans 8 1096-99 (1956)

64. M.I. Sherman and J.D.H. Strickland;
ibid. 9 1386-88 (1957)

65. M.I. Sherman and J.D.H. Strickland;
ibid 9 795-800 (1957)

66. N.V. Sidgwick;
Chemical Elements and Their Compounds (1950)

67. F.G. Smith;
Am. Mineral 27 1 - 19 (1942)

68. C.S. Smithells ;
Tungsten 3rd Ed. (1952)

69. J.F. Stenhouse and W.M. Armstrong ;
Canad. Inst. Min. Met. Trans 55 38. (1952)

70. Sullivan;
Trans. Am. Inst. Min. Met. Engsr. 106
515 - 46 (1933)

71. G. Thomas and B.J.P. Whalley;
Canad. J. Chem. Engng. 36 (1) 37-43 (1958)

72. V.G. Tronev and S.M. Bondin;
Comptes Rendus Acad. Sci. URSS (23 541 (1937)

73. I.H. Warren;
Aust. J. Appl. Sci. 9 36-51 (1958)

74. I.H. Warren;
Aust. J. Appl. Sci 7 346-58 (1956)

75. A.F. Wells;
Structural Inorganic Chemistry (3rd Edition 1962)

76. H.A. White;
J. Chem. Soc. S.Afr. 20 1 (1919)

77. B.T.M. Willis and H.P. Rooksby;
Acta Crys. 6 827 - 31 (1953)

78. J.T. Woodcock;
Aust. Inst. Min. Met. Proc. 198 47-84

79. R.W.G. Wyckoff;
Crystal Structures. Vol 1. Chap. III Pyrite and Wustite